1-1-2015

Regulation of Functional Amyloid formation and Pigmentation During Melanosome Biogenesis

Tina Ho
University of Pennsylvania, hotina7@gmail.com

Regulation of Functional Amyloid formation and Pigmentation During Melanosome Biogenesis

Abstract
Melanosomes are subcellular organelles specialized for the synthesis and storage of melanin pigments. Within epidermal and ocular pigment cells, melanosomes are generated from endosomal precursors in discrete stages. Early stages are characterized by the accumulation of premelanosome protein (PMEL) and its assembly into nontoxic amyloid fibrils, while later stages are characterized by the arrival of proteins important for the production of pigment. In this thesis, I will discuss two important findings relevant to melanosome biology.

The first finding addresses the molecular mechanisms that regulate the transformation of PMEL from an integral membrane protein to fibrillar structures with properties of amyloid. These data show that native disulfide-bonded PMEL dimers prevent premature fibril formation early in the secretory pathway but must be resolved prior to the assembly of functional amyloid fibrils in early stage melanosomes. Failure to resolve the dimeric intermediates – as occurs with mutagenesis of a PMEL regulatory domain – decreases amyloid production in a heterologous expression system. Since the oligomerization of amyloid precursors is hardly unique, detailed characterization of the different intermediates formed by functional versus pathological amyloid proteins may bring us one step closer to understanding the mechanisms of neurodegenerative amyloid disease.

The second finding addresses the localization and potential function of SLC45A2, a proton-dependent sucrose transporter encoded by the gene that is mutated in the hypopigmentary disorder oculocutaneous albinism type 4 (OCA4). While melanocytes derived from patients and mouse models of OCA4 are known to contain hypopigmented melanosomes, it is unclear why mutations in SLC45A2 lead to decreased pigment production. Our data show that SLC45A2 localizes to and functions from distinct punctate structures on/near stage III and IV melanosomes. Mislocalization of SLC45A2 leads to hypopigmentation suggesting that the transporter must be present on melanosomal structures to function. Preliminary data also suggest that SLC45A2-deficient melanocytes harbor melanosomes that are hypopigmented but normally shaped and that SLC45A2 function can be bypassed by overexpression of a different melanosomal transporter, OCA2. Along with other preliminary data, these results suggest that SLC45A2 likely maintains a neutral pH within maturing melanosomes to ensure sustained melanin deposition.

Together, these two studies provide insight into the molecular mechanisms that regulate nontoxic amyloid and melanin production within healthy melanocytes.

Degree Type
Dissertation

Degree Name
Doctor of Philosophy (PhD)

Graduate Group
Cell & Molecular Biology

REGULATION OF FUNCTIONAL AMYLOID FORMATION AND PIGMENTATION DURING MELANOSOME BIOGENESIS

Tina Ho

A DISSERTATION

in

Cell and Molecular Biology

Presented to the Faculties of the University of Pennsylvania

in

Partial Fulfillment of the requirements for the

Degree of Doctor of Philosophy

2015

Supervisor of Dissertation

_____

Michael S. Marks

Professor of Pathology and Laboratory Medicine

Graduate Group Chairperson

_____

Daniel S. Kessler, Associate Professor of Cell and Developmental Biology

Dissertation Committee

Robert W. Doms, Professor of Pathology and Laboratory Medicine

Rahul M. Kohli, Assistant Professor of Medicine and Biochemistry and Biophysics

Virginia M.Y. Lee, Professor of Pathology and Laboratory Medicine

James Shorter, Associate Professor of Biochemistry and Biophysics

ABSTRACT

REGULATION OF FUNCTIONAL AMYLOID FORMATION AND PIGMENTATION DURING MELANOSOME BIOGENESIS

Tina Ho

Michael S. Marks

Melanosomes are subcellular organelles specialized for the synthesis and storage of melanin pigments. Within epidermal and ocular pigment cells, melanosomes are generated from endosomal precursors in discrete stages. Early stages are characterized by the accumulation of premelanosome protein (PMEL) and its assembly into nontoxic amyloid fibrils, while later stages are characterized by the arrival of proteins important for the production of pigment. In this thesis, I will discuss two important findings relevant to melanosome biology.

The first finding addresses the molecular mechanisms that regulate the transformation of PMEL from an integral membrane protein to fibrillar structures with properties of amyloid. These data show that native disulfide-bonded PMEL dimers prevent premature fibril formation early in the secretory pathway but must be resolved prior to the assembly of functional amyloid fibrils in early stage melanosomes. Failure to resolve the dimeric intermediates – as occurs with mutagenesis of a PMEL regulatory domain – decreases amyloid production in a heterologous expression system. Since the oligomerization of

amyloid precursors is hardly unique, detailed characterization of the different intermediates formed by functional versus pathological amyloid proteins may bring us one step closer to understanding the mechanisms of neurodegenerative amyloid disease.

The second finding addresses the localization and potential function of SLC45A2, a proton-dependent sucrose transporter encoded by the gene that is mutated in the hypopigmentary disorder oculocutaneous albinism type 4 (OCA4). While melanocytes derived from patients and mouse models of OCA4 are known to contain hypopigmented melanosomes, it is unclear why mutations in SLC45A2 lead to decreased pigment production. Our data show that SLC45A2 localizes to and functions from distinct punctate structures on/near stage III and IV melanosomes. Mislocalization of SLC45A2 leads to hypopigmentation suggesting that the transporter must be present on melanosomal structures to function. Preliminary data also suggest that SLC45A2-deficient melanocytes harbor melanosomes that are hypopigmented but normally shaped and that SLC45A2 function can be bypassed by overexpression of a different melanosomal transporter, OCA2. Along with other preliminary data, these results suggest that SLC45A2 likely maintains a neutral pH within maturing melanosomes to ensure sustained melanin deposition.

Together, these two studies provide insight into the molecular mechanisms that regulate nontoxic amyloid and melanin production within healthy melanocytes.

TABLE OF CONTENTS

LIST OF TABLES

LIST OF FIGURES

CHAPTER 1

Introduction: Functional Amyloid and Melanosome Biogenesis

1.1 Introduction

Pigmentation has a variety of purposes in metazoans including mate selection, camouflage, and communication (1). In humans and some other mammals, melanin is primarily important for protection from UV damage and for proper development of the visual system. Produced in specialized organelles known as melanosomes that are present within pigment cells of the skin and eye, melanins are polymers composed of a heterogenous mixture of redox-active compounds derived initially from the amino acid tyrosine (2). Eumelanins, which are composed of indole products of tyrosine hydroxylation and oxidation, serve as sinks for reactive oxygen species and thus protect the skin and eyes from oxidative damage (2). Pheomelanin polymers result from cysteinylation of tyrosine and are thought to be more pro-oxidative, correlating with higher risk of skin cancers (2).

The melanosomes that harbor primarily eumelanins are specialized, membrane-bound structures that are generated in skin and choroidal melanocytes and in the retinal, iris, and ciliary body pigment epithelia of the eye. They are among the best characterized of a series of cell type-specific "lysosome-related organelles" (LROs) that coexist with lysosomes in their respective cell types (3). A challenge for pigment cells and other LRO-containing cell types is the ability to generate LROs during their development; in retinal pigment epithelial cells, melanosomes are generated only during a short period of prenatal development, but in other mammalian pigment cell types, they are generated constantly. Proteins that underlie melanosome structure and that contribute to melanin formation must be synthesized by the cell, processed through the classical secretory

pathway, and then diverted to newly forming melanosomes. How this occurs is just beginning to be understood (4).

Eumelanosomes are particularly unusual in having a cylindrical shape and an intralumenal fibrillar scaffold upon which melanins deposit as the melanosome matures (5). This fibrillar scaffold develops prior to the onset of melanogenesis and is comprised largely – if not entirely – of the functional amyloid protein PMEL (also known as Pmel17, Silver, gp100 and ME20) (6). As discussed below, the amyloid fold is more typically thought of in the context of disease, such as in Alzheimer or Parkinson disease, but PMEL production in pigment cells is non-toxic.

The production of nontoxic amyloids and how this process differs from that of pathological amyloid proteins is not known. We hypothesize that the formation of nontoxic amyloid requires highly coordinated and robust mechanisms of regulation that either do not exist or malfunction in amyloid disease. Therefore, in the first half of this thesis, we examine one mechanism of regulation in which PMEL – a model functional amyloid protein of the endomembrane system – forms dimers that maintain the protein in a non-amyloid conformation as it traffics en route to early stage melanosomes.

Once fibrillar melanosome precursors are generated, they undergo a process of maturation in which the enzymes and transporters that contribute to melanin synthesis are delivered and activated. The key enzyme in the synthesis of all melanins is tyrosinase (TYR), which catalyzes the limiting steps of tyrosine hydroxylation to L-DOPA and oxidation of L-DOPA to DOPAquinone (2). Importantly, however, TYR is inactive at acidic pH (7). This belies the fact that PMEL amyloid formation requires low pH, at least

initially to activate the proteolytic enzymes involved in PMEL maturation ((8); see below). Thus, the internal environment of melanosomes must be modified for efficient melanin biosynthesis to occur. This involves both a rise in pH (9) and changes to the divalent cation composition (10-12). This is accomplished by the delivery of transmembrane transporters specifically to the melanosome during maturation. For example, delivery of the copper transporter ATP7A facilitates loading of copper into the TYR active site (10), and delivery of the chloride channel, OCA2, facilitates pH neutralization (13,14). Mutations in the genes encoding these transporters result in hypopigmentation in animal models and oculocutaneous albinism (OCA) in humans.

Other transporters also likely function to maintain the proper intralumenal environment within melanosomes. In the second half of this thesis, I investigate the molecular basis of OCA type 4 (OCA4). This disorder is caused by mutations in SLC45A2 (15); however, the role of SLC45A2 in melanosome biology is not well understood. I preliminarily define the localization of SLC45A2 and present preliminary data to suggest that the protein contributes to maintaining the neutral pH of late-stage melanosomes.

1.2 Amyloid

Associated with pathological conditions since the time of Virchow, the study of amyloid today is still virtually synonymous with that of disease. The formation of amyloid has been linked to both systemic amyloid diseases in which the deposition of amyloid disrupts tissue architecture and stiffens affected organs as well as neurodegenerative diseases in which the mechanism of disease is less well understood. However, not all

amyloid proteins are associated with pathology. Functional amyloid proteins such as curli (16), RIP1/RIP3 (17), and PMEL (18) form nontoxic amyloid fibrils that actually contribute to the well-being of the organism and do not participate in disease processes under normal physiological conditions. By studying and comparing the formation of functional amyloid with that of pathological amyloid, we hope to gain insight into the molecular basis of Alzheimer, Parkinson, and other neurodegenerative amyloid diseases.

All amyloid proteins are defined by their ability to polymerize into cross-β-sheet fibrils that are insoluble, resistant to protease degradation, and readily apparent by electron microscopy (19). Most also bind traditional amyloid dyes such as Congo red and thioflavin T. They are typically thought to be produced via a nucleated assembly mechanism in which soluble monomers associate to form a stable nucleus during the lag phase of fibril formation (**Figure 1.1**; (20)). This thermodynamically unfavorable process either requires unstructured proteins to adopt a specific conformation or folded proteins to partially unfold and adopt a new conformation. Once sufficient nuclei have formed, however, soluble monomers are rapidly incorporated into the ends of growing fibrils during the elongation phase of fibril formation.

The nucleated self-assembly process creates a diverse array of intermediates as well as a heterogeneous final product. The intermediates are often crudely categorized as soluble oligomers (such as dimers and trimers), nonfibrillar aggregates of higher molecular weight, and protofibrils (21). The inherently metastable nature of these pre-amyloid species makes it difficult for biophysicists to study their structure by traditional methods such as X-ray crystallography or NMR and even harder for cell biologists to generalize

Figure 1.1

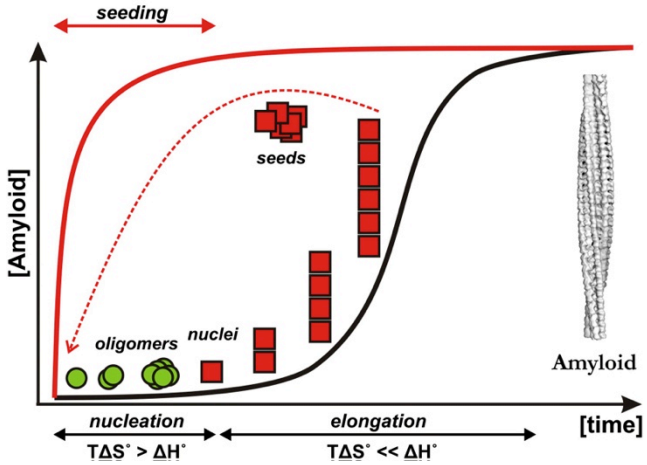

Nucleated assembly of amyloid fibrils. The kinetics of amyloid fibril formation are consistent with a nucleation dependent mechanism in which the thermodynamically unfavorable process of nucleus formation occurs during a lag phase but grow rapidly during the elongation phase (black line). However, the lag phase is significantly shortened if the process is seeded with preformed fibrils (red line). *Adapted from: A Diversity of Assembly Mechanisms of a Generic Amyloid Fold (20).*

about the effect of these species on cell health. Attempts have been made to isolate relatively homogenous preparations of stable intermediates, however, and comparison of the stable intermediates formed by functional versus pathological amyloid proteins might one day be helpful in determining whether oligomers are responsible for the toxicity associated with pathological amyloid formation and, if so, which particular intermediates are to blame.

1.2.1 Aβ and Alzheimer Disease

Amyloid precursor protein (APP) is linked to Alzheimer's disease (AD) since mutations in APP result in familial forms of AD (22). In patients with AD, APP is cleaved first by β-secretase and then by γ-secretase to form Aβ peptides. These peptides can be 39-42 amino acids in length; however, the most amyloidogenic is Aβ42. Aβ42 is the major component of the amyloid plaques that accumulate in AD brains (23,24) and forms highly insoluble amyloid fibrils more rapidly *in vitro* (25,26). Mutations in presenilin-1, the catalytic subunit of the γ-secretase complex, can also increase the Aβ42:Aβ40 ratio and cause familial AD (27).

Aβ plaques are a defining feature of AD; however, it remains controversial whether these plaques constitute the pathogenic species of AD or whether pre-amyloid intermediates of fibril formation are responsible for the neuronal loss and neurocognitive decline observed in patients with AD. It is known that plaque burden correlates poorly with clinical severity while levels of soluble non-fibrillar Aβ are a much better indicator of both synaptic loss and disease progression (28,29). It has also been shown that Aβ dimers

isolated from human brain tissue by size exclusion chromatography disrupted synaptic function in rat brain slices – an effect that could be blocked by the addition of antibodies to Aβ (30). Soluble AD brain lysate also impaired memory formation in live rats, while the same lysate immunodepleted for Aβ did not suggesting that soluble Aβ intermediates disrupt normal brain function *in vivo.*

These experiments raise many more questions than they answer, but the one we are most interested in is what makes the brain-derived Aβ dimers in this experiment so toxic. Moreover, how might functional amyloid proteins avoid such toxicity?

1.2.2 α-Synuclein and Parkinson Disease

Parkinson disease (PD) is genetically linked to α-synuclein since mutations in the protein cause familial PD (31). α-Synuclein fibrils are the principal component of Lewy bodies, the defining pathological feature of PD (32). Here too, oligomers emerged as a way to explain the poor correlation between Lewy pathology and clinical features of PD. Lewy bodies are observed in 12% of asymptomatic individuals on autopsy (33), and many patients with familial forms of PD show no evidence of Lewy pathology postmortem (34). Additionally, in a rat model system, variants of α-synuclein that were more prone to form oligomers than fibrils led to greater dopaminergic loss than mutants that were more prone to form fibrils than oligomers (35).

However, not all oligomers of α-synuclein appear to be toxic. The most interesting debate in the field currently centers on the existence of native α-synuclein tetramers. Isolated from cells in culture, mouse brain tissue, and red blood cells under non-denaturing

conditions or from *E. coli* using *n*-octylglucoside detergent, these tetramers exhibit α-helical structure and are resistant to amyloid formation (36,37). Physiological tetramers of α-synuclein previously escaped detection because harsh conditions are often used to purify recombinant α-synuclein based on studies characterizing α-synuclein as a natively unfolded, intrinsically disordered protein (38). In addition, the α-helical structure of α-synuclein is stabilized by N-terminal acetylation, a post-translational modification found *in vivo* but not in recombinant bacterially produced protein (at least not without co-expression of the fission yeast N-terminal acetylation B complex) (36,39,40). Together, these data suggest that α-synuclein oligomerization may inhibit pathological amyloid formation *in vivo*. They also demonstrate that *in vitro* studies performed using recombinant protein should be interpreted with caution.

1.2.3 Functional amyloid

Functional amyloid proteins are a group of proteins that have all the biochemical and biophysical properties of amyloid but are actually beneficial to the cells and organisms that produce them (41). They have been observed in a wide variety of species ranging from bacteria to humans and include extracellular amyloid proteins important in biofilm formation (**Figure 1.2A**; (16)) as well as intracellular amyloid proteins that function in learning and memory (42), innate immunity (17), and pigmentation (**Figure 1.2C**; (18)). In order to be evolutionarily beneficial, however, these proteins must form amyloid without destroying their hosts. How does the assembly of functional amyloid occur

Figure 1.2

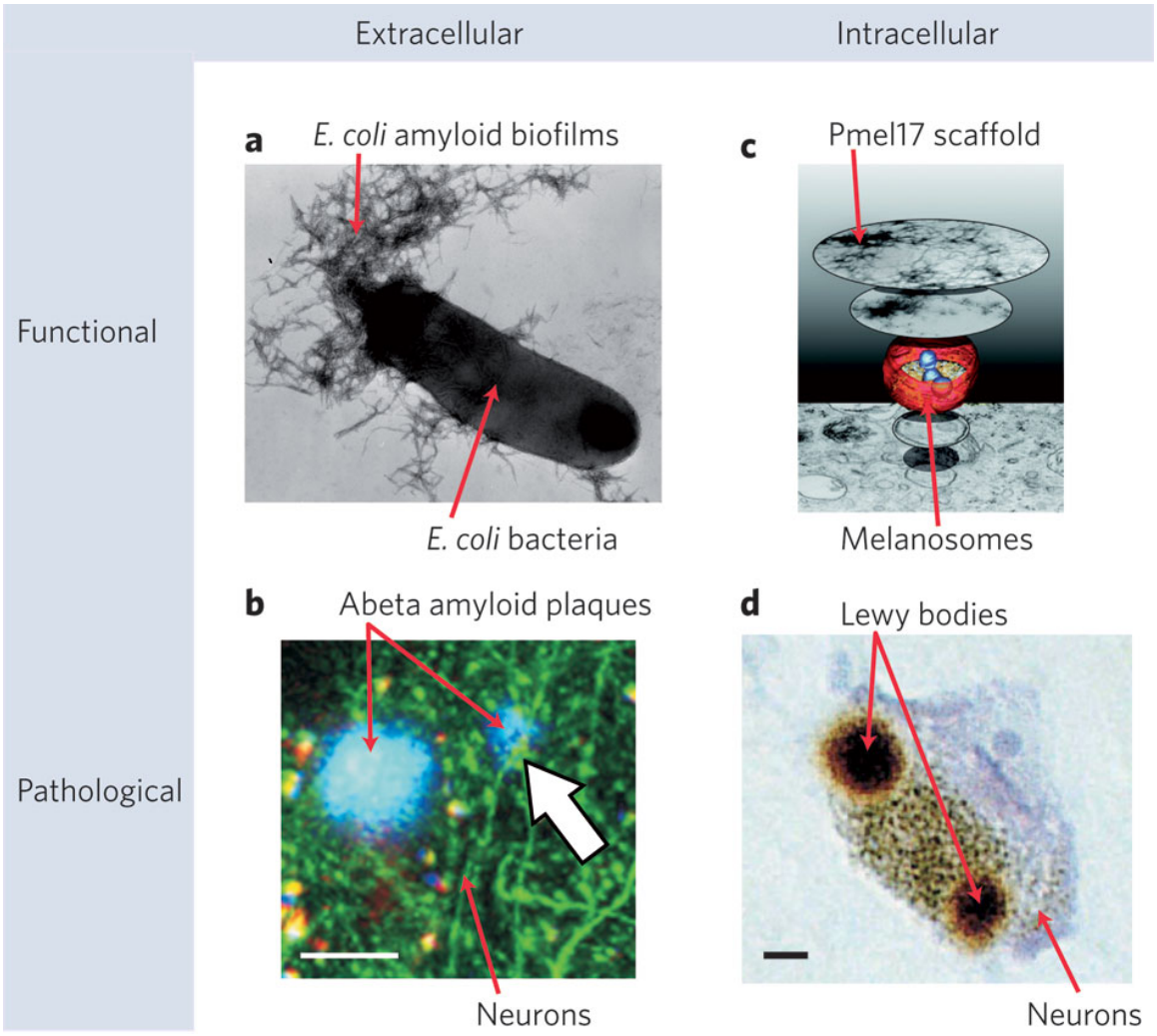

Examples of amyloid. Amyloid fibrils can form extracellularly (A, B) or intracellularly (C, D) and be functional (A, C) or pathological (B, D). *Adapted from: Nanomechanics of functional and pathological amyloid materials (50).*

without inducing any of the toxic effects associated with the deposition of pathological amyloid proteins such as Aβ (**Figure 1.2B**) or α-synuclein (**Figure 1.2D**)?

An especially well-studied example of functional amyloid formation is that of curli fiber production. The two curli operons *csgBAC* and *csgDEFG* encode seven proteins, all of which are important for biofilm formation in *E. coli*. The primary component of curli fibers, CsgA, has five imperfect repeats that are predicted to form the amyloid core (43). CsgB is a minor subunit that both nucleates CsgA fibril formation (44) and cooperates with CsgF to anchor growing fibers to the bacterial outer membrane (45). CsgC is a very recently identified protein chaperone that prevents premature amyloid formation in the bacterial periplasm; incredibly, CsgC can inhibit not only CsgA amyloid formation at a 1:500 molar ratio but also α-synuclein fibril formation at a 1:10 molar ratio (46). CsgD is a transcription factor that activates the *csgBAC* operon (47). CsgG oligomerizes to form a channel in the outer membrane necessary for CsgA and CsgB to pass from the periplasm into the extracellular space (48,49), while the specificity factor CsgE binds to CsgG and caps the periplasmic side of the channel (49). Together, these seven proteins illustrate the complex regulation involved in functional amyloid formation – even in a prokaryote.

Several functional amyloid proteins have also been identified in yeast. The majority of these are prions, or proteins that confer heritable and infectious traits to the yeast in which they are present. They include Ure2p, which interferes with the ability of yeast to adapt to nitrogen-rich environments (51,52), Sup35p, which regulates stop codon readthrough (53,54), and Rnq1p, which helps other prion proteins adopt their amyloid state (55). Remarkably, yeast can remodel both pre-amyloid oligomers and mature

amyloid fibrils using Hsp104, a chaperone with robust disaggregation activity. Using ATP as an energy source, Hsp104 functions in concert with Hsp40 and Hsp70 chaperones to solubilize and recover enzymatically active monomers from misfolded aggregates (56).

Cytoplasmic polyadenylation element-binding proteins (CPEBs) regulate protein synthesis at the neuronal synapse, and isoforms in the sea snail *Aplysia* (ApCPEB) as well as in *Drosophila* (Orb2) have been shown to play a role in the formation of long-term memories (42,57). With bacteria and yeast, structural studies are performed directly on the amyloid proteins of interest. In higher organisms, however, detailed biophysical characterizations are often done on recombinant protein with maybe one or two studies performed *in vivo* to support the findings *in vitro*. This is true for ApCPEB and Orb2. Recombinant ApCPEB forms fibrils visible by electron microscopy that bind Thioflavin T and have a cross-β sheet X-ray diffraction pattern (57,58). Cells expressing an HA-tagged variant of ApCPEB also stained with the amyloid dye Thioflavin S; however, endogenous ApCPEB did not. Even fewer structural studies have been performed on the *Drosophila* isoforms Orb2A and Orb2B, though recombinant versions of these proteins do assemble into fibrils by electron microscopy (42).

Detailed structural studies were performed, however, on both light and heavy secretory granules purified from rat pituitary (59). These experiments suggested that at least some of the peptide hormones that form fibrils *in vitro* are indeed stored as amyloid *in vivo* as the granules exhibited Congo Red birefringence, bound Thioflavin T, and had a cross-β sheet X-ray fiber diffraction pattern. Of note, these functional amyloid fibrils

depolymerized and released active monomers when dialyzed in Tris buffers of pH 6.0 or pH 7.4. Some were also moderately toxic when applied to a neuronal cell line.

The diversity of functional amyloid suggests that there may be many ways to generate amyloid without causing damage to cells and/or surrounding tissues. However, one property that will likely be shared by all examples mentioned as well as functional amyloid proteins yet to be discovered is a high degree of regulation. It is our hope that future studies will not only reveal additional mechanisms of regulation governing the conversion of functional amyloid proteins from non-amyloid to amyloid forms but also highlight processes that may be misregulated in amyloid disease.

1.2.4 PMEL amyloid

Melanosomes are lysosome-related organelles that mature from early endosomes in four morphologically distinct stages. Stage I melanosomes are characterized by intraluminal vesicles (ILVs) from which short fibrillar structures appear to emanate (**Figure 1.3**; (60)). Lateral association of these fibrils occurs as the organelle matures to stage II. Thus stage II melanosomes are characterized by the presence of longer, thicker fibrils arranged in parallel sheets (**Figure 1.3**; (60)). As the organelle continues to mature, melanins are synthesized and deposited on these proteinaceous sheets until the underlying fibrillar scaffold is completely obscured by the deposition of pigment.

Premelanosome protein (PMEL; also referred to as Pmel17, Silver, ME20, or gp100) was originally identified as a component of the "melanosomal matrix" by antisera raised against the Triton X-100 insoluble fraction of melanosomes that (1) labeled the

Figure 1.3

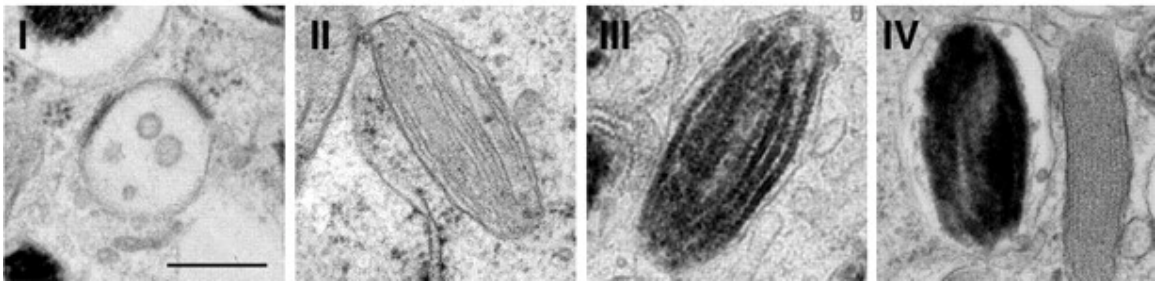

Melanosome maturation. Cells from a pigmented human melanoma cell line, MNT-1, were analyzed by thin section electron microscopy. Note the cytoplasmic coats on the limiting membrane and fibrils extending from ILVs in stage I melanosomes, the parallel sheets of amyloid present in stage II melanosomes, the deposition of melanins in stage III melanosomes, and how the underlying melanosomal matrix is masked in stage IV melanosomes. Scale bar, 200 nm. *Adapted from: Electron tomography of early melanosomes: implications for melanogenesis and the generation of fibrillar amyloid sheets (60).*

melanosomal matrix of B16 mouse melanoma cells and (2) immunoprecipitated a full-length protein that was soluble in Triton X-100 as well as a proteolytically processed form of PMEL that required the harsher detergent SDS to be solubilized (61). This was subsequently supported by experiments showing an interaction between PMEL with newly synthesized melanin polymers (62) as well as additional immuno-electron microscopy studies in MNT-1 human melanoma cells that showed clear labeling of fibrils within stage II melanosomes (9). Importantly, PMEL is both necessary and sufficient for fibril formation. Fibrillar structures are absent from the melanosomes of PMEL knockout mice (63), while expression of PMEL cDNA is sufficient to support fibril formation in non-pigment cells (64). Together, these data indicate that PMEL is the primary component of the fibrillar structures observed in early stage melanosomes.

It is now known that the fibrils formed by PMEL are in fact functional amyloid. Recombinantly produced PMEL fragments purified from *E. coli* inclusion bodies using 8 M guanidinium hydrochloride rapidly assemble into fibrils following dilution into non-denaturing buffers (18). The fibrils are visible by electron microscopy, accelerate the rate of melanin deposition *in vitro*, bind the amyloid dyes Thioflavin T and Congo Red, and have the characteristic cross-β sheet X-ray diffraction pattern of amyloid (18). *In vivo*, melanosomes isolated from bovine retinal pigment epithelia stain with Thioflavin S and Congo Red, and the Thioflavin S staining overlaps with that of PMEL in detergent-insoluble clusters extracted from the bovine melanosomes (18).

As the first functional amyloid protein to be identified in mammals, PMEL was the first to challenge the notion that functional amyloid proteins would be limited to more

primitive organisms due to the risk of forming large insoluble protein structures in longer-lived multicellular species. Yet PMEL is highly conserved throughout vertebrate evolution suggesting that the process of PMEL fibril formation is (1) regulated such that very little of the protein adopts toxic/misfolded conformations and (2) so evolutionarily beneficial as to be worth the risk.

1.2.5 PMEL regulation

PMEL fibril formation must be constrained to a specific time and place because unregulated amyloid formation could rapidly wreak havoc on both melanocytes and the organism as a whole. Without a doubt, many redundant layers of regulation exist to prevent such a catastrophe; however, only a small handful of these layers have been identified. Understanding more of these layers will help us determine whether the regulatory mechanisms that govern functional amyloid formation are shared by pathological amyloid proteins and perhaps shed some light on what makes pathological amyloid proteins so devastating in patients with neurodegenerative disease.

Tissue-specific expression

Of the regulatory mechanisms that have been identified, the pigment-cell-specific expression of PMEL is the most straightforward. Under control of the microphthalmia-associated transcription factor (MITF) (65), PMEL is expressed only in those cells that produce eumelanin: pigment cells of the skin, eye, heart, and inner ear. Note that the

production of pheomelanin pigments does not involve MITF, PMEL, or the production of amyloid fibrils (66,67).

Compartmentalization

Regulatory mechanisms also exist to ensure that PMEL forms amyloid only on intraluminal vesicles (ILVs) of early endosomes/stage I melanosomes. PMEL is initially synthesized in the ER as a type I transmembrane protein (**Figure 1.4**; (68-70)). Once folded, PMEL traffics through the Golgi where O-linked glycans are added and 3 of the 4 N-linked glycans mature to the complex type (64,71,72). PMEL is then cleaved by a proprotein convertase in the TGN (73) and/or in endosomes (74), and at least some quantity of PMEL traffics to the plasma membrane (75). At the plasma membrane, a small fraction of PMEL is released into the extracellular space by ectodomain shedding (76), while the rest is taken back up into the cell and targeted to clathrin-coated early endosomes/stage I melanosomes via a dileucine-based sorting signal in the cytoplasmic domain of the protein (77). Within stage I melanosomes, PMEL is sorted to ILVs in a process dependent on CD63 and ApoE but not ESCRT components (78,79) and cleaved by BACE2 (80). The protein then assembles into amyloid fibrils that can be seen emanating from ILVs by electron microscopy. The fibrils then associate laterally to form parallel sheets of amyloid in stage II melanosomes. As the melanosomes mature, melanins are synthesized and deposited on the fibrillar PMEL scaffold, forming stage III melanosomes. These pigmented stage III melanosomes ultimately mature to stage IV

Figure 1.4

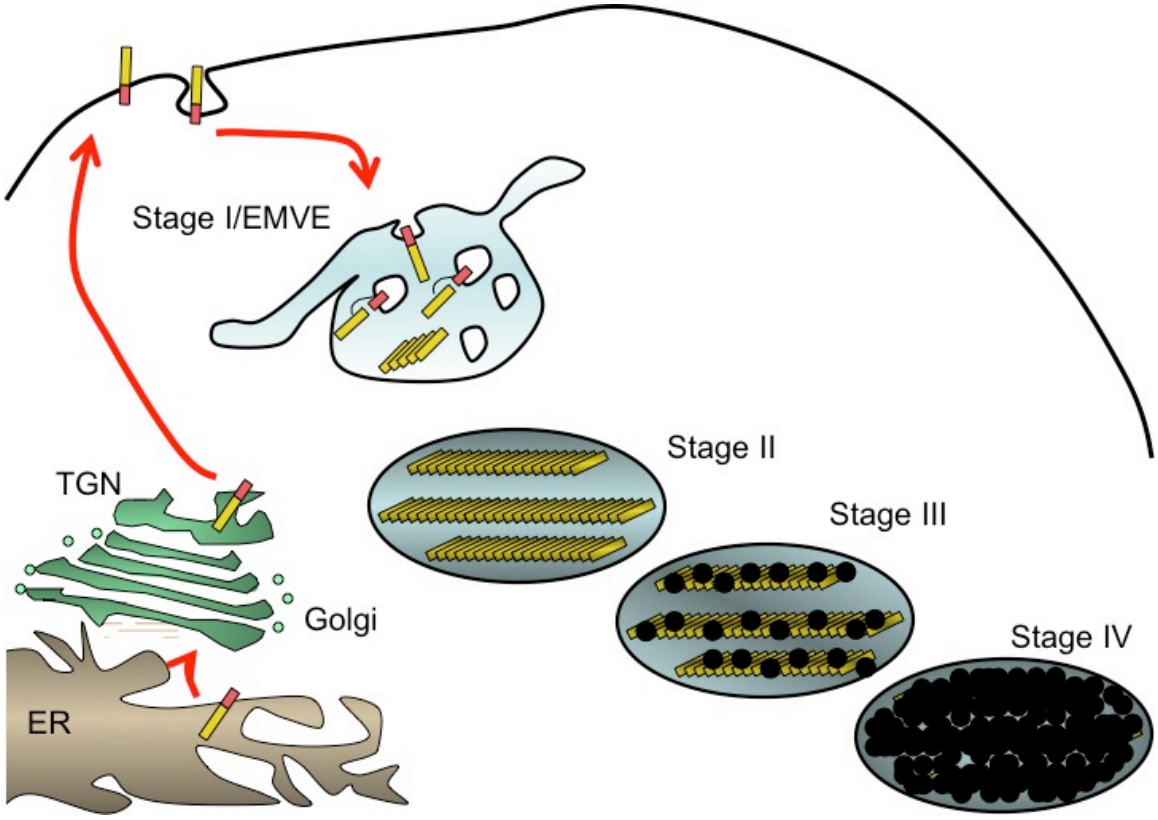

Trafficking of PMEL from the ER to stage I melanosomes. Schematic showing PMEL as it traffics from its site of synthesis in the ER to stage I melanosomes. At least a fraction of PMEL transits through the Golgi, TGN, and plasma membrane en route to stage I melanosomes. *Adapted from: PMEL: a pigment cell-specific model for functional amyloid formation (6) by B. Watt.*

melanosomes which have so much melanin that the underlying PMEL scaffold can no longer be visualized by electron microscopy or detected using PMEL antibodies (9).

Notably, PMEL amyloid fibrils are not observed in the ER, Golgi, trans-Golgi network (TGN) or any organelle preceding early endosomes/stage I melanosomes. Therefore, the conformational switch that converts PMEL from a non-amyloid protein to an amyloid protein likely occurs in association with ILVs or membranes that later invaginate to form ILVs. Several properties of ILVs could aid in this conversion. Association with lipids of a specific composition or curvature may be required to partially unfold and/or stabilize a β-sheet rich conformation of PMEL – a hypothesis strengthened by the new link between PMEL and ApoE, a protein that not only coats lipoprotein particles but alleles of which are a risk factor for AD (81). Additionally, the presence of proprotein convertases (82), BACE2 (80), ADAM proteases (83), and/or cysteine proteases (see chapter 2) in an environment favorable for their activity may facilitate this process. Chaperones or other regulatory mechanisms designed to prevent premature fibril formation elsewhere in the cell could also simply be absent in ILVs, and concentrating PMEL monomers into a small patch of membrane likely facilitates nucleation. Regardless, the secreted form of PMEL is soluble (64,84,85) and does not form fibrils in the culture medium (unpublished results) suggesting that the environment of ILVs is necessary for the conversion of PMEL from a non-amyloid to an amyloid form. Restricting the formation of PMEL amyloid to a specific membrane-enclosed organelle likely decreases the potential for toxicity arising from interactions between cytosolic proteins and misfolded oligomers, nonfibrillar aggregates, protofibrils, and/or the completed PMEL matrix.

Kinetics

A toxic intermediate with a short half-life may have fewer opportunities to interact with other cellular components and cause damage than one with a longer half-life. Therefore, extremely rapid polymerization kinetics have been proposed as one mechanism by which functional amyloid proteins avoid the toxic effects observed with the formation of pathological amyloid. *In vitro*, recombinant PMEL purified using 8 M guanidinium hydrochloride forms fibrils within 3 s of dilution into a non-denaturing buffer (18). While the kinetics of PMEL fibril formation is difficult to measure *in vivo*, metabolic pulse-chase experiments indicate that the entire process – from translation in the ER to polymerization into insoluble amyloid fibrils – occurs in a matter of hours.

Rapid fibril formation that occurs within seconds has also been observed for recombinantly produced CPEB (58). This is in contrast to the hours or days required for synthetic Aβ42 to form fibrils without seeding (25). Intriguingly, the functional amyloid protein RIP1/RIP3 also took hours to polymerize into amyloid fibrils after dilution into non-denaturing buffer (17) suggesting that this mechanism of regulation may not be shared among all functional amyloid proteins.

Cleavage

At least two regulated proteolytic cleavage events are absolutely essential for PMEL fibril formation. A furin-like proprotein convertase cleaves full-length PMEL into two fragments: an N-terminal Mα fragment and a C-terminal Mβ fragment (82). The Mα fragment contains the fibril-forming domains of PMEL and can be incorporated into

insoluble amyloid fibrils without additional processing (82,86). The Mβ fragment contains a cysteine-rich luminal domain (the KLD; see below), transmembrane domain, and cytoplasmic domain. Since Mα and Mβ are connected by at least one disulfide bond (8), subsequent cleavage by an ADAM protease at the plasma membrane (76) or by BACE2 within endosomes (80) is required to generate soluble PMEL. In this second cleavage step, Mβ is cleaved into an Mβ' fragment that is covalently associated with Mα to form the soluble Mα+Mβ' species and a C-terminal fragment (CTF) that contains the transmembrane and cytoplasmic domains and is eventually degraded in lysosomes via an ESCRT-dependent process (78).

The PMEL primary structure can be subdivided into several domains (see **Figure 2.1A**). The very N-terminus of PMEL contains a 23-amino-acid signal sequence (69,87) that targets the protein for translocation into the ER. Adjacent to the signal sequence is an N-terminal region (NTR) that is necessary for both the trafficking of PMEL to ILVs and for the formation of functional amyloid fibrils (74). Other than a homologous region in the GPNMB protein (88), the NTR has no identifiable conserved characteristics except for three N-linked glycosylation sites and three cysteine residues that might participate in disulfide bonds (see below). Also required for both PMEL trafficking and fibril formation, the polycytic kidney disease (PKD) domain has homology to a repeated β-sheet-rich domain of polycistin-1, a protein in which mutations lead to polycystic kidney disease. The last domain present in the Mα region of PMEL is the RPT domain, a highly glycosylated region of the protein containing 7-10 imperfect repeats of a 13-amino-acid sequence (71,89). The RPT domain is highly modified by O-linked sialylated glycans in the mature PMEL protein, and although conserved in nature and position, this domain is

not conserved in sequence across vertebrate evolution. A recombinant form of the RPT domain, produced in bacteria and lacking O-linked glycans, has been shown to produce amyloid structures when incubated at low pH for prolonged periods of time, but unlike physiological PMEL amyloid, these structures dissolve at neutral pH (90-93).

Proprotein convertase cleavage occurs in the TGN (73) and/or in endosomes (74) and is required for the formation of PMEL amyloid fibrils. If the cleavage site is mutated or proprotein converatase cleavage is inhibited using α_1-antitrypsin Portland (α_1-PDX), a furin-specific variant of α_1-antitrypsin, PMEL forms disordered electron-dense aggregates instead of the usual parallel arrays of amyloid visible by electron microscopy (82).

Within pigment cells, BACE2 cleavage releases Mα+Mβ' into the lumen of early endososomes/stage I melanosomes (80). Interestingly, BACE2 is a homolog of BACE1, the enzyme that cleaves and defines the N terminus of Aβ. However, BACE2 knockout mice are hypopigmented whereas BACE1 knockout mice are not (80), suggesting that only BACE2 functions in melanosome maturation. Indeed, when BACE2 was depleted by siRNA, the number of fibril-containing organelles decreased threefold and the number of organelles containing unstructured aggregates increased sixfold in thin sections examined by electron microscopy (80). By electron tomography, some small fibrils were visible in the BACE2-depleted cells; however, none of these fibrils were organized into the parallel sheets observed in control cells. Together, these data indicate that BACE2 cleavage is required for the efficient assembly of PMEL amyloid fibrils.

Summary

Regulatory mechanisms ensure that the conversion of PMEL from a non-amyloid to an amyloid form occurs in a manner beneficial to the organism. So far, we know that PMEL must be expressed and appropriately cleaved to rapidly assemble into amyloid fibrils on ILVs within pigment cells. However, it is not known how – or if – the KLD contributes to the regulation of PMEL amyloid formation. Therefore, in chapter 2 we examine the role of disulfide bonding, dimerization, and the KLD in regulating when and where PMEL is transformed into functional amyloid.

1.3 Stage III and stage IV melanosomes

Once PMEL has been appropriately cleaved and assembled into sheets of functional amyloid, the delivery of additional melanosomal cargo results in the maturation of these unpigmented stage II melanosomes to pigmented stage III and stage IV melanosomes (**Figure 1.2**). Both enzymes responsible for the synthesis of melanin and proteins that alter the environment of the melanosome to optimize enzymatic activity must be present to achieve full pigmentation. Defects in any of these proteins leads to hypopigmentation of the skin and eyes in a group of disorders collectively known as oculocutaneous albinism (94).

1.3.1 Melanosomal proteins associated with oculocutanous albinism

Oculocutaneous albinism type 1 (OCA1) is caused by mutations in tyrosinase (TYR), the rate-limiting enzyme in the synthesis of melanins (95). TYR is an integral membrane protein synthesized in the ER (96) with two copper binding sites (97). Copper is supplied to apo-tyrosinase by the copper transporter ATP7A, which pumps copper from the cytosol into the lumen of the TGN or endosomal compartments (98). Therefore, tyrosinase is transiently active when loaded with copper in the TGN but loses its copper cofactors prior to its arrival in stage III melanosomes. Therefore, a cohort of ATP7A must be delievered to melanosomes in melanocytes to resupply TYR with copper for full enzymatic activity (10). When ATP7A delivery is impaired, as it is in some forms of HPS, TYR is inactive and melanosome maturation is suspended at stage II.

Oculocutanous albinism type 2 (OCA2) is caused by mutations in the OCA2 protein (also known as pink-eyed dilution or P protein), a chloride-sensitive ion channel (13) that regulates melanosomal pH. The internal pH of a melanosome rises as the organelle matures (9). Endosomes, from which melanosomes are derived, generally have an internal pH between 5 and 6 (99). This low pH is important for proprotein convertase activity but may also facilitate PMEL fibril formation by destabilizing the protein and promoting conformational change (8). However, optimal TYR activity requires a pH of 6.8 (7,100). Therefore, the pH of melanosomes must increase for maximum pigment production.

Specialized transporters such as OCA2 neutralize the acidic pH of early stage melanosomes. In the absence of OCA2, melanosomes are hypopigmented. However, treatments that increase melanosomal pH restore pigmentation in OCA2-deficient

melanocytes (101). In addition, exogenous expression of OCA2 in non-pigment cells raises the pH of endosomes and lysosomes (13).

Oculocutaneous albinism type 3 (OCA3), also known as rufous oculocutaneous albinism, is caused by mutations in tyrosinase-related protein 1 (TYRP1), a protein that directly or indirectly facilitates the conversion of DHICA to eumelanin (102). Patients with OCA3 therefore have a higher ratio of pheomelanin to eumelanin, resulting in reddish skin and hair.

None of the proteins associated with oculocutanous albinism type 4, 5, 6, or 7 are very well characterized. Oculocutaneous albinism type 4 (OCA4) is caused by mutations in SLC45A2, a 12-transmembrane domain H^+-sucrose symporter (103). The exact gene associated with oculocutaneous albinism type 5 (OCA5) has yet to be identified (104). Oculocutaneous albinism type 6 (OCA6) is caused by mutations in SLC24A5 (11), a sodium/calcium exchanger that localizes to the TGN, and oculocutaneous albinism type 7 (OCA7) is caused by mutations in the uncharacterized orphan gene, C10orf11 (105). Given the phenotype of patients with these disorders, however, each one must contribute in some way to melanosome maturation or melanin biosynthesis.

1.3.2 Trafficking of melanosomal cargo

Melanosomes rely on specialized cellular machinery for the delivery of TYR and other melanosome-specific proteins. Proteins that traffic directly to mature melanosomes such as TYR, TYRP1, and OCA2 typically contain acidic dileucine-based motifs [D/E]XXXL[L/I] (14,106,107) that bind to AP-1 in the TGN and/or AP-3 in endosomes

(14,108-110). These adaptor proteins then direct TYR, TYRP1, and OCA2 into clathrin-coated vesicles for delivery to melanosomes in a process that requires the biogenesis of lysosome-related organelles complexes BLOC-1 and BLOC-2 (111-113).

However, some melanosomal proteins including dopachrome tautomerase (DCT) and SLC45A2 lack dileucine-based motifs. While the mechanisms regulating the transport of these two proteins have not been closely examined, both proteins have cytoplasmic tyrosine-based Yxxϕ sorting motifs and tyrosine-based motifs have been shown to bind the μ subunits of AP-1 and/or AP-3 (114). Therefore, in chapter 3, we test whether mutation of the critical tyrosine residue in the Yxxϕ sorting motif affects the steady-state localization of SLC45A2.

1.3.3 SLC45A2

Very little is known about the localization, trafficking, or function of SLC45A2. SLC45A2 expression in yeast resulted in proton-dependent sucrose uptake (103). However, one paper reported that the protein localizes to BLOC-1 trafficking intermediates (115), another suggested localization to early stage melanosomes (116), and yet another rudimentary study found co-localization of SLC45A2 with both early and late stage melanosomes (117). Likewise, one study suggested that SLC45A2 functions in trafficking TYR to melanosomes (118), while another implicated SLC45A2 in the regulation of melanosomal pH. (119). Therefore, in chapter 3, we thoroughly examine the localization of a functional HA-tagged variant of SLC45A2 and present preliminary data that suggest SLC45A2 facilitates sustained TYR activity by maintaining a neutral pH.

1.4 Dissertation Aims

Melanosomes are lysosome-related organelles with a unique complement of proteins specialized for the synthesis and storage of pigments. In early stage melanosomes, a fibrillar matrix is assembled in preparation for melanin biosynthesis. This matrix is comprised primarily of the functional amyloid protein PMEL, which must traverse the secretory pathway in a non-amyloid form prior to its polymerization into amyloid fibrils in stage I and stage II melanosomes. In stage III and stage IV melanosomes, transporters optimize conditions within the organelle for the production of melanins. One pigment cell-specific transporter, SLC45A2, is hypothesized to contribute to this process by trafficking to the melanosomal membrane and helping to regulate melanosomal pH; however, studies performed prior to the beginning of this thesis were at best suggestive of these findings. We thus pursued the following questions:

Question 1: What regulates the conversion of PMEL from a non-amyloid to an amyloid protein? The difference between functional amyloid and pathological amyloid may lie in regulatory mechanisms that prevent and/or encourage amyloid formation within the cell. However, our understanding of the molecular mechanisms that govern functional amyloid formation is far from complete. For instance, proprotein convertase and BACE2 cleavage are required for PMEL fibril formation since inhibition of either cleavage event results in disordered aggregates by electron microscopy; however, other factors must regulate the assembly of PMEL amyloid fibrils as proteolytically processed, secreted forms of PMEL are soluble.

We hypothesize that disulfide bonds promote a non-amyloid conformation of PMEL, thereby preventing unwanted fibril formation early in the secretory pathway. The formation and resolution of disulfide-stabilized PMEL species is discussed in chapter 2 where we show that dimerization may inhibit PMEL amyloid formation en route to melanosomes.

Question 2: How does SLC45A2 contribute to melanosome maturation? Mutations in human SLC45A2 result in oculocutaneous albinism type 4; therefore, it stands to reason that the protein is necessary for efficient melanin biosynthesis. In chapter 3, we determine the localization of a functional HA-tagged variant of SLC45A2 and show that the H^+-sucrose symporter requires a cytoplasmic tyrosine-based Yxxϕ sorting motif to traffic appropriately. We also discuss some preliminary data suggesting a requirement for SLC45A2 in maintaining a neutral environment during late stages of melanosomal maturation.

CHAPTER 2

Dimerization prevents PMEL functional amyloid formation in early secretory compartments

Tina Ho[1,2,3], Brenda Watt[1,2,3], Lynn A. Spruce[1], Steven H. Seeholzer[1], and Michael S. Marks[1,2,3,4]

[1]Department of Pathology and Laboratory Medicine, Children's Hospital of Philadelphia, Philadelphia, PA 19104

[2]Cell and Molecular Biology Graduate Group

[3]Department of Pathology and Laboratory Medicine, University of Pennsylvania, Philadelphia, PA 19104

[4]Department of Physiology, University of Pennsylvania, Philadelphia, PA 19104

The text and figures of this chapter have been submitted for publication in *The Journal of Biological Chemistry*.

ABSTRACT

The formation of functional amyloid must be carefully regulated to prevent the accumulation of potentially toxic products. Premelanosome protein (PMEL) forms non-toxic functional amyloid fibrils that assemble into sheets upon which melanins ultimately deposit within the melanosomes of pigment cells. PMEL is synthesized in the endoplasmic reticulum (ER) but forms amyloid only within post-Golgi melanosome precursors; thus, PMEL must traverse the secretory pathway in a non-amyloid form. Here, we identify a native disulfide-bonded PMEL dimer that impedes premature fibril formation early in the secretory pathway. Analyses by non-reducing SDS-PAGE, size exclusion chromatography, and sedimentation velocity revealed two native high M_r disulfide-bonded species that contain Golgi-modified forms of PMEL. These species correspond to disulfide bond-containing dimeric and monomeric PMEL isoforms that contain no other proteins as judged by 2D-PAGE of metabolically labeled/immunoprecipitated PMEL and by mass spectrometry of affinity-purified complexes. Metabolic pulse-chase analyses, small molecule inhibitor treatments, and evaluation of site-directed mutants suggest that the PMEL dimer forms around the time of ER exit and is resolved by disulfide bond rearrangement into a monomeric form within the late Golgi or in a post-Golgi compartment. Mutagenesis of individual cysteine residues within the non-amyloid cysteine-rich Kringle-like domain stabilizes the disulfide-bonded dimer and impairs functional amyloid fibril formation as determined by electron microscopy. Our data suggest that PMEL dimerization helps prevent premature fibril formation in early secretory compartments and that resolution of the dimer must occur prior to the assembly of functional amyloid fibrils.

INTRODUCTION

Amyloid is a "cross beta sheet" polymeric protein conformation in which beta strands are stacked perpendicularly to the long axis of the amyloid fibril (19). The amyloid fold is traditionally associated with pathological protein misfolding in neurodegenerative diseases such as Alzheimer and Parkinson diseases (120). However, the amyloid fold has also been exploited for diverse physiological processes in a wide range of organisms (41) including biofilm formation in bacteria (16), learning and memory in *Drosophila* (42), and programmed necrosis in mammals (17). Molecular mechanisms that limit the toxicity of such “functional amyloids” or their folding intermediates during synthesis are incompletely understood, but likely regulate when and where these proteins assemble into amyloid fibrils. For example, curli biofilm formation in *E. coli* is regulated by three proteins: CsgB, CsgC, and CsgF. CsgB is a minor curli subunit required to nucleate amyloid fibril formation *in vivo* (44). CsgC is a chaperone protein that prevents premature amyloid formation in the bacterial periplasm (46), and CsgF is an extracellular protein important for the attachment of curli fibers to the cell surface (45). However, much less is known about functional amyloid regulation in mammals where the formation of large, self-assembling, insoluble protein structures likely carries increased risk due to the multicellular nature and longer lifespan of higher organisms.

The best characterized mammalian functional amyloid protein is premelanosome protein (PMEL; also referred to as Pmel17, Silver, ME20, or gp100). Within immature melanosomes of pigment cells in the skin and eye, PMEL polymerizes into amyloid fibrils (18) that associate laterally into sheets upon which melanins deposit as they are

synthesized during melanosome maturation (reviewed in (6)). The amyloid sheets are critical determinants of the ellipsoid melanosome shape (63,77), which has been shown to be required for proper melanosome motility into the apical processes of retinal pigment epithelial cells (121). The amyloid sheets have also been proposed to accelerate melanin polymerization (18,122,123), and organisms that lack PMEL or carry mutations in the PMEL gene are characterized by various degrees of hypopigmentation (63,124-128). Because PMEL is synthesized in the endoplasmic reticulum (ER) as a type I transmembrane protein (68-70) but only initiates amyloid fibril formation within the lumen of endosomal membrane compartments (60,64,129), PMEL must navigate the secretory pathway from the ER to endosomes in a non-amyloid form. It is thus an excellent model system in which to dissect the regulation of amyloid formation within the endomembrane system.

Our current understanding of the processes involved in PMEL biosynthesis and amyloidogenesis is as follows. Following synthesis and addition of four core N-linked glycans within the ER (generating a "P1" precursor form), PMEL is exported to the Golgi where it is extensively modified by *O*-glycosylation (71,72) and maturation of the N-linked glycans to the complex type (64). This generates a full-length "P2" form that is subsequently cleaved by a proprotein convertase into two disulfide-linked fragments, Mα and Mβ (82), either in the trans Golgi network (73) or within endosomes (74) (see **Figure 2.1A**). A subsequent proteolytic cleavage by BACE2 within endosomes (80) or by an ADAM protease at the plasma membrane (76) cleaves Mβ into two fragments; the C-terminal fragment (CTF) contains the transmembrane domain and is eventually degraded in a γ-secretase-dependent manner in lysosomes (78), while the other fragment (Mβ') is

liberated from the membrane covalently bound to Mα (80,84). No longer anchored to the membrane, most of the Mα undergoes additional proteolytic processing events prior to forming the parallel arrays of functional amyloid fibrils characteristic of early stage melanosomes (60,72,130). A small fraction of Mα may also be secreted (64,84) or directly incorporated into growing fibrils without further processing (82,86). Proprotein convertase and BACE2 cleavage are necessary for functional amyloid fibril formation since interference with either of these two proteolytic processing events results in the formation of disordered PMEL aggregates instead of ordered fibrils (80,82). However, these cleavage events are not sufficient to induce fibril formation since a fraction of cleaved PMEL is secreted from cells in culture (64,84,85) in a non-amyloid form (unpublished results). Therefore, additional regulatory mechanisms must govern PMEL fibril formation.

Regulated disulfide bond rearrangements have the potential to affect both protein conformation and protein function. For example, interaction of the β-barrel protein LptD with the LptE subunit of the LPS translocon in the *E. coli* outer membrane triggers a disulfide bond rearrangement within LptD that activates the translocon (131). PMEL has 13 cysteine residues (black circles, **Figure 2.1A**), of which 11 are exposed to the lumen of the endomembrane system and thus might participate in disulfide bonds. Indeed, the existence of intermolecular disulfide bonds can be inferred from experiments showing that P2 and non-fibrillar Mα and Mβ fragments are incorporated into higher order oligomers when samples are analyzed by non-reducing SDS-PAGE (64). Here we show that disulfide bonds maintain PMEL in a tethered oligomeric form that is incompatible with amyloidogenesis. Our data suggest that generation and destruction of a disulfide-

stabilized dimer contributes an additional layer of regulation to the timing of PMEL amyloid formation.

RESULTS

p250 and p160 are disulfide-bonded species composed of Golgi-modified PMEL

The Golgi-matured P2 form of PMEL and the products of proprotein convertase cleavage, Mα and Mβ (**Figure 2.1A**), migrate with M_r of approximately 120,000, 100,000, and 28,000, respectively, when analyzed by reducing SDS-PAGE (64,130). However, when analyzed by non-reducing SDS-PAGE, most detergent-soluble forms of Golgi-matured PMEL migrate with a higher M_r (64), indicating that the vast majority of pre-amyloid P2, Mα, and Mβ isoforms exist as components of disulfide-bonded species. To further investigate the nature of these species, immunoblots were performed using antibodies that can distinguish between immature and mature PMEL isoforms. MNT-1 human melanoma cells (which endogenously express PMEL) or transfected HeLa cells transiently expressing full-length PMEL (isoform 1) were treated with NEM prior to and during lysis in TritonX-100 to prevent the formation of artifactual disulfide bonds. Detergent-soluble lysates were then fractionated by SDS-PAGE on low percentage polyacrylamide gels under non-reducing (NR) or reducing (R) conditions and analyzed by immunoblotting using the antibodies HMB45, αPMEL-I, αPMEL-N, or αPMEL-C. The HMB45 monoclonal antibody recognizes the *O*-glycosylated RPT region of mature PMEL isoforms present only in post-Golgi compartments (72,132). The αPMEL-I antibody recognizes the same domain in its non-glycosylated form as is characteristic of

Figure 2.1

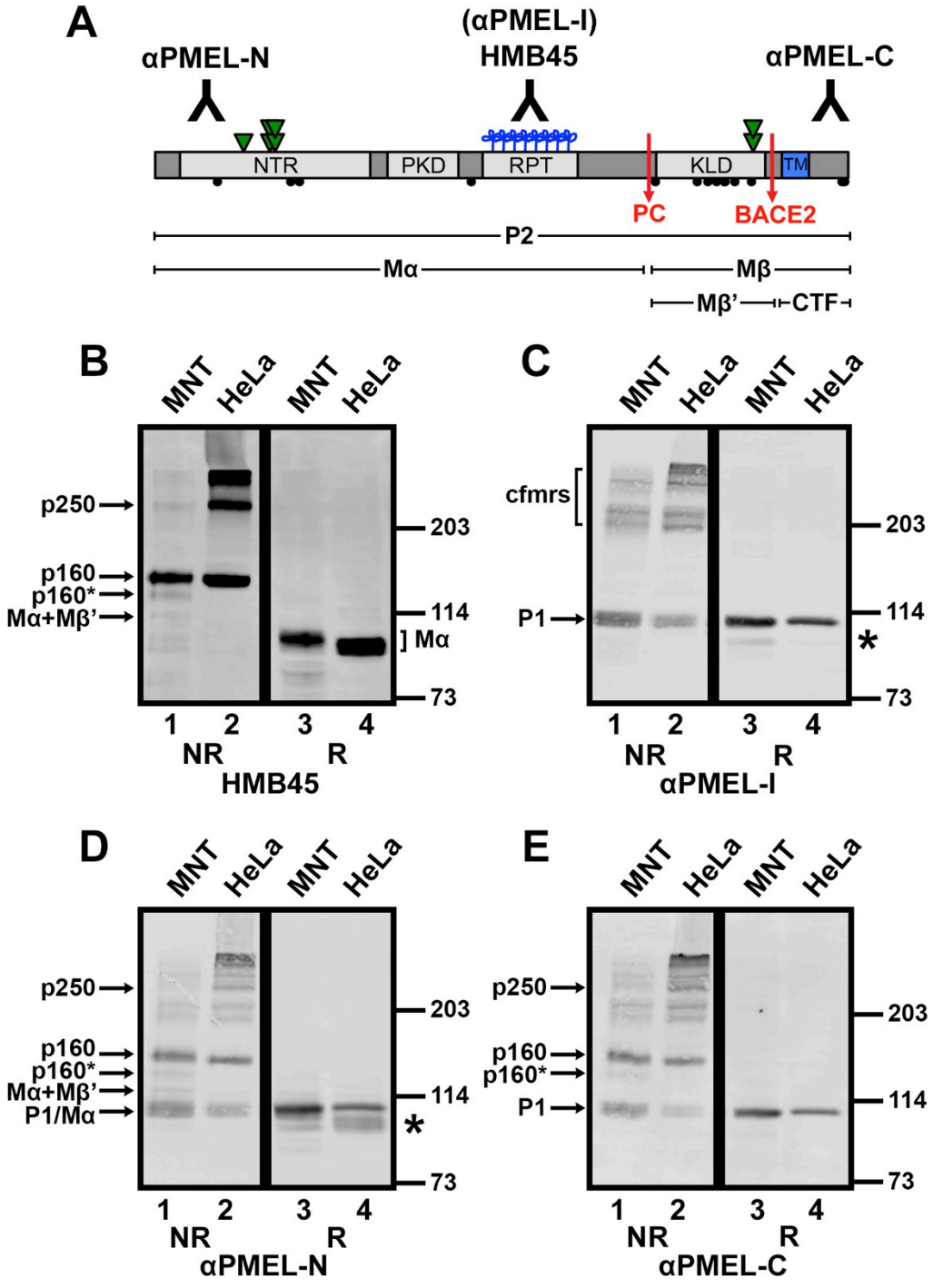
A
αPMEL-N
(αPMEL-I)
HMB45
αPMEL-C
NTR
PKD
RPT
KLD
TM
PC
BACE2
P2
Mα
Mβ
Mβ'
CTF
B
MNT
HeLa
MNT
HeLa
p250
p160
p160*
Mα+Mβ'
203
114
] Mα
73
1 2 3 4
NR R
HMB45
C
MNT
HeLa
MNT
HeLa
cfmrs
P1
203
114
*
73
1 2 3 4
NR R
αPMEL-I
D
MNT
HeLa
MNT
HeLa
p250
p160
p160*
Mα+Mβ'
P1/Mα
203
114
*
73
1 2 3 4
NR R
αPMEL-N
E
MNT
HeLa
MNT
HeLa
p250
p160
p160*
P1
203
114
73
1 2 3 4
NR R
αPMEL-C

Golgi-matured PMEL exists predominantly in high M_r disulfide-bonded species. (A) Schematic diagram of the mature PMEL primary structure showing the sites of antibody recognition for αPMEL-N, αPMEL-I, HMB45, and αPMEL-C (note that αPMEL-I recognizes only the immature form of PMEL lacking O-glycans), cleavage sites for a proprotein convertase (PC) and BACE2, and resulting cleavage fragments Mα, Mβ, Mβ', and C-terminal fragment (CTF). Also noted are the domain structure, N-linked glycosylation sites (green triangles; double triangles indicate sites that are modified to the complex type in the Golgi), O-linked glycosylation sites (blue clovers), and cysteine residues (black circles). The N-terminal region (NTR), a region with homology to a repeated domain in polycystin 1 (PKD), a highly glycosylated repeat (RPT) domain, and the Kringle-like Domain (KLD) are indicated in light gray, and the transmembrane domain (TM) is indicated in blue. (B-E) MNT-1 melanoma cells (MNT, lanes 1 and 3) or transiently transfected HeLa cells (HeLa, lanes 2 and 4) expressing wild-type PMEL were lysed in buffer containing 1% (w/v) Triton X-100, and the soluble material was fractionated by SDS-PAGE under non-reducing (NR) or reducing (R) conditions. Proteins transferred to membranes were then probed with the PMEL antibodies HMB45 (B), αPMEL-I (C), αPMEL-N (D), or αPMEL-C (E). The migration of molecular weight standards is indicated to the right of each blot. Bands corresponding to p250, p160, p160*, Mα+Mβ', Mα, immature PMEL conformers (cfmrs), and P1 are indicated by arrows; note that Mα and P1 comigrate in MNT-1 cells. *, an alternatively spliced PMEL product (PMEL-ss). Lane numbers are indicated at bottom.

immature PMEL isoforms located in the ER (133). The αPMEL-N and αPMEL-C antibodies recognize the N-terminus and C-terminus of PMEL, respectively, regardless of maturation status (64,133).

Under non-reducing conditions, HMB45 detected two major species that migrate with M_r of approximately 160,000 (p160) and 250,000 (p250). Also detected were larger PMEL species retained at the boundary between the stacking and separating gel and minor amounts of p160*, Mα+Mβ', and free Mα (**Figure 2.1B**, lanes 1-2). The p160* species is a slightly faster migrating version of p160 resulting from an alternatively spliced PMEL variant expressed in melanocytic cells but not transfected HeLa cells (133). The Mα+Mβ' species is composed of Mα covalently bound to Mβ' based on the following: (i) its detection by the HMB45 and αPMEL-N antibodies but not the αPMEL-C antibody, indicating that it lacks the PMEL C-terminus; (ii) its comigration with the major form of secreted PMEL (see **Figure 2.5A**), which consists predominantly of disulfide-bonded Mα+Mβ' complexes (84); and (iii) its depletion following inhibition of BACE2 (see **Figure 2.7A**), the enzyme that cleaves Mβ into CTF and Mβ' fragments. Since only a single band corresponding to Mα is observed under reducing conditions (**Figure 2.1B**, lanes 3-4; note that Mα migrates with a higher M_r when derived from MNT-1 cells than when derived from HeLa cells due to differences in terminal glycosylation (64)), disulfide bonds must be necessary to maintain the integrity of p250 and p160 as well as that of p160* and Mα+Mβ'.

The p250 and p160 bands were not labeled by αPMEL-I under non-reducing conditions; instead, this antibody detected a band that corresponds to monomeric P1 as well as a

series of high M_r bands ranging from approximately 220,000 to the top of the separating gel (**Figure 2.1C**, lanes 1-2). Since the high M_r bands collapse into P1 under reducing conditions (**Figure 2.1C**, lanes 3-4; note that the slightly faster migrating band * corresponds to the P1 form of the alternatively spliced PMEL variant, PMEL-ss (133)), these species most likely represent partially folded disulfide-bonded conformers of PMEL in the ER (cfmrs, **Figure 2.1C**). The αPMEL-N and αPMEL-C antibodies recognized p250 and p160 as well as the immature PMEL conformers detected by αPMEL-I, indicating that all of these high M_r species contain either full-length PMEL or Mα disulfide-bonded to Mβ (**Figure 2.1D, E**). Therefore, only Golgi-matured forms of full-length or proprotein convertase-cleaved PMEL are present in p250 and p160. Furthermore, the presence of p250 and p160 both in MNT-1 cells that endogenously express PMEL and in non-pigment HeLa cells expressing a PMEL transgene suggests that no additional pigment cell-specific proteins are required for the formation of mature disulfide-bonded PMEL species.

p250 and p160 represent distinct physiological complexes

To test whether the disulfide-bonded p250 and p160 species observed by non-reducing SDS-PAGE correspond to physiological PMEL-containing complexes, we assessed the biophysical properties of p250 and p160 under non-denaturing conditions. First, we examined the PMEL species by sedimentation velocity analysis. Lysates of MNT-1 cells were prepared using *n*-octylglucoside, a non-ionic detergent with a small micelle size and a relatively high partial specific volume (134). After fractionation through sucrose

gradients containing *n*-octylglucoside, mature PMEL species were identified by immunoblot analysis of gradient fractions separated by non-reducing SDS-PAGE (**Figure 2.2A**). Sedimentation coefficients were then calculated by comparing the peak position of mature PMEL species, detected using the HMB45 antibody, with the peak position of globular protein standards (**Figure 2.2B, C**). Distinct sedimentation coefficients were calculated for p250, p160, Mα+Mβ', and "free" Mα. Consistent with the relative order of their migration by non-reducing SDS-PAGE, p250 had the highest calculated *s* value followed by p160, Mα+Mβ', and lastly free Mα. This suggests that p250 and p160 are not artifacts of non-reducing SDS-PAGE but distinct native disulfide-bonded PMEL complexes. The sedimentation coefficients of all four PMEL species were substantially smaller than expected given the magnitude of their migration by non-reducing SDS-PAGE (**Table 2.1**), suggesting that these species might have extended glycoprotein structures.

To further characterize the PMEL species under native conditions, MNT-1 cell lysates were fractionated by size exclusion chromatography in *n*-octylglucoside. Aliquots of each fraction were separated by non-reducing SDS-PAGE, and mature PMEL species were detected by immunoblotting with HMB45. As observed in the sedimentation analyses, the four PMEL species – p250, p160, Mα+Mβ' and Mα – migrated with distinct elution volumes by size exclusion chromatography (**Figure 2.3A, B**). However, when the peak elution volume of each species was compared with that of globular protein standards, the mature PMEL species had peak elution volumes much smaller – and therefore Stokes radii much larger – than expected for globular proteins of similar molecular weight (**Figure 2.3C, Table 2.1**). For example, the Stokes radius of p250 (10.4 nm) was

Figure 2.2

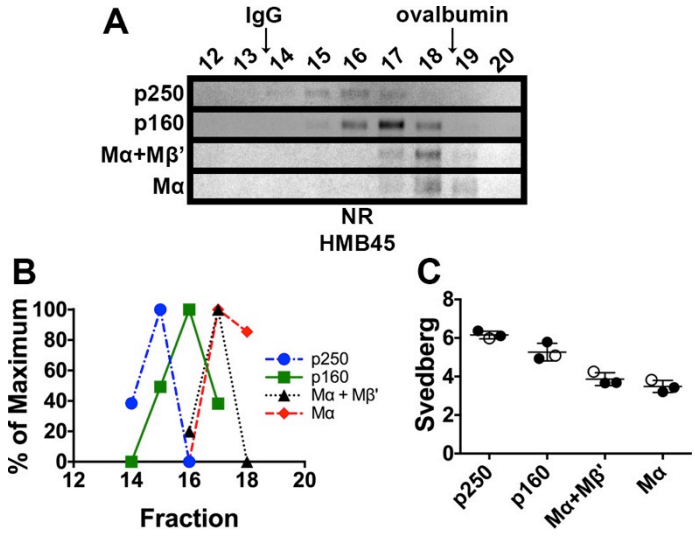

p250, p160, and Mα monomers have distinct sedimentation properties. MNT-1 cell lysates prepared using 250 mM *n*-octylglucoside were subject to sedimentation velocity analyses in 5-20% sucrose gradients. (A) Aliquots of the gradient fractions were analyzed by non-reducing (NR) SDS-PAGE and immunoblotted using HMB45. Shown are regions of the immunoblots corresponding to p250, p160, Mα+Mβ', and Mα as indicated to the left. Fraction numbers are indicated above each lane (bottom of the gradient is to the left; top of the gradient is to the right), and the migration of globular protein standards IgG and ovalbumin are indicated with arrows at top. Immunoblot contrast was optimally adjusted for each individual species. (B) HMB45 immunoreactivity was quantified to determine the peak elution fraction for p250, p160, Mα+Mβ', and Mα. The lowest value quantified for each species was set to 0% and the highest value was set to 100%. (C)

Svedberg values were calculated for each species by comparison of peak fractions with those of protein standards with known *s* values in three independent experiments. Circles, values calculated from each experiment; open circles, values calculated from the experiment shown in panels A and B; horizontal lines, mean value; error bars, standard deviation. Mean and standard deviation are also shown in Table 2.1.

Figure 2.3

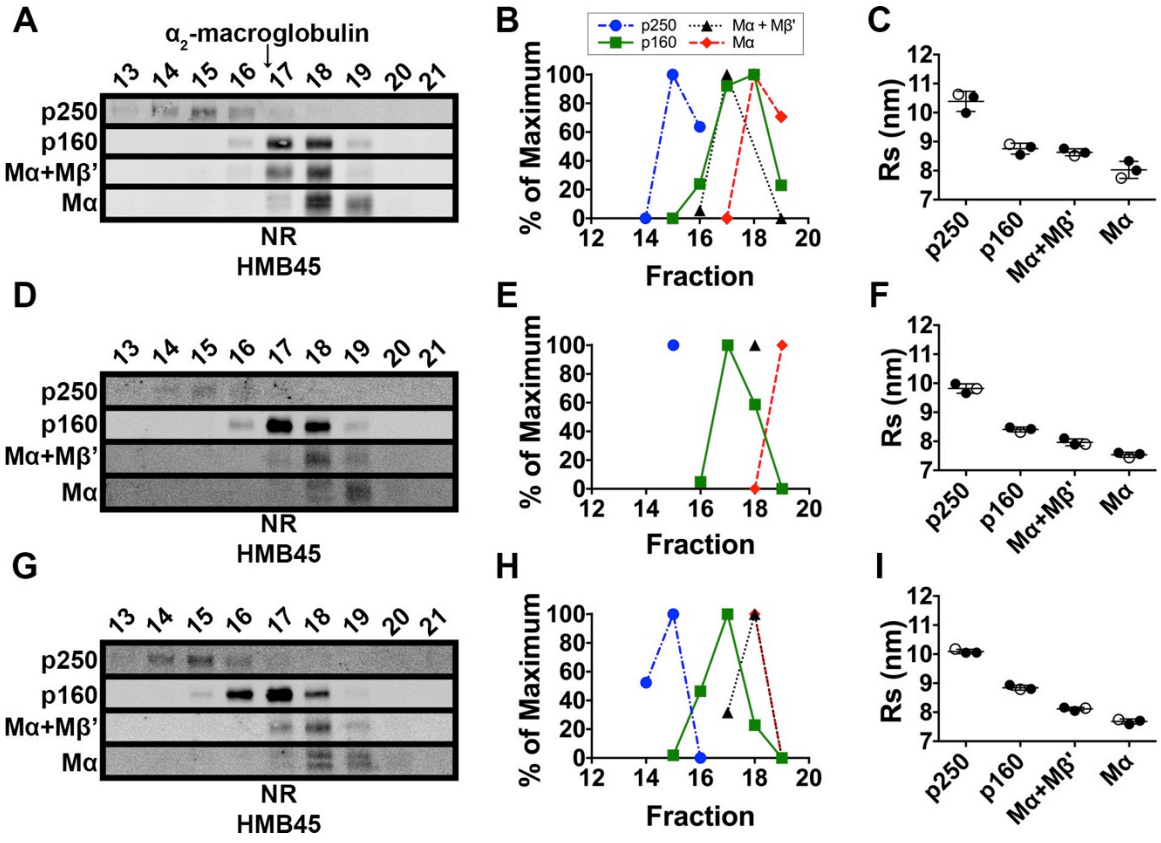

p250, p160, and Mα monomers have distinct Stokes' radii that are minimally altered by solubilization in detergents with different micelle sizes. MNT-1 cells were lysed using *n*-octylglucoside (A-C), dodecyl-β-D-maltoside (D-F), or Triton X-100 (G-I), and the detergent extracts fractionated by size exclusion chromatography in the corresponding detergent. (A, D, G) Eluted fractions were analyzed by SDS-PAGE under non-reducing (NR) conditions and immunoblotted using the HMB45 antibody. Shown are regions of the immunoblots corresponding to p250, p160, Mα+Mβ', and Mα as

indicated to the left. Fraction numbers are indicated above each lane, and the migration of α_2-macroglobulin indicated with an arrow. Immunoblot contrast was optimally adjusted for each individual species in each experiment. (B, E, H) HMB45 immunoreactivity was quantified to determine the elution volume of p250, p160, Mα+Mβ', and Mα. The lowest value quantified for each species was set to 0% and the highest value was set to 100%. (C, F, I) The Stokes radius of each species was then calculated by comparing the peak elution fraction of that species with those of globular protein standards in three independent experiments. Circles, values calculated from each experiment; open circles, values calculated from the experiments shown in panels A, D, and G; horizontal lines, mean value; error bars, standard deviation. Mean and standard deviation are also shown in Table 2.1.

Table 2.1

Species	$s_{20,w}$ (S)	Stokes radius (nm)		
		***n*-octylglucoside**	**dodecyl-β-D-maltoside**	**Triton X-100**
p250	6.15 +/- 0.20	10.38 +/- 0.34	9.82 +/- 0.16	10.09 +/- 0.07
p160	5.27 +/- 0.46	8.76 +/- 0.19	8.41 +/- 0.08	8.84 +/- 0.08
Mα+Mβ'	3.86 +/- 0.33	8.63 +/- 0.12	7.96 +/- 0.12	8.12 +/- 0.06
Mα	3.49 +/- 0.31	8.03 +/- 0.29	7.54 +/- 0.09	7.68 +/- 0.08

Summary of calculated sedimentation coefficients and Stokes radii.

calculated to be larger than that of α_2-macroglobulin (8.8 nm), a 720-kDa tetrameric protein (135). To test whether the exceptionally large Stokes radii reflected association with multiple detergent micelles, cell lysates were prepared and analyzed by size exclusion chromatography using detergents with different micelle sizes: *n*-octylglucoside (average micelle size of 8 kDa (136)), dodecyl-β-D-maltoside (average micelle size of 50-76 kDa (136)) or Triton X-100 (average micelle size of 81 kDa (137)). If any of the PMEL species had been associated with multiple detergent micelles, those species would have eluted with distinct volumes in each of the three detergents. However, the elution volume of each PMEL species was roughly similar in all three detergents (**Figure 2.3, Table 2.1**), suggesting that detergent micelles do not contribute substantially to the large Stokes radii of the mature PMEL species. Therefore, the unusually high Stokes radii and low sedimentation coefficients of p250, p160, Mα, and Mα+Mβ' most likely reflect extended glycoprotein conformations resulting from the heavily glycosylated RPT domain of mature PMEL.

PMEL is the sole component of both p250 and p160

To determine whether p250 and p160 contain additional polypeptides besides PMEL, we analyzed the contents of PMEL immunoprecipitates by 2-dimensional non-reducing/reducing SDS-PAGE (2D-PAGE). We used transfected HeLa cells transiently expressing wild-type PMEL in this experiment because Mα is more clearly identified in HeLa cell lysates analyzed by reducing SDS-PAGE. This is because, unlike melanocytic cells, transfected HeLa cells typically do not express the alternatively spliced form of

PMEL (PMEL-ss) that comigrates with Mα by reducing SDS-PAGE (see **Figure 2.1B-D**). In addition, Mα comigrates with P1 in MNT-1 cells but not in transfected HeLa cells as a result of differences in terminal glycosylation. After extensively labeling biosynthesized proteins with ^{35}S-methionine/cysteine, PMEL species in detergent cell lysates were immunoprecipitated using αPMEL-N, αPMEL-C, or NKI-beteb (138) – a monoclonal antibody to the PKD domain (72) – and then fractionated by 2D-PAGE and analyzed by Phosphorimaging. Using this technique, the higher M_r bands observed by standard SDS-PAGE (**Figure 2.1**) were resolved into their individual components. Similar results were obtained using all three PMEL antibodies (**Figure 2.4**). Spots corresponding to the core-glycosylated P1 and the Golgi-modified P2 forms of PMEL were identified close to the diagonal and thus represent monomeric forms of these PMEL species. The p160 band typically observed by 1-D non-reducing SDS-PAGE resolved into two species by 2D-PAGE, one of which contained the Mα and Mβ products of proprotein convertase cleavage and the other of which contained uncleaved, full-length, Golgi-modified P2. The p250 band also resolved into both cleaved and uncleaved forms of Golgi-modified PMEL. A number of other bands present in the non-reducing dimension resolved into P1 under reducing conditions and thus most likely represent disulfide-bonded ER folding intermediates. Importantly, no other radiolabeled polypeptide was reproducibly detected within the p250 band or the p160 band. Furthermore, three independent attempts to identify additional components by tandem mass spectrometry analysis of affinity purified PMEL from MNT-1 cells yielded no reasonable candidates other than chaperones and protein disulfide isomerases that were present in vastly substoichiometric amounts (**Table 2.2 and Supplemental Table S1**)

Figure 2.4

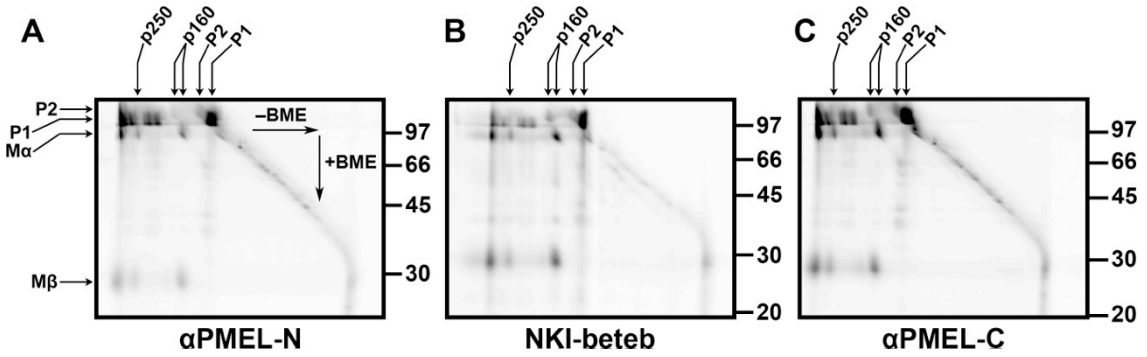

p250 and p160 are comprised of Golgi-matured P2 and Mα/Mβ fragments of PMEL. Transiently transfected HeLa cells expressing wild-type PMEL were metabolically labeled for 2 h with ^{35}S-methionine/cysteine, immunoprecipitated using αPMEL-N (A), NKI-beteb (B), or αPMEL-C (C), and analyzed by 2D-PAGE under non-reducing conditions in the first dimension (left to right; -BME) and reducing conditions in the second dimension (top to bottom; +BME). The migrations of p250, p160, P2, and P1 in the first dimension are indicated by arrows at the top; the migration of molecular weight standards in the second dimension is indicated to the right of each blot; and the positions of P2, P1, Mα and Mβ in the second dimension are indicated to the left.

Table 2.2

Summed Intensity	Protein	MW (kDa)
10,459,000,000	PMEL	120
9,310,000,000	Trypsin (*Sus scrofa*)	24
3,643,900,000	AspN (*Pseudomonas fragi*)	16
2,444,500,000	Clathrin heavy chain 1	188
1,113,200,000	Mucin-19	357
1,060,400,000	Keratin, type I cytoskeletal 13	50
1,052,500,000	UDP-glucose:glycoprotein glucosyltransferase 1	175
908,870,000	Keratin, type II cytoskeletal 1	66
720,070,000	Trypsin	15
477,000,000	Keratin, type I cytoskeletal 10	59
431,880,000	Keratin, type II cytoskeletal 6A	60
352,060,000	Keratin, type II cytoskeletal 4	57
351,310,000	Keratin, type II cytoskeletal 2 epidermal	65
350,080,000	Methionine synthase	135
292,260,000	Solute carrier family 12 member 7	119
264,970,000	Filamin-A	280
248,250,000	Protein disulfide-isomerase A3	57
194,490,000	Myosin-9	227
161,510,000	Keratin, type I cytoskeletal 9	62
152,110,000	Endoplasmic reticulum resident protein 44	47
125,550,000	Kappa-casein (*Bos taurus*)	21
120,610,000	Ubiquitin	10
117,270,000	Unconventional myosin-Ic	118
113,980,000	Unconventional myosin-Id	116
112,810,000	Fatty acid synthase	273
105,730,000	Keratin, type I cytoskeletal 19	44
100,700,000	Vinculin	117
100,210,000	Protein disulfide isomerase A4	73
97,113,000	Transferrin receptor protein 1	85
86,599,000	4F2 cell-surface antigen heavy chain	65
70,376,000	78 kDa glucose-regulated protein (BiP)	72
67,557,000	Protein disulfide isomerase A6	48
65,533,000	Myosin-10	231
64,584,000	Ras GTPase-activating-like protein IQGAP1	189
64,038,000	Protein S100-A9	13

61,131,000	Protein disulfide isomerase	57
60,047,000	Alpha-synuclein	14
54,174,000	Exportin-1	123
54,029,000	Small proline-rich protein 3	17
44,466,000	Keratin, type II cytoskeletal 5	62
43,245,000	Actin	42
42,124,000	Protein S100-A8	11
40,829,000	Heat shock protein beta-1	23
39,343,000	Tetraspanin-10	36
36,125,000	Solute carrier family 12 member 4	119
34,172,000	Annexin A1	39
32,707,000	Transcription elongation factor SPT5	121
32,563,000	Transmembrane protein 65	25
31,993,000	Filamin-B	276
31,932,000	Talin-1	270

Analysis of p250 and p160 by LC-MS/MS. Affinity-purified PMEL was fractioned on a non-reducing SDS-PAGE gel, relevant bands excised and digested using trypsin or AspN, and the samples analyzed by mass spectrometry. This table is a brief summary of the top 50 “hits” obtained. Summed intensity refers to the sum of the eXtracted ion currents from three independent experiments analyzing higher Mr disulfide-bonded PMEL species. The proteins listed are of human origin unless otherwise noted. A more detailed table with the results of each band analyzed in each of the three experiments is provided in the supplemental Microsoft Excel file.

and only associated with immature forms of PMEL (unpublished data). Other identified peptides derived from either common contaminants, such as keratins, and/or from proteins with molecular weights that were inconsistent with that of p250 and p160, or were very poorly recovered relative to PMEL-derived peptides. We therefore conclude that p250 and p160 are comprised exclusively of PMEL or PMEL fragments.

When considered together with the results from non-reducing SDS-PAGE, size exclusion chromatography, and velocity sedimentation analyses, the simplest interpretation of our data is that p250 represents a PMEL dimer and p160 represents a disulfide-dependent conformation of a single PMEL monomer or Mα/Mβ complex.

p250 and p160 are intermediates of PMEL fibril formation

The reactivity of p250 and p160 with HMB45 but not with αPMEL-I suggests that these two species are primarily present in post-ER compartments. In order to define the kinetics of their formation, we performed a metabolic pulse/chase and immunoprecipitation analysis. MNT-1 cells were metabolically labeled for 15 min with ^{35}S-methionine/cysteine and then chased in medium containing excess unlabeled amino acids for 0-120 min. PMEL isoforms in detergent-soluble cell lysates and the culture medium from each time point were immunoprecipitated using NKI-beteb and analyzed by non-reducing or reducing SDS-PAGE. At the pulse, the primary PMEL species detected under non-reducing conditions was monomeric P1, which migrated with a M_r of approximately 110,000 (**Figure 2.5A**, lane 1). The p250 band first appeared after 5 min of chase and peaked at 30 min (**Figure 2.5A**, lanes 2-4). This resembles the kinetics of P2

Figure 2.5

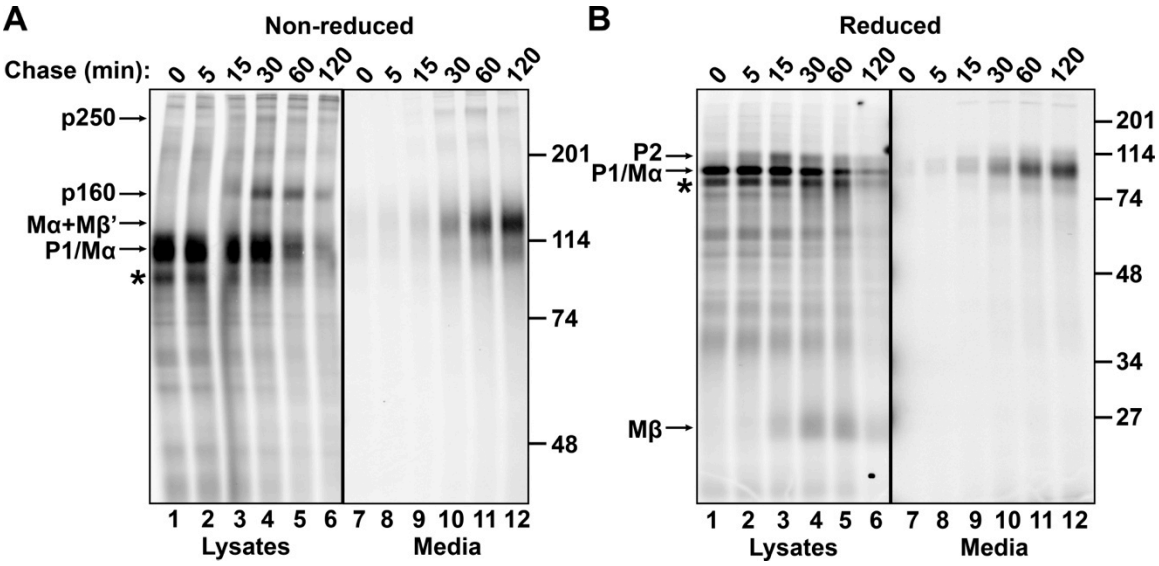

p250 and p160 are transient PMEL intermediates present only in cell lysates. MNT-1 cells were metabolically labeled with ^{35}S-methionine/cysteine for 15 min and chased for the times indicated (min). PMEL in detergent cell lysates or culture media, as indicated, was then immunoprecipitated using NKI-beteb and fractionated by SDS-PAGE under non-reducing (A) or reducing (B) conditions. The migration of molecular weight standards is shown to the right of each gel. Bands corresponding to p250, p160, Mα+Mβ', P1, and Mα on the non-reducing gel and P2, P1, Mα, and Mβ on the reducing gel are indicated by arrows; note that P1 and Mα largely comigrate. *, product of alternatively spliced PMEL mRNA (PMEL-ss). Lane numbers are indicated at bottom.

formation/accumulation, as observed under reducing conditions (**Figure 2.5B**, lanes 1-6), suggesting that dimer formation occurs just prior to ER exit or in the early Golgi. The p160 band was first observed after 15 min of chase and peaked at 30-60 min (**Figure 2.5A**, lanes 3-5). This resembles the kinetics of proprotein convertase cleavage, as indicated by the appearance of the Mβ cleavage product observed under reducing conditions (**Figure 2.5B,** lanes 1-6). Essentially similar results were obtained upon pulse/chase analysis of PMEL expressed in transiently transfected HeLa cells (**Figure 2.6**). Thus, p160 is likely generated in the TGN or in a post-Golgi compartment. Importantly, at no point did monomeric forms of P2 or Mα appear in cell lysates analyzed under non-reducing conditions. This indicates that the vast majority of post-ER/prefibrillar PMEL must be present in disulfide bond-dependent intermediates.

As previously observed (64,70,84,138), a small fraction of PMEL was secreted into the medium of MNT-1 cells starting at 30 min of chase and peaking at 120 min (**Figure 2.5A**, **B**, lanes 7-12). Completely consistent with those reports (84), PMEL secreted in this manner was comprised primarily of Mα+Mβ' with lesser amounts of free Mα.

To verify band identity and to probe for potential precursor-product relationships, MNT-1 cells were treated with small molecule inhibitors of trafficking and processing steps. Detergent-soluble lysates were then analyzed by non-reducing SDS-PAGE and immunoblotted with HMB45 or αPMEL-C. Treatment of MNT-1 cells with monensin, an inhibitor of intra-Golgi transport (139), led to the accumulation of p250 and higher M_r oligomers as well as the concomitant depletion of p160 (**Figure 2.7A, B**, lane 2). This supports the conclusions that p250 forms during ER exit or in the early Golgi and that

Figure 2.6

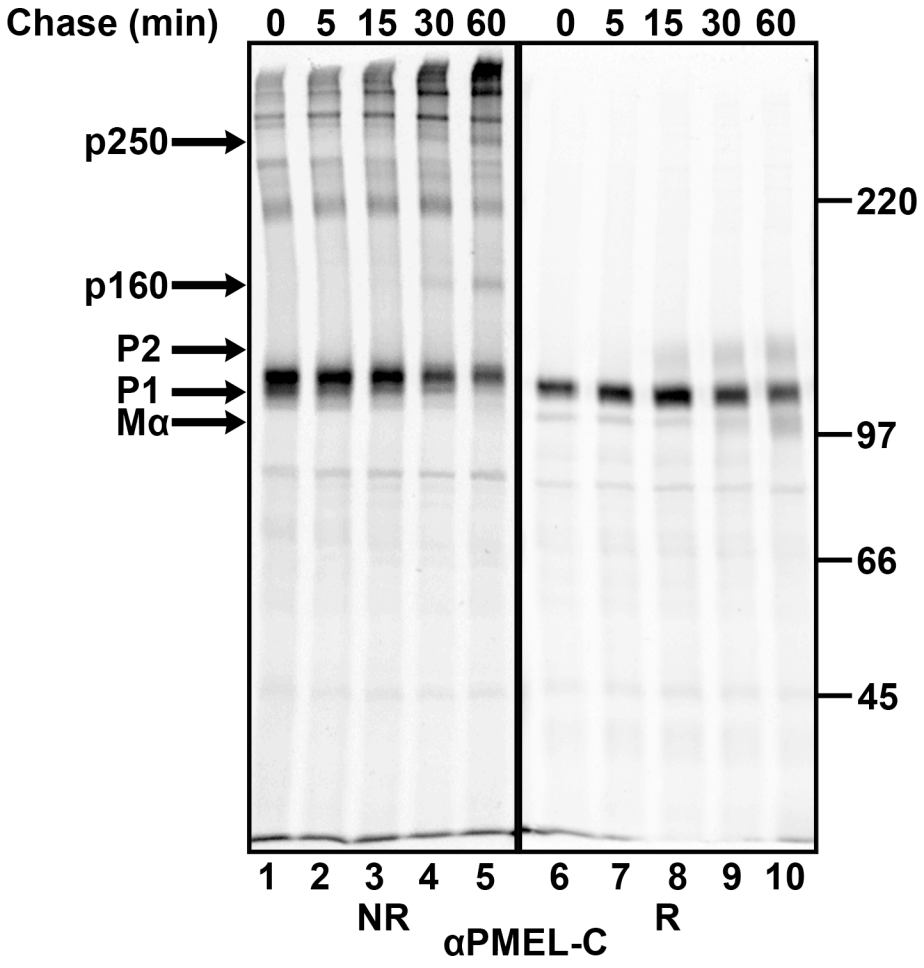

The kinetics of p250 and p160 formation in PMEL-expressing HeLa cells resembles that of MNT-1 cells. Transiently transfected HeLa cells expressing wild-type PMEL (long form) were metabolically pulse labeled with ^{35}S-methionine/cysteine for 10 min and chased for the indicated amounts of time. Cell lysates prepared using Triton X-100 were then immunoprecipitated using αPMEL-C and fractionated by SDS-PAGE under non-reducing (lanes 1-5) or reducing (lanes 6-10) conditions. The migration of molecular

weight standards is shown to the right. Bands corresponding to p250, p160, and P1 on the non-reducing gel and P2, P1, and Mα on the reducing gel are indicated to the left. Lane numbers are indicated across the bottom.

Figure 2.7

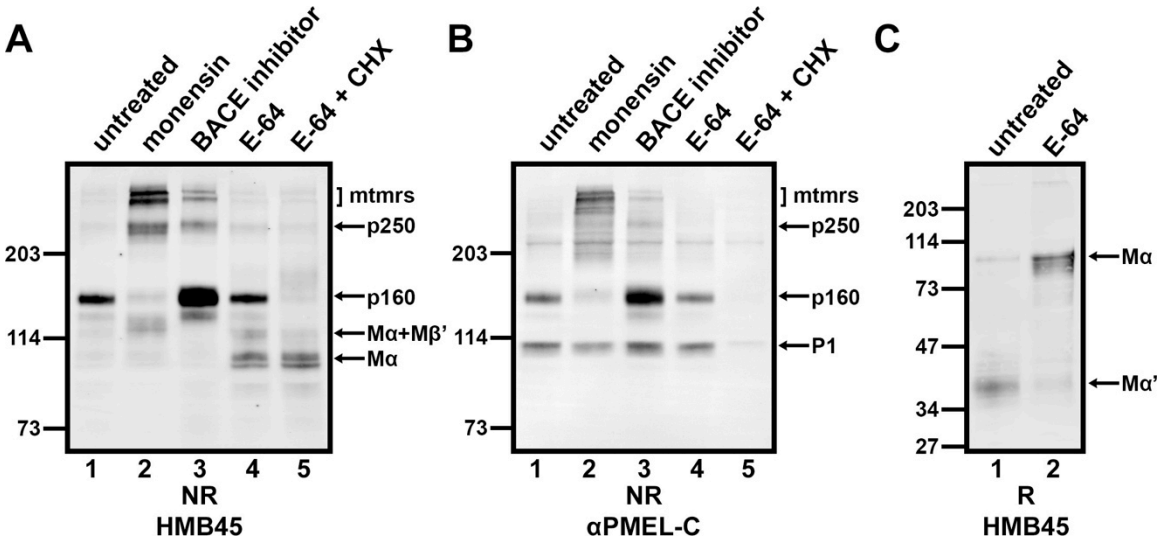

Potential precursor/procuct relationships among p250, p160, and Mα monomers. (A, B) MNT-1 cells were untreated (lane 1) or treated for 3 h with 10 μM monensin (lane 2), 100 μM β-secretase inhibitor IV (lane 3), or 1 mg/mL E-64 (lanes 4 and 5). Cells treated with E-64 were then either immediately harvested (lane 4) or additionally treated with 10 μg/mL cycloheximide in the presence of E-64 for 2 h (lane 5). After lysis in Triton X-100, detergent-soluble cell lysates were analyzed by non-reducing (NR) SDS-PAGE followed by immunoblotting with HMB45 (A) or αPMEL-C (B). (C) MNT-1 cells that were untreated (lane 1) or treated for 2 d with 1 mg/mL E-64 (lane 2) were lysed in Triton X-100, and detergent-insoluble cell lysates were analyzed by reducing (R) SDS-PAGE followed by immunoblotting with HMB45. The migration of molecular weight standards is indicated to the left of each blot, and bands corresponding to p250, p160,

Mα+Mβ', Mα, P1, Mα' fragments, and higher M_r multimers (mtmrs) are indicated with arrows.

p160 forms in the TGN or later. It also suggests that p250 might be the precursor of p160. Treatment with β-secretase inhibitor IV at concentrations that inhibit BACE2 cleavage (140) resulted in the substantial accumulation of p160 and the minor accumulation of p250 and higher M_r oligomers (**Figure 2.7A, B**, lane 3). This result indicates that the resolution of p160 – and perhaps a fraction of p250 – requires BACE2 cleavage, which is known to cleave Mβ to Mβ' and the CTF (80). Since BACE2 inhibition has been shown to impede PMEL fibril formation (80), this also suggests that p160 cannot directly assemble into functional amyloid fibrils. Lastly, treatment with the cysteine protease inhibitor E-64 resulted in the accumulation of free Mα and Mα+Mβ' (as detected by HMB45 but not by αPMEL-C) but had no effect on p250 or p160 (**Figure 2.7A, B**, lane 4). Prolonged treatment with E-64 also resulted in the accumulation of Mα and the depletion of Mα' fragments in the detergent-insoluble fraction of MNT-1 cells (**Figure 2.7C**) suggesting that, in addition to ADAM proteases (83), cysteine proteases are required to cleave Mα and Mα+Mβ' into the Mα' fragments that typically accumulate in PMEL amyloid fibrils.

Importantly, treatment of these cells for an additional 2 hours in the presence of both E-64 and the protein synthesis inhibitor cycloheximide (CHX) to allow for further processing in the absence of new PMEL biosynthesis led to the depletion of p160 but not of Mα or Mα+Mβ' (**Figure 2.7A, B**, lane 5). This suggests that p160 is a true intermediate in PMEL processing that precedes the formation of free Mα and Mα+Mβ'. Finally, none of the inhibitor treatments (except for cycloheximide) affected the level of P1 detected by αPMEL-C (**Figure 2.7B**) as is consistent with the notion that immature PMEL monomers are predominantly located in pre-Golgi compartments (i.e. the ER).

Cysteine 301 participates in a cross-subunit disulfide bond in p250 and a disulfide bond between Mα and Mβ derived from the same PMEL precursor in p160

To determine which cysteine residues participate in the disulfide bonds that stabilize p250 and p160, we evaluated the effect of single cysteine mutations on the disulfide-bonded PMEL species. The 11 luminal cysteine residues within PMEL (**Figure 2.8A**) were each individually mutagenized to serine and the single point mutants expressed in HeLa cells by transient transfection. Like wild-type PMEL, all mutants were able to exit the ER and localize to a subset of late endosomes and lysosomes labeled with LAMP1 by immunofluorescence microscopy (**Figure 2.9**). The mutants were also all appropriately cleaved in post-Golgi compartments by a proprotein convertase since every one produced Mβ fragments when analyzed by reducing SDS-PAGE followed by immunoblotting with αPMEL-C (**Figure 2.8B**). These data indicate that no single disulfide bond is necessary for PMEL to pass ER quality control checkpoints or to be appropriately modified by Golgi enzymes and proprotein convertase. To assess p250 and p160 formation, lysates were then fractionated by non-reducing SDS-PAGE and immunoblotted with HMB45 (**Figure 2.8C-E**). Of the four cysteine residues within the region of PMEL that corresponds to Mα, individual mutations in three of them had little to no effect on p250 and p160. Mutagenesis of C60 resulted in disulfide-bonded PMEL species that were undistinguishable from those produced by wild-type PMEL (**Figure 2.8C**, lane 2), and mutagenesis of C130 or C138 produced only slight increases in the M_r of p250 and p160 (**Figure 2.8C**, lanes 3-4). This suggests that although C130 and C138 likely participate in

Figure 2.8

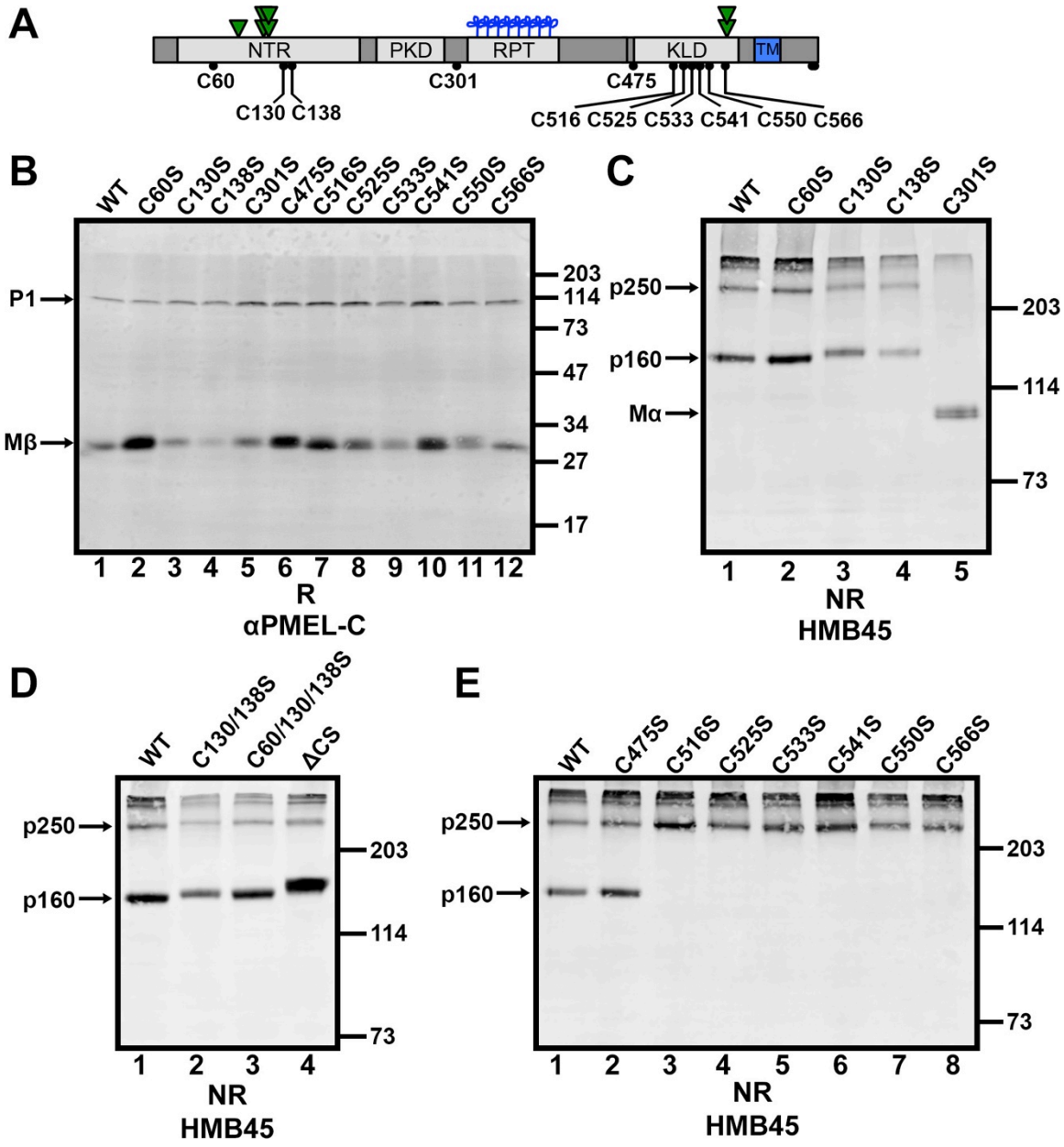

p250 has a C301-dependent intermoelcular disulfide bond and p160 has a C301-dependent intramolecular disulfide bond. (A) Schematic from Figure 2.1A showing

luminal cysteine residues labeled with their amino acid numbers. (B-E) Lysates from transiently transfected HeLa cells expressing wild-type PMEL, indicated cysteine-to-serine mutants of PMEL, or the ΔCS variant were analyzed by reducing (R) SDS-PAGE and immunoblotted with αPMEL-C (B) or by non-reducing (NR) SDS-PAGE and immunoblotted with HMB45 (C-E). Single point mutants are analyzed in B, C, and E; double and triple mutants are analyzed in D together with ΔCS. Positions of molecular weight standards are indicated to the right of each blot, and relevant PMEL bands are indicated with arrows.

Figure 2.9

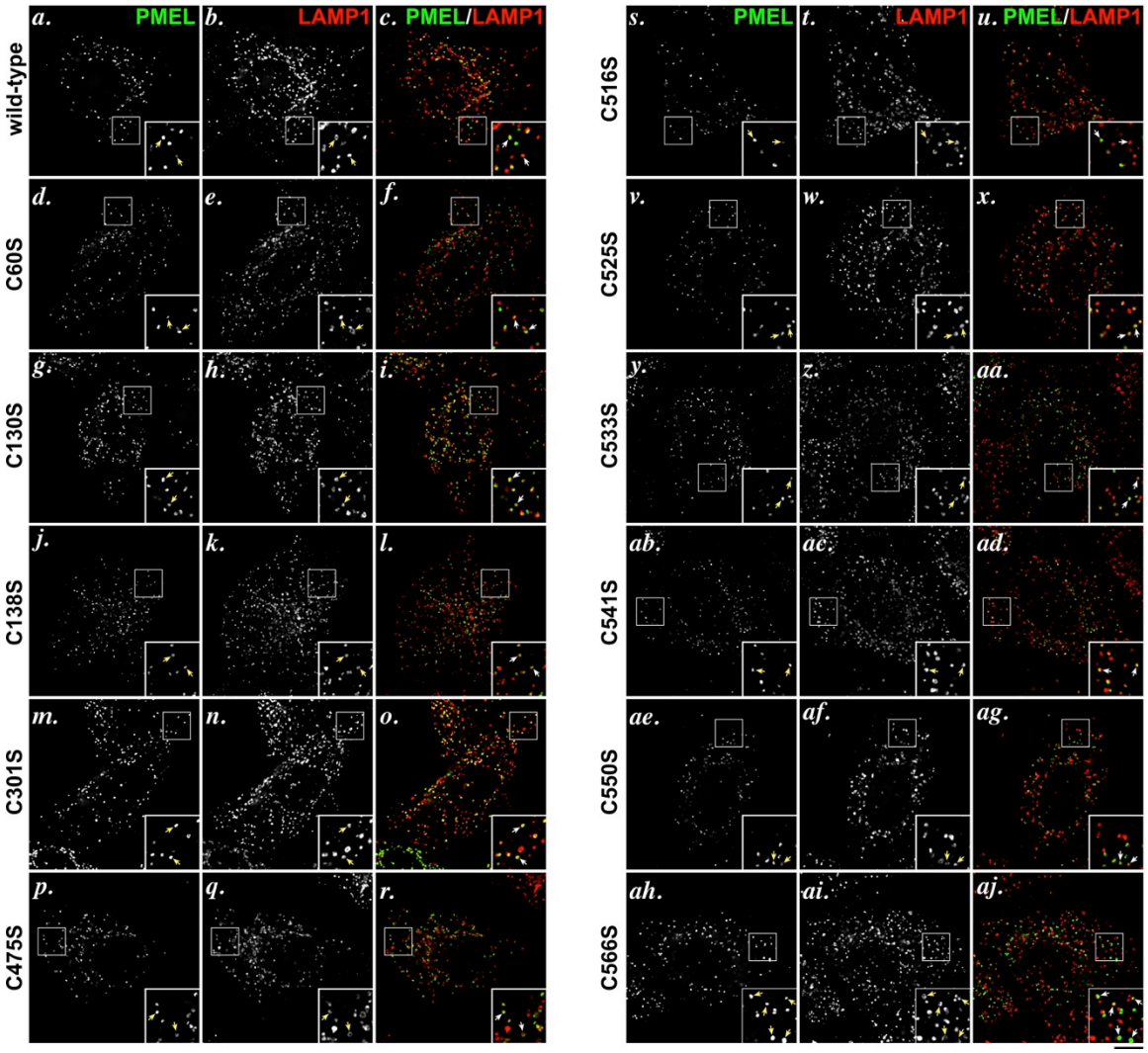

PMEL cysteine mutants mutants traffic appropriately to late endosomal compartments when expressed in HeLa cells. HeLa cells transiently transfected with wild-type PMEL (A-C), PMEL C60S (D-F), PMEL C130S (G-I), C138S (J-L), C301S (M-O), C475S (P-R), C516S (S-U), C525S (V-X), C533S (Y-AA), C541S (AB-AD),

C550S (AE-AG), or C566S (AH-AJ) were fixed, labeled with antibodies to PMEL (NKI-beteb, red; A, D, G, J, M, P, S, V, Y, AB, AE, AH) and LAMP1 (H4A3, green; B, E, H, K, N, Q, T, W, Z, AC, AF, AI), and analyzed by deconvolution immunoflourescence microscopy. Shown are representative images of each label separately and merged together (C, F, I, L, O, R, U, X, AA, AD, AG, AJ). Insets show 4X magnifications of the boxed regions. Scale bar represents 10 μm.

an intramolecular disulfide bond, neither C60, C130, nor C138 is critical for maintaining the integrity of p250 or p160. By contrast, mutagenesis of C301 ablated formation of both p250 and p160, causing most mature PMEL to migrate as free Mα by non-reducing SDS-PAGE (**Figure 2.8C**, lane 5). Since C301 was the only cysteine residue within the Mα region of PMEL required to stabilize both disulfide-bonded PMEL species, C301 must participate in a disulfide bond with a cysteine residue in the Mβ region of PMEL to generate p250 and p160.

In order to generate p250, a disulfide bond must connect the two PMEL monomers within the dimer. Because p250 contains both Mα and Mβ products of proprotein convertase cleavage (**Figure 2.4**), a disulfide bond must also form a bridge between the Mα and Mβ fragments. If C301 is the only cysteine residue in the Mα region of PMEL that actively functions to fulfill both of these requirements, then C301 of one PMEL molecule must form an intermolecular disulfide bond with the Mβ region of the other PMEL molecule within the p250 dimer. Alternatively, the other cysteine residues in the Mα region of PMEL could participate in a disulfide bond with Mβ in a redundant manner such that mutagenesis of any one is insufficient to disrupt disulfide bond formation. We therefore tested whether combined mutagenesis of the other Mα cysteine residues impacted p250 or p160 formation. Relative to single point mutations in C130 or C138, simultaneous mutation of two (C130 and C138) or all three (C60, C130, and C138) of these cysteine residues had no additional impact on the migration or the formation of p250 (**Figure 2.8D**, lanes 2-3). Therefore, C301 must participate in cross-subunit

disulfide bonds that both (a) link the two PMEL monomers present within the p250 dimer and (b) link Mα to Mβ within p250.

To generate p160, a disulfide bond must connect C301 of Mα to a cysteine residue of Mβ in the cleaved version of this species. However, this disulfide bond could form between Mα and Mβ fragments derived from the same PMEL molecule or from different PMEL molecules. To distinguish between these possibilities, we analyzed a mutated form of PMEL lacking the proprotein convertase cleavage site (ΔCS; (82)) by non-reducing SDS-PAGE. As predicted by the migration of uncleaved P2 in the "larger" form of p160 by 2D-PAGE (**Figure 2.4**), the ΔCS variant generates both p250 and p160 with only small shifts in migration (**Figure 2.8D**, lane 4). Thus, p160 must contain a disulfide bond that connects Mα and Mβ regions originating from the same PMEL molecule. Given that C301 is required for the formation of both the interchain disulfide bond in p250 and the intrachain disulfide bond in the uncleaved version of p160, a disulfide bond exchange must occur during the maturation of p250 to p160.

In an attempt to identify the cysteine residue within the Mβ region of PMEL that forms a disulfide bond with C301, the 7 cysteine residues in this region were individually mutagenized to serine and the single point mutants analyzed for their effects on the stability and migration of p250 and p160 by non-reducing SDS-PAGE. Mutagenesis of C475 resulted in disulfide-bonded PMEL species undistinguishable from those produced by wild-type PMEL, but mutagenesis of any one cysteine residue within the cysteine-rich KLD (C516, C525, C533, C541, C550, or C566) completely ablated formation of p160 without disrupting that of p250 (**Figure 2.8E**). Although these data fail to isolate which

cysteine residue within the Mβ region of PMEL participates in the disulfide bond with C301, they suggest that an intact KLD is critical for the formation of p160.

Stabilization of p250 impairs amyloid fibril formation

The ability of KLD cysteine mutants to preferentially stabilize p250 provides a useful tool with which to investigate the function of this disulfide-bonded PMEL intermediate. Previous studies have shown that, when overexpressed in non-pigmented cells such as HeLa or Mel220, PMEL forms melanosome-like fibrillar structures within multivesicular endosomes that can be visualized and distinguished from non-fibrillar aggregates by electron microscopy (73,82,141,142). In our experiments, transient expression of wild-type PMEL led to the formation of fibrillar sheets in 36 ± 4.6% (mean ± SEM) of the multivesicular bodies present within a given HeLa cell (**Figure 2.10**). However, following comparable expression of the C566S PMEL mutant – which forms p250 but not p160 (**Figure 2.8E**, lane 8) – many fewer multivesicular bodies (18 ± 3.5%; $p < 0.01$) showed evidence of fibril formation (**Figure 2.10**). This result suggests that stabilization of p250 can impair the formation of functional amyloid fibrils and that resolution of this disulfide-bonded intermediate may be necessary for fibril formation to ensue.

Surprisingly, expression of the C301S variant – which fails to form both p250 and p160 (**Figure 2.8C**, lane 5) – resulted in levels of fibril formation (34 ± 3.8% of multivesicular bodies) that were not significantly different from wild-type PMEL (**Figure 2.10**). This could have been interpreted to suggest that p250 and p160 are not required for fibril formation. However, given that p250 and p160 were detected as distinct entities under

Figure 2.10

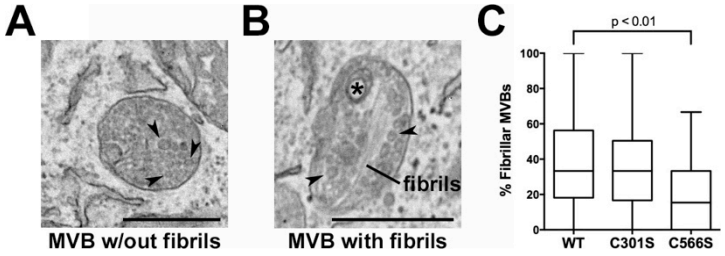

Cells expressing the C566S PMEL mutant exhibit decreased fibril formation while those expressing C301S PMEL appear similar to wild-type. HeLa cells transiently transfected with wild-type PMEL, the C301S mutant, or the C566S mutant were analyzed by transmission electron microscopy. (A) An example of a multivesicular body with intraluminal vesicles (arrowheads). (B) An example of a multivesicular body with fibrils, intraluminal vesicles (arrowheads), and a small multilamellar structure commonly found in late endosomes and lysosomes (asterisk). (C) Fibril-containing organelles and multivesicular bodies without any evidence of fibril formation were quantified in at least one field of view per cell, and the percentage of fibril-containing multivesicular bodies calculated for each cell. Box plots show the combined results of three experiments with the line in the center representing the median, the box representing the 25th and 75th percentiles, and the whiskers denoting the minimum and maximum values. Statistics were performed using a two-tailed unpaired t-test comparing each mutant to wild-type PMEL. Scale bars are 500 nm.

non-denaturing conditions by sedimentation and size exclusion chromatography analyses (**Figures 2.2**, **2.3**), we considered the possibility that similar complexes might form non-covalently in the absence of C301. Indeed, co-immunoprecipitation analyses show that Mα and Mβ remain associated in cells expressing the C301S mutant of PMEL (**Figure 2.11A-B**). Moreover, when transfected HeLa cells were analyzed by size exclusion chromatography, the C301S mutant generates PMEL complexes that have elution volumes identical to those of wild-type PMEL (**Figure 2.11C-H**). Thus, while C301-dependent disulfide bonds may provide additional stability to p250 and p160, the data suggest that formation of the corresponding non-covalent complexes is sufficient for function.

DISCUSSION

Very little is known about the regulation of functional amyloid formation, especially in mammalian systems. Here we show that the pigment cell-specific amyloid protein PMEL forms a disulfide-bonded dimer in the ER or early Golgi. Resolution of this dimer to a disulfide-bonded monomer requires an intact KLD, and inhibiting this process interferes with the assembly of functional amyloid fibrils. Our data are consistent with a model in which formation of a disulfide bond-stabilized PMEL dimer in the ER or early Golgi functions to prevent premature fibril formation early in the secretory pathway (**Figure 2.12**). The dimer must then be resolved to monomeric forms by disulfide bond rearrangements in the late Golgi or in a post-Golgi compartment in order to be incorporated into growing amyloid fibrils.

Figure 2.11

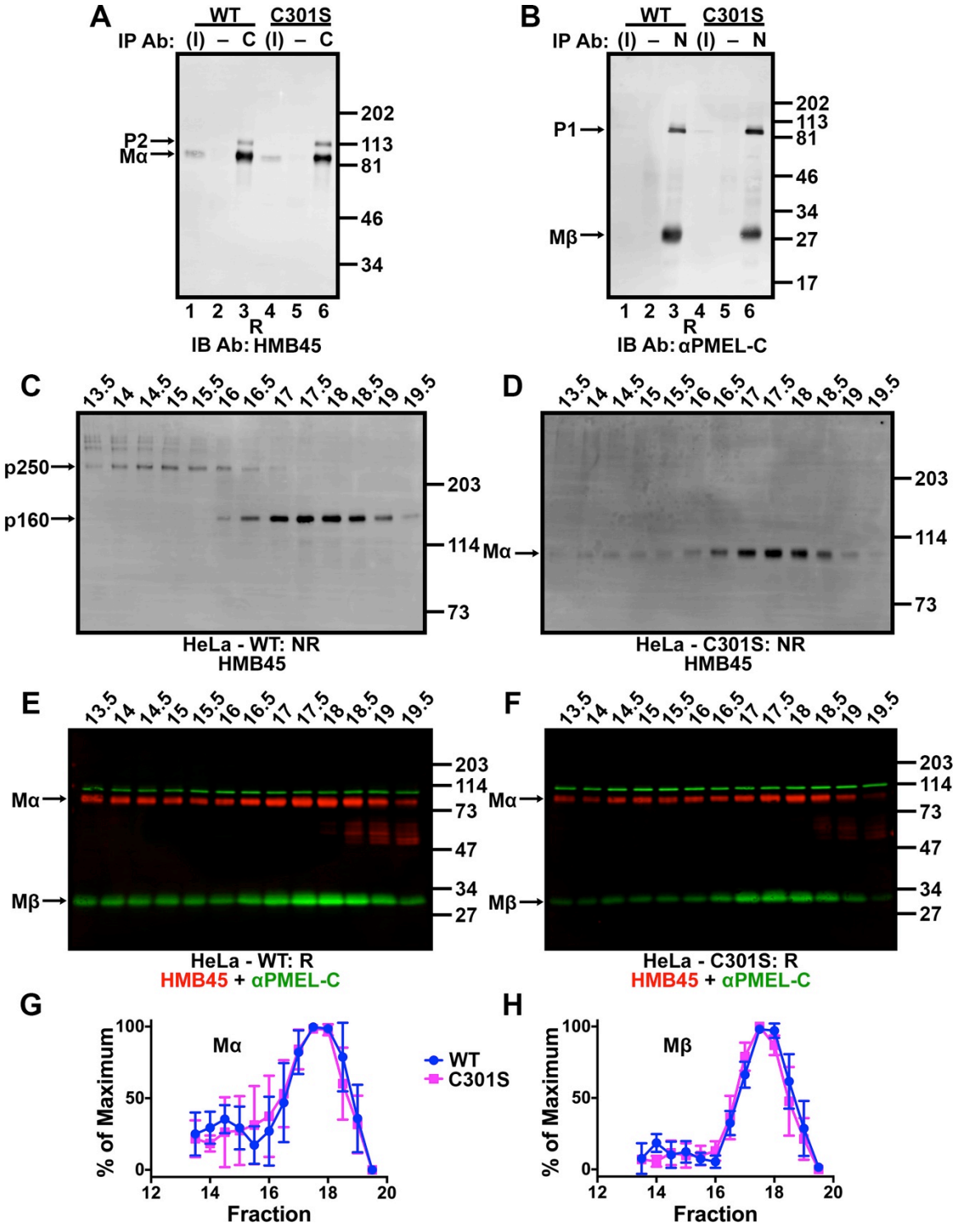
A
WT C301S
IP Ab: (I) – C (I) – C
P2
Mα
202
113
81
46
34
1 2 3 4 5 6
R
IB Ab: HMB45
B
WT C301S
IP Ab: (I) – N (I) – N
P1
Mβ
202
113
81
46
34
27
17
1 2 3 4 5 6
R
IB Ab: αPMEL-C
C
13.5 14 14.5 15 15.5 16 16.5 17 17.5 18 18.5 19 19.5
p250
p160
203
114
73
HeLa - WT: NR
HMB45
D
13.5 14 14.5 15 15.5 16 16.5 17 17.5 18 18.5 19 19.5
Mα
203
114
73
HeLa - C301S: NR
HMB45
E
13.5 14 14.5 15 15.5 16 16.5 17 17.5 18 18.5 19 19.5
Mα
Mβ
203
114
73
47
34
27
HeLa - WT: R
HMB45 + αPMEL-C
F
13.5 14 14.5 15 15.5 16 16.5 17 17.5 18 18.5 19 19.5
Mα
Mβ
203
114
73
47
34
27
HeLa - C301S: R
HMB45 + αPMEL-C
G
Mα
% of Maximum
100
50
0
12 14 16 18 20
Fraction
WT
C301S
H
Mβ
% of Maximum
100
50
0
12 14 16 18 20
Fraction

Non-covalent complexes with properties similar to p250 and p160 persist despite C301 mutagenesis. (A, B) Detergent-soluble lysates prepared from transiently transfected HeLa cells expressing wild-type PMEL (lanes 1-3) or PMEL C301S (lanes 4-6) were immunoprecipitated using αPMEL-C to the Mβ fragment (C; panel A, lanes 3 and 6), NKI-beteb to the Mα fragment (N; panel B, lanes 3 and 6) or matched negative (-) controls (normal rabbit serum in panel A, lanes 2 and 5, or the irrelevant monoclonal antibody OKT4 in panel B, lanes 2 and 5). The immunoprecipitated material and 3% of the inputs (I; lanes 1 and 4) were analyzed by reducing SDS-PAGE and immunoblotted with antibodies to the opposite fragment – HMB45 to Mα (panel A) or αPMEL-C to Mβ (panel B). The migration of molecular weight standards are shown to the right; bands corresponding to P2, Mα, P1, and Mβ are indicated with arrows. (C-F) HeLa cells transfected with wild-type PMEL (C, E) or the C301S PMEL variant (D, F) were lysed in 250 mM *n*-octylglucoside lysis buffer and the detergent extract fractionated by size exclusion chromatography in 25 mM *n*-octylglucoside running buffer. Eluted fractions were analyzed by SDS-PAGE under non-reducing (C, D) or reducing (E, F) conditions and immuoblotted using the antibodies indicated. The migration of molecular weight standards is indicated to the right of each blot, and bands corresponding to p250, p160, Mα, and Mβ are indicated by arrows. Lanes are labeled with fraction numbers as in Figure 2.3A. (G-H) HMB45 and αPMEL-C immunoreactivity were quantified to determine the amount of Mα (G) and Mβ (H) present in each fraction. The lowest value quantified for each species was set to 0% and the highest value was set to 100% for each experiment. Data represent the mean ± SD of three independent experiments.

Figure 2.12

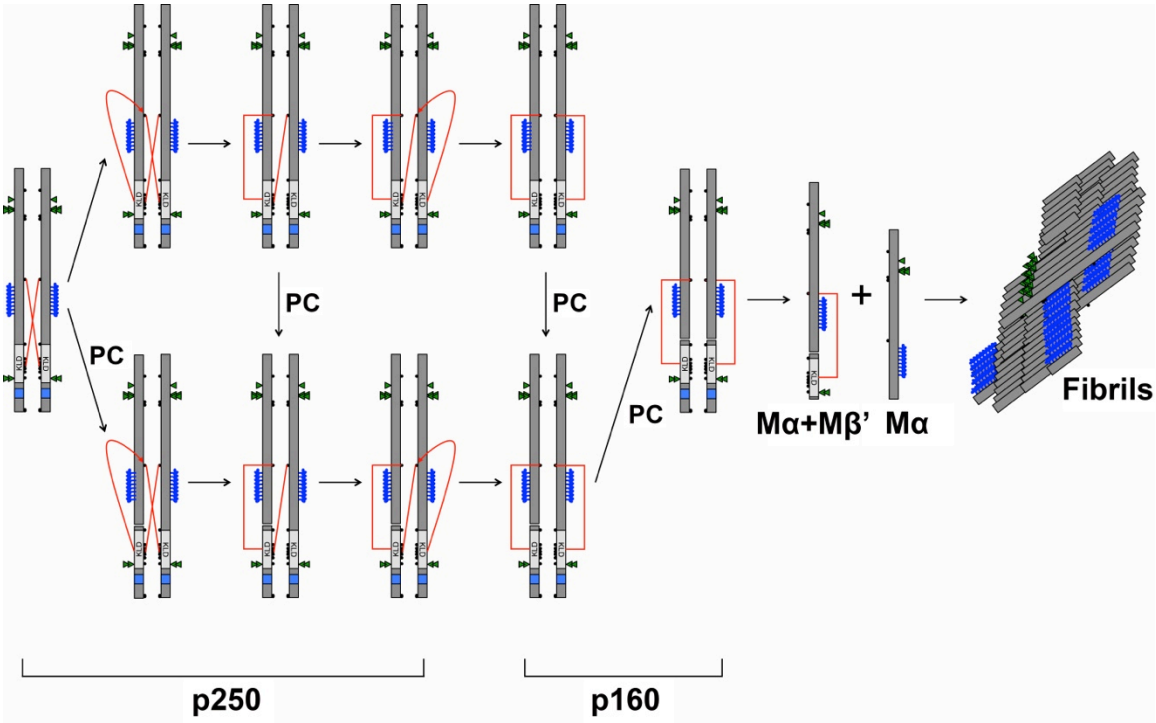

Model of PMEL fibril formation. Schematic diagram showing maturation of p250 into functional amyloid fibrils. The p250 PMEL dimer is resolved to p160 via disulfide bond rearrangement with proprotein convertase cleavage occuring before, during, or after this process. The p160 monomers then mature to form the soluble PMEL species Mα+Mβ' and Mα. These are further cleaved by cysteine proteases into smaller fragments that assemble into functional amyloid fibrils along with Mα. For simplicity, only one subunit of the original dimer is shown after p160. Red lines represent disulfide bonds between C301 and the KLD.

The discovery of higher molecular weight disulfide-bonded p250 and p160 PMEL species that react with an antibody known to detect mature – but not immature – PMEL isoforms originally suggested to us that Golgi-modified forms of PMEL might be covalently bound to one or more unidentified partner proteins. However, several observations led us to conclude that these species contain only PMEL. First, p250 and p160 were detected in both melanocytic cells and transfected HeLa cells. Since pigment cell-specific proteins are not expressed in HeLa cells, this eliminated the possibility of covalent association with a pigment cell-specific binding partner. Second, no polypeptides other than PMEL-derived P2, Mα, and Mβ were consistently detected as components of p250 or p160 by 2D-PAGE of PMEL immunoprecipitated from cells metabolically labeled with ^{35}S-methionine/cysteine for an extended period of time. This was surprising given that the hypothesized binding partners were expected to be stoichiometrically represented within the disulfide-bonded PMEL complexes. Third, no candidate binding partners of the appropriate molecular weight, relative abundance to PMEL, and subcellular localization were identified by mass spectrometry analysis of trypsin- or AspN-digested p250 and p160 bands (see **Table 2.2** and **Supplemental Table S1**). Several ER chaperones were detected in moderate abundance; however, these are common contaminants of protein purification by affinity chromatography, and detailed analyses of two abundant protein disulfide isomerase family members revealed interactions with immature ER forms of PMEL but not p250 or p160 (data not shown). The mass spectrometry data effectively rule out the possibility that a stoichiometric constituent of p250 or p160 was missed by 2D-PAGE due to poor labeling with ^{35}S-methionine/cysteine. Thus, while it remains remotely possible that a poorly radiolabeled,

ubiquitous binding partner might fail to generate peptides detectable by mass spectrometry using either of two proteases, we favor the more likely interpretation that p250 and p160 are comprised entirely of PMEL.

With a molecular weight approximately twice that of a PMEL monomer, p250 is most likely a PMEL dimer. The exact composition of p160, however, was less obvious at first. The migration of p160 by non-reducing SDS-PAGE is considerably slower than that of a completely reduced, Golgi-modified PMEL monomer. We initially interpreted this to suggest that p160 is comprised of a full-length PMEL monomer – or linked Mα/Mβ cleavage products – in complex with an additional PMEL fragment such as Mβ. However, the migration of p160 by non-reducing SDS-PAGE was only minimally altered in the absence of Mβ production as tested using the proprotein convertase cleavage site mutant ΔCS. In addition, the naturally occurring p160 comprised of uncleaved, full-length, Golgi-modified P2 contained no additional PMEL fragments when analyzed by 2D-PAGE. As such, we interpret the data to indicate that P2 migrates with a M_r of ~160,000 when constrained by disulfide bonds but a M_r of ~120,000 when fully reduced. We speculate that the disulfide-bonded structure of p160 limits accessibility to SDS, thus reducing the migration of this species by non-reducing SDS-PAGE.

Our results are consistent with a model in which the p250 dimer is an obligate precursor of the p160 monomer since (i) the formation of p250 occurs prior to that of p160 by metabolic pulse/chase analysis, (ii) inhibition of intra-Golgi transport in cells treated with monensin leads to the accumulation of p250 and depletion of p160, and (iii) none of the cysteine mutants produce p160 independently of p250. Complicating this interpretation,

however, is the finding that both p250 and p160 contain the full-length Golgi-modified P2 form of PMEL and the Mα/Mβ form cleaved by proprotein convertase when analyzed by 2D-PAGE. Since Mα and Mβ are generated by proprotein convertase cleavage of P2 in the TGN (73) or endosomes (74), ideally p250 would contain only uncleaved P2 and p160 would contain only cleaved Mα/Mβ. While these data raise the possibility that p250 represents an independent "dead-end" pathway for PMEL that never generates fibrils, we consider it more likely that p250 is converted to p160 at the same intracellular site but independently of proprotein convertase cleavage such that cleavage can occur before, during, or after resolution of the p250 dimer (**Figure 2.12**).

Our data further suggest that a disulfide bond rearrangement is required to convert p250 to p160. This is because C301 – a cysteine residue conserved throughout vertebrate evolution (88) – participates in a cross-subunit disulfide bond between two different PMEL molecules within p250 but in a disulfide bond between Mα and Mβ derived from the same PMEL precursor within p160. Although proprotein convertase cleavage of both monomers within the p250 dimer would immediately resolve p250 into a "monomeric" form in which Mα derived from one protomer is linked to Mβ from the other protomer, the observation that p160 can form without proprotein convertase cleavage suggests that the cross-subunit disulfide bond of p250 is broken to form a new disulfide bond connecting Mα and Mβ derived from the same PMEL protomer. While disulfide bonds are typically formed and remodeled in the ER (143), disulfide bond rearrangements outside the ER have been reported (131,144). Interestingly, if our model is correct, the disulfide exchange likely occurs without the enzymatic activity of a protein disulfide isomerase; typical ER protein disulfide isomerases such as PDIA1 and PDIA3 associate

exclusively with ER forms of PMEL (T. Ho, unpublished data), and melanocytes do not express the only known protein disulfide isomerase of the endocytic pathway, GILT (γ-interferon inducible lysosomal thiol reductase) (145), unless they are stimulated with γ-interferon ((146) and M. Marks, unpublished data). In addition, failure to treat cells with fresh NEM prior to lysis resulted in poor preservation of the disulfide-bonded PMEL species (T. Ho, unpublished data), suggesting that nearby cysteine residues rapidly reduce p250 and p160 when not blocked by alkylation. Since the integrity of the PMEL KLD is required for the resolution of p250 to p160, we speculate that cysteine residues within the KLD initiate this disulfide exchange in an autocatalytic manner. Assessment of this model would require the purification of properly folded recombinant PMEL isoforms, which are not currently available.

Many layers of regulation must exist to protect organisms against the dire consequences of inappropriate amyloid formation. Our data indicate that the KLD domain protects against premature PMEL fibril formation by regulating the resolution of a disulfide-stabilized PMEL dimer. The importance of an intact KLD is supported by the finding that fibril formation is impaired in HeLa cells expressing the C566S mutant, a variant of PMEL that generates p250 dimers but not p160 monomers. Given that mutagenesis of any single cysteine residue within the KLD – and even a small deletion (B. Watt, unpublished data) – results in the same biochemical effect on p250 and p160, we predict that any disruption to the cysteine arrangement within the KLD will interfere with fibril formation. Surprisingly, all of the individual cysteine mutants pass quality control checkpoints in the ER, are cleaved by proprotein convertases in the TGN or endosomes, and localize appropriately to late endosomes and lysosomes. This suggests that the KLD

acts primarily in a post-Golgi compartment to regulate p160 formation and promote the assembly of functional amyloid fibrils. Whether the KLD can promote fibril formation independent of its effect on the disulfide-bonded PMEL species cannot be determined with the present data, but the progressive disulfide bond changes during PMEL maturation suggest that a primary function of the KLD is to regulate these changes.

Intriguingly, mutagenesis of C301 – the only cysteine residue integral to the formation of both p250 and p160 – does not impair PMEL fibril formation. As shown by size exclusion chromatography, this is most likely because the C301S PMEL variant forms non-covalent complexes similar to the disulfide-bonded species formed by wild-type PMEL. This indicates that C301-dependent disulfide bonds are not required for amyloid fibril formation but rather stabilize energetically favorable conformations at distinct stages of the PMEL biosynthetic pathway. We speculate that loss of this additional stability under physiological expression conditions might lead to premature fibril formation and consequent pathology that is not detectable in the short-term assays used here, as has been observed for several dominant PMEL mutants (147).

PMEL is not the only amyloid protein influenced by disulfide bonds. Reduction of the single disulfide bond in the functional amyloid protein somatostatin-14 *in vitro* results in fibrils that form faster, are more resistant to denaturation, and have decreased monomer release (148). Reduction of the intrachain and/or one of two interchain disulfide bonds in porcine insulin also accelerates fibril formation (149). Interestingly, the cysteine residues of tau can participate in intramolecular or intermolecular disulfide bonds; the intramolecular disulfide bonds retard fibril formation by restricting the protein to

conformations incompatible with the amyloid fold, whereas the intermolecular disulfide bonds accelerate amyloid fibril formation (150). However, many proteins including insulin have the ability to form amyloid aggregates *in vitro* but do not typically do so *in vivo* (151). Since many proteins of the secretory pathway contain disulfide bonds, we suggest that the use of disulfide bonds to stabilize pro- or anti-amyloidogenic folding intermediates might be a common mode of regulation for amyloid proteins within the endomembrane system.

ACKNOWLEDGMENTS

We thank Mark A. Lemmon for helpful discussions, Dewight Williams and the University of Pennsylvania Electron Microscopy Resource Laboratory for assistance high-pressure freezing, Nathan Roy (Children's Hospital of Philadelphia), John A. Wolf and Michael Grovola (Philadelphia VA Medical Center), and Frank E. Herbert and Jesse B. DeWitt (Nikon Instruments) for assistance with super-resolution microscopy that was not included in the manuscript, and James Z. Hui, Andrew Tsourkas, Elizabeth A. Sweeny, and James Shorter (University of Pennsylvania) for assistance with size exclusion chromatography. This work was supported by funding from the National Institutes of Health including R01 AR048155 and training program T32 AR007465 from the National Institute of Arthritis, Musculoskeletal and Skin Diseases, and training programs T32 AG000255 from the National Institute on Aging and T32 GM007170 from the National Institute of General Medical Sciences.

CHAPTER 3

Localization of SLC45A2 to Punctate Structures on or near Melanosomes

Tina Ho[1,2,3], Ariel J. Lefkovith[1,2,3], Kirk D. Haltaufderhyde[4], Elena Oancea[4], and Michael S. Marks[1,2,3,5]

[1]Department of Pathology and Laboratory Medicine, Children's Hospital of Philadelphia, Philadelphia, PA 19104

[2]Cell and Molecular Biology Graduate Group

[3]Department of Pathology and Laboratory Medicine, University of Pennsylvania, Philadelphia, PA 19104

[4]Department of Molecular Pharmacology, Physiology and Biotechnology, Brown University, Providence, RI

[5]Department of Physiology, University of Pennsylvania, Philadelphia, PA 19104

ABSTRACT

Mutations in the proton-dependent sucrose transporter SLC45A2 lead to a disorder known as oculocutaneous albinism type 4 (OCA4). Here, we show that HA-tagged human SLC45A2 localizes to punctate structures on or near the limiting membrane of melanosomes in a process that requires an intact tyrosine-based sorting motif located within a cytoplasmic loop of the transporter. Mutagenesis of the critical tyrosine residue within this sorting motif leads to mislocalization of HA-SLC45A2 to the plasma membrane and decreased pigmentation suggesting that SLC45A2 functions most effectively when present on or near melanosomes. Preliminary data also indicate that SLC45A2-deficient melan-uw1 mouse melanocytes accumulate hypopigmented mature melanosomes and that SLC45A2 may be required to maintain the neutral pH of late-stage melanosomes in order to achieve efficient melanin biosynthesis.

INTRODUCTION

Oculocutaneous albinism (OCA) is a group of autosomal recessive disorders characterized by hypopigmentation of the hair, skin, and eye. To date, seven types of non-syndromic oculocutaneous albinism have been identified, each resulting from mutation in a different gene associated with melanin production. OCA1 is caused by mutations in tyrosinase (TYR) (152), the rate-limiting enzyme in the synthesis of both eumelanins and pheomelanins. OCA2 is caused by mutations in the pink-eyed dilution protein (also known as the P protein or simply OCA2) (153), which is a chloride-selective ion channel that neutralizes the pH of maturing melanosomes (154). OCA3 results from mutations in tyrosinase related protein 1 (TYRP1) (155) which directly or indirectly facilitates the conversion of DHICA to eumelanin (102), and OCA4 results from mutations in SLC45A2 (15), a proton-dependent sucrose symporter (103). OCA5 is caused by mutations in an unidentified gene located on chromosome 4 (4q24) (104), OCA6 is caused by mutations in SLC24A5 (11), a putative potassium-dependent sodium/calcium exchanger, and OCA7 is caused by mutations in the uncharacterized orphan gene *C10orf11* (105).

Despite the different underlying mutations, patients with OCA2 and OCA4 are clinically indistinguishable and must be characterized by molecular genetic testing. While all patients with oculocutaneous albinism present with hypopigmented skin and hair and some degree of ocular defects including reduced retinal pigment and foveal hypoplasia leading to poor visual acuity, those with OCA1 are usually the most severely affected (94). Patients with OCA1 tend to have hair that is completely white and the worst vision,

whereas patients with OCA3 typically have the least severe disease, red hair, and reddish skin due to an increased ratio of pheomelanin to eumelanin. In contrast, patients with OCA2 and OCA4 have decreased production of both eumelanin and pheomelanin with light pigmentation of the hair and skin. OCA5, OCA6, and OCA7 have only recently been identified, and the range of clinical phenotypes exhibited by these patients has yet to be thoroughly characterized (156). Analyses of hair from mouse models of OCA2 and OCA4 are also much more similar to one another than to the other mouse models of oculocutaneous albinism, suggesting that the function of SLC45A2 may be related to that of OCA2 in the melanosome (**Table 3.1**).

OCA2 increases melanosomal pH to optimize the activity of the enzyme TYR, which functions best at pH 6.8 (7,100). Ectopic expression of the chloride channel in non-pigment cells causes endolysosomal pH to rise (154), likely by facilitating the export of H^+ as well as Cl^-. Consistent with a similar function in melanocytes, inhibition of the vacuolar-type H^+-ATPase (V-ATPase) by bafilomycin A1 restores pigmentation in OCA2-deficient melanocytes (101). Though far less is known about SLC45A2, all available evidence suggests that this H^+-sucrose symporter regulates melanosomal pH through an independent mechanism. Knockdown of a catalytic subunit of the V-ATPase complex in SLC45A2-deficient zebrafish larvae or overnight treatment of SLC45A2-deficient zebrafish embryos with bafilomycin A1 increases melanin production, suggesting that SLC45A2, like OCA2, helps to neutralize the pH of melanosomes (119). However, SLC45A2 and OCA2 appear to regulate melanosomal pH independently. Mice carrying mutations in both SLC45A2 and OCA2 are more severely hypopigmented than mice carrying only one of the two mutations (157). In addition, primary mouse

Table 3.1

Mouse	Corresponding Human Disorder	PTCA (ng/mg)	Total AHP (ng/mg)	Reference
C57BL-*a/a*, black	---	1590	49	(158)
B10-*a/a*, black	---	1560	43	(159)
B10-*c/c*, albino	OCA1	2	18	(159)
B10-*p/p*, pink-eyed	OCA2	70	91	(159)
B10-*b/b*, brown	OCA3	459	89	(159)
C57BL-*uw/uw*, underwhite	OCA4	29	80	(157)
C57BL-uw^{d}/uw^{d}, underwhite	OCA4	89	108	(157)
C57BL-Uw^{dbr}/Uw^{dbr}, underwhite	OCA4	85	114	(157)

Eumelanin (PTCA) and pheomelanin (AHP) content of mouse hair. *Adapted from: Quantitative Analysis of Eumelanin and Pheomelanin in Humans, Mice, and Other Animals: a Comparative Review (160).*

melanocytes from *underwhite* (*uw*) mice with a nonsense mutation in SLC45A2 secrete dark vesicles containing tyrosinase, TYRP1, and DOPAchrome tautomerase (DCT) that are easily pelleted by centrifugation (118) while melanins present in the media of cells lacking OCA2 are not easily pelleted by centrifugation at 12,000g (161).

To better understand how SLC45A2 contributes to melanosome biogenesis, we studied the subcellular localization of ectopically expressed SLC45A2. Our results show that SLC45A2 localizes to melanosomes, concentrating in punctate structures in or near the melanosomal membrane, and that mutagenesis of the critical tyrosine residue within a tyrosine-based signaling motif of SLC45A2 causes mislocalization to the plasma membrane and a consequent decrease in pigmentation. Preliminary data also suggest that SLC45A2 maintains the elevated pH of mature melanosomes and that overexpression of OCA2 can compensate for defects in SLC45A2.

RESULTS

Wild-type SLC45A2 localizes to punctate structures associated with melanosomes

Since antibodies that recognize endogenous SLC45A2 are not suitable for immunofluorescence microscopy, we studied the localization of SLC45A2 using a functional HA-tagged version of the protein. To determine whether the epitope tag interfered with SLC45A2 activity, we tested the ability of human HA-SLC45A2 to rescue pigmentation in immortalized melan-uw1 melanocytes derived from the SLC45A2-deficient OCA4 mouse model, *underwhite*. Toward this end, we both transiently transfected and stably expressed human HA-SLC45A2, a HA-tagged Y268A variant

(described below), and an unrelated HA-tagged transporter with multiple transmembrane domains (HA-SLC35D3) and evaluated the degree to which pigmentation was restored in these cells. The melan-uw1 cells transiently expressing HA-SLC45A2, the Y268A variant, or the HA-tagged negative control were examined 48 or 72 h after transfection, and the number of transfected melanocytes that were unpigmented (**Figure 3.1A**), partially pigmented (**Figure 3.1B**), or fully pigmented (**Figure 3.1C**) quantified by bright-field microscopy. At 48 h, 69 ± 3.4% (mean ± SD) of the melanocytes transfected with HA-SLC45A2 exhibited some degree of pigmentation, with about half the cells pigmented at levels comparable to immortalized wild-type melanocytes derived from C57BL/6 mice (melan-Ink4a) and half more modestly pigmented (**Figure 3.1D**). At 72 h, 79 ± 7.3% exhibited some degree of pigmentation, again with approximately half fully pigmented and half partially pigmented (**Figure 3.1E**). In contrast, very few cells transiently expressing the HA-SLC35D3 negative control showed evidence of pigmentation. Restoration of pigment in melan-uw1 cells stably expressing HA-SLC45A2, the Y268A variant, or the HA-tagged SLC35D3 negative control was evaluated by measuring the amount of melanin per mg of detergent-soluble lysate. Consistent with our results by bright-field microscopy, the melan-uw1 melanocytes stably expressing human HA-SLC45A2 had 3-fold more melanin than melanocytes stably expressing HA-SLC35D3 in this assay (**Figure 3.2**). Together, these data indicate that human HA-SLC45A2 is functional in melan-uw1 mouse melanocytes and that the behavior of this epitope-tagged human construct will likely reflect that of the endogenous mouse protein.

Figure 3.1

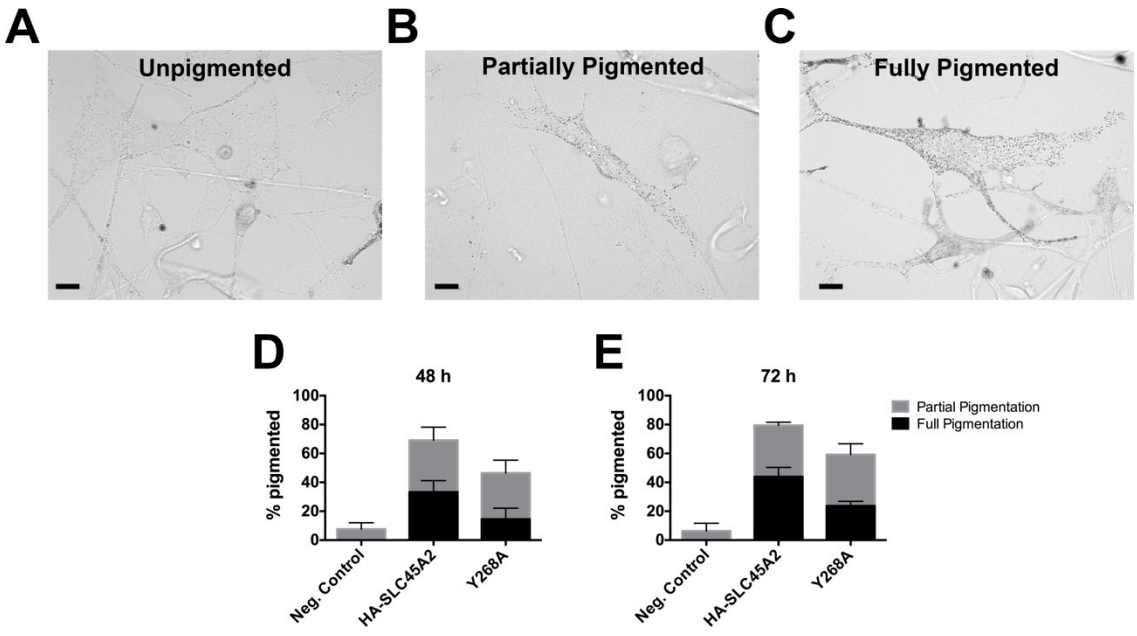

HA-SLC45A2 restores pigmentation to hypopigmented underwhite melanocytes. Immortalized SLC45A2-deficient underwhite melanocytes (melan-uw1) transiently expressing human HA-SLC45A2, the Y268A variant of HA-SLC45A2 (Y268A), or HA-SLC35D3 as a negative control (Neg. Control) were categorized as unpigmented (A), partially pigmented (B), or fully pigmented (C) by A. Lefkovith and the percentage of cells in each category analyzed 48 h (D) or 72 h (E) after transfection. Shown is the mean ± SD of three independent experiments in which at least 10 cells were evaluated for each transfected cell type. Scale bars represent 10 μm.

Figure 3.2

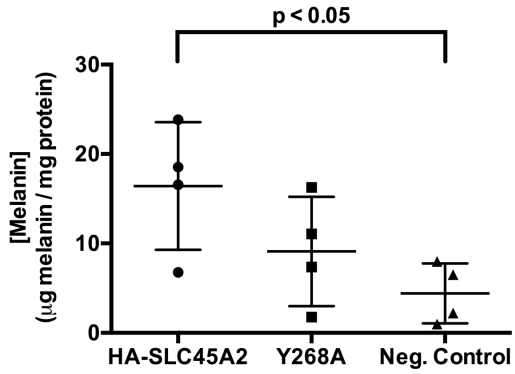

Restoration of pigment is also observed in stable cell lines expressing HA-SLC45A2 and related variants. The amount of melanin per mg protein in melan-uw1 cell lines stably expressing human HA-SLC45A2, the Y268A variant of HA-SLC45A2, or HA-SLC35D3 as a negative control (Neg. Control) was analyzed by K. Haltaufderhyde. Shown is the mean ± SD of four independent experiments.

While rudimentary studies of SLC45A2 localization in MNT-1 cells (117) and primary human melanocytes (116) have been reported, the subcellular localization of SLC45A2 has yet to be characterized in detail. Therefore, to thoroughly and accurately define the subcellular localization of SLC45A2, we expressed our HA-tagged construct transiently or stably in wild-type mouse melanocytes and analyzed the cells by immunofluorescence microscopy. Following transient transfection, the epitope-tagged protein was observed in rings surrounding pigment granules as is commonly observed for proteins of the melanosome limiting membrane (**Figure 3.3**). Also consistent with localization to melanosomes, HA-SLC45A2 staining overlapped with that of TYR and TYRP1 but not LAMP2 (**Figure 3.4**). Interestingly, careful examination of some of these images showed that HA-SLC45A2 frequently clustered in punctate spots within the rings surrounding pigment granules and/or the melanosomal marker proteins TYR or TYRP1. This pattern of localization was even more pronounced in melan-uw1 melanocytes stably expressing HA-SLC45A2 with the epitope-tagged protein localizing primarily to bright puncta adjacent to pigment granules or within rings labeled by antibodies to TYR or TYRP1 (**Figure 3.5**). These data suggest that SLC45A2 localizes to a distinct domain in the melanosomal membrane or to small vesicles closely associated with melanosomes when expressed at modest levels. More uniform labeling of the entire melanosome limiting membrane frequently observed in transiently transfected cells likely reflects an artifact of overexpression.

Melanosomal proteins often localize to late endosomes and lysosomes when expressed in non-pigment cells. To test whether the same is true for SLC45A2, we transiently expressed the HA-tagged construct in HeLa cells and evaluated the subcellular

Figure 3.3

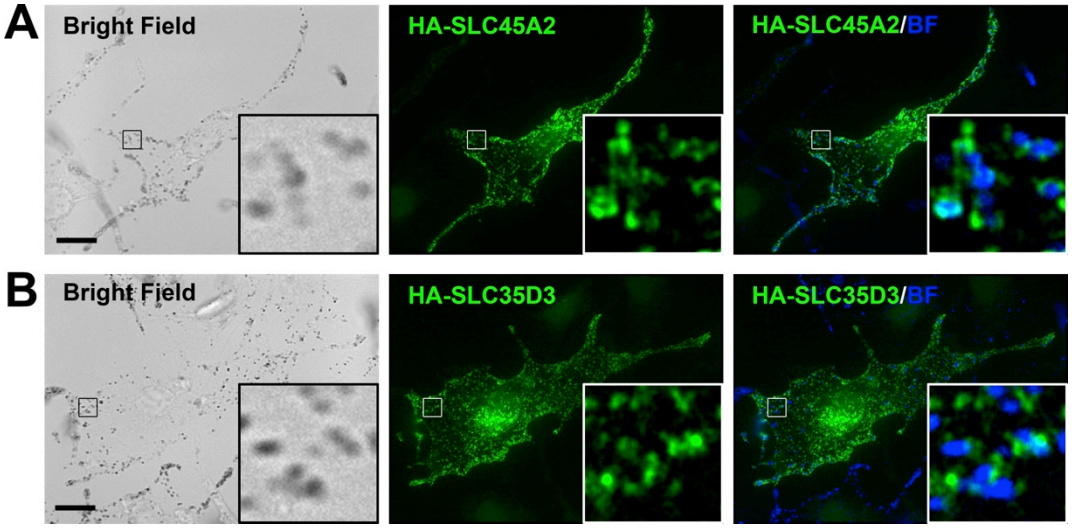

HA-SLC45A2 localizes to rings surrounding pigment granules when transiently overexpressed in wild-type melanocytes. Immortalized melan-Ink4a melanocytes transiently expressing HA-SLC45A2 (A) or HA-SLC35D3 as a negative control (B) were fixed 2 d after transfection, labeled with an antibody to the HA tag, and analyzed by A. Lefkovith using bright field and deconvolution immunofluorescence microscopy. Shown are representative bright field and deconvolution immunoflourescence images separately and merged together. Pigment granules have been pseudocolored blue in the merged image. Insets show 8.25x magnifications of the boxed regions. Scale bars represent 10 μm.

Figure 3.4

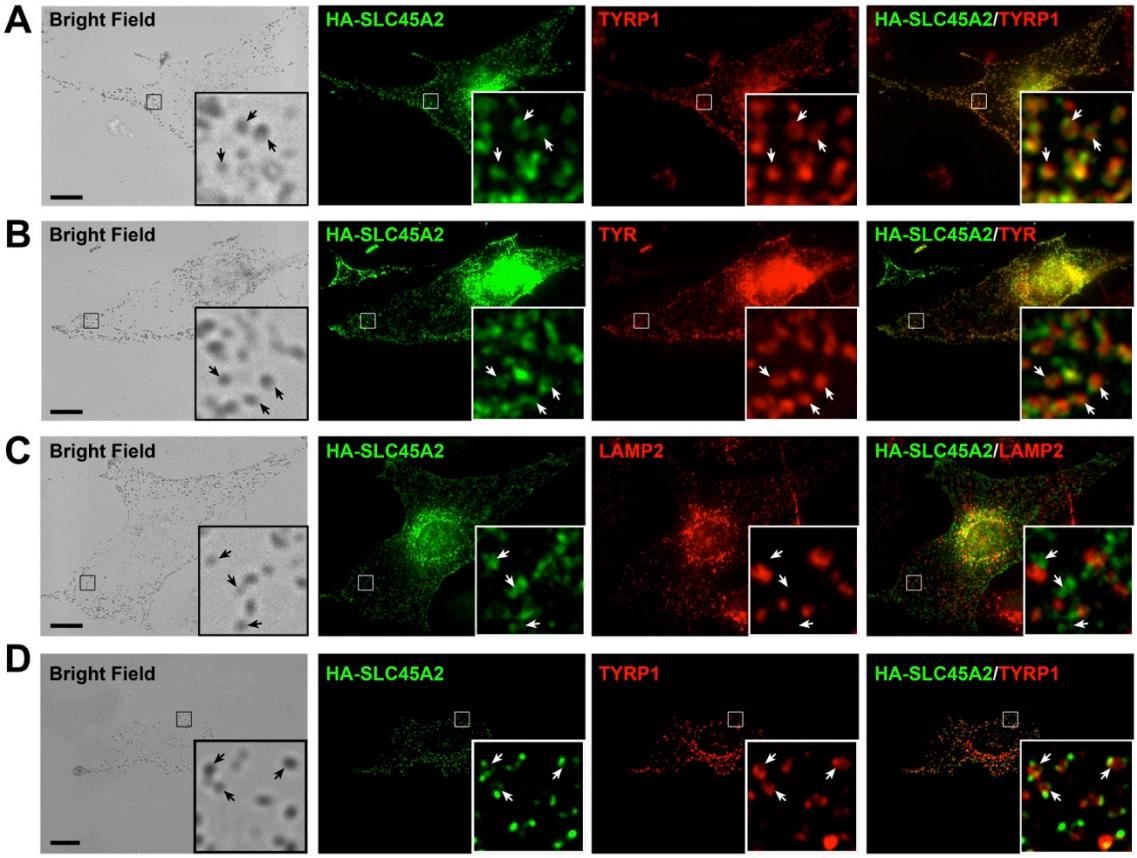

HA-SLC45A2 colocalizes with melanosomal membrane proteins in wild-type melanocytes. (A, B, C) Immortalized melan-Ink4a melanocytes transiently expressing HA-SLC45A2 were fixed 2 d after transfection, labeled with antibodies against TYRP1 (TA99; A), TYR (αPEP7h; B), or LAMP2 (GL2A7; C) and the HA tag, and analyzed by A. Lefkovith using bright field and deconvolution immunofluorescence microscopy. (D) Melan-Ink4a melanocytes stably expressing HA-SLC45A2 were also fixed, stained with

antibodies to TYRP1 (TA99) and the HA tag, and analyzed by T. Ho using bright field and deconvolution immunofluorescence microscopy. Shown are representative images of each label separately and merged together. Insets show 8.25x magnifications of the boxed regions. Scale bars represent 10 μm.

Figure 3.5

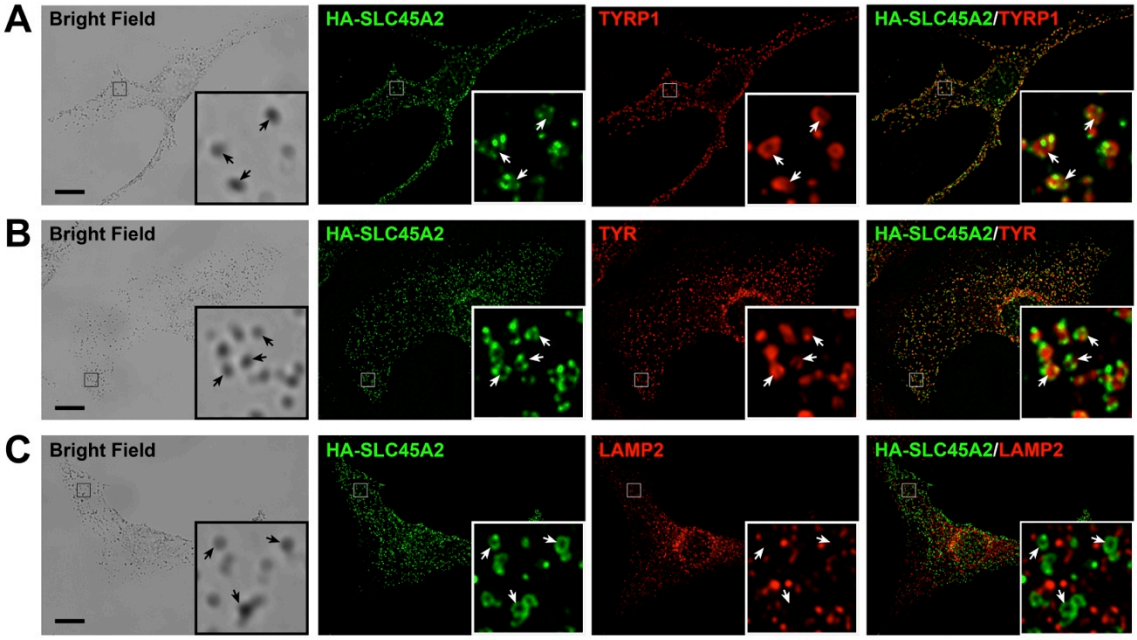

HA-SLC45A2 concentrates in puncta on or near melanosomes when stably expressed in SLC45A2-deficient melan-uw1 cells. Immortalized melan-uw1 melanocytes stably rescued with HA-SLC45A2 were fixed, labeled with antibodies against TYRP1 (TA99; A), TYR (αPEP7h; B), or LAMP2 (C) and the HA tag, and analyzed by T. Ho using bright field and deconvolution immunofluorescence microscopy. Shown are representative images of each label separately and merged together. Insets show 8.25x magnifications of the boxed regions. Scale bars represent 10 μm.

localization of HA-SLC45A2 by immunofluorescence microscopy. As shown in **Figure 3.6**, punctate clusters of HA-SLC45A2 were observed near or within the limiting membrane of late endosomes and lysosomes labeled with LAMP1 suggesting that pigment cell-specific proteins are not required for the localization of HA-SLC45A2 to these domains.

SLC45A2 localization to melanosomes requires a tyrosine-based signal (Yxxϕ)

Melanosome maturation involves the sequential delivery of melanosomal cargo to precursor organelles. TYR, TYRP1, and OCA2 contain acidic dileucine-based sorting signals that interact with AP-1 and/or AP-3 in the cytoplasm to deliver these proteins to melanosomes (14,107,162). Examination of the primary sequence of SLC45A2 reveals no dileucine-based motif within any of the predicted cytoplasmic domains of SLC45A2. However, between the 6^{th} and 7^{th} transmembrane domains of SLC45A2 lies a predicted AP-binding tyrosine-based motif (Yxxϕ) starting with Y268. This motif is conserved in vertebrates – all of which have specialized pigmented cells – but not in invertebrates, plants, or yeast which either lack pigment cells or harbor distinct classes of pigments (**Figure 3.7**). Since these more distant homologs of SLC45A2 are thought to function at the plasma membrane, this pattern of evolutionary conservation suggests that the melanosomal localization of human SLC45A2 could be mediated by the tyrosine-based motif between the 6^{th} and 7^{th} transmembrane domain.

To test this hypothesis, we developed a Y268A variant of SLC45A2 that disrupts the tyrosine-based motif. When expressed in wild-type melanocytes, this variant is expressed

Figure 3.6

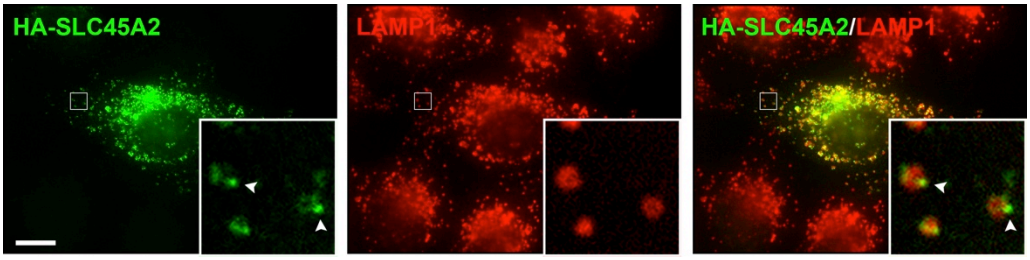

HA-SLC45A2 concentrates in puncta on or near late endosomes and lysosomes when expressed in non-pigment HeLa cells. HeLa cells transiently expressing HA-SLC45A2 were fixed 2 d after transfection, labeled with antibodies to the HA tag (green) and LAMP1 (H4A3, red), and analyzed by T. Ho using deconvolution immunoflourescence microscopy. Shown are representative images of each label separately and merged together. Insets show 8x magnifications of the boxed regions. Scale bar is 10 μm.

Figure 3.7

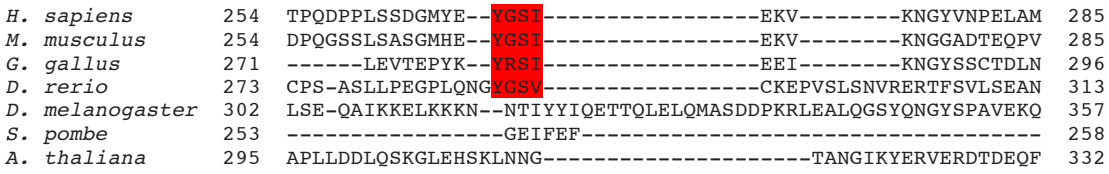

The tyrosine-based motif of SLC45A2 is conserved in vertebrates but not in lower organisms. Amino acid sequence comparison was performed on SLC45A2 orthologs in the species indicated using COBALT Constraint-based Multiple Protein Alignment Tool (163). Shown is the region surrounding the SLC45A2 tyrosine-based motif located in the cytoplasmic loop between the 6th and 7th transmembrane domains. Highlighted in red is the conserved Yxxϕ tyrosine-based motif. The GenBank accession numbers from which the sequences are derived are as follows: *Homo sapiens* SLC45A2 [Q9UMX9.2], *Mus musculus* SLC45A2, [P58355.1], *Gallus gallus* SLC45A2 [ABK51634.1], *Danio rerio* SLC45A2 [AAI54628.1], *Drosophila melanogaster* SLC45A2 ortholog 1, isoform A [NP_648292.1], *Schizosaccharomyces pombe* SUT1 [CAB16264.1], *Arabidopsis thaliana* SUC3 [O80605.1].

both diffusely throughout the cell – likely on the plasma membrane – and in puncta that did not colocalize with pigment (**Figure 3.8**). Consistent with this observation, expression of the Y268A variant of HA-SLC45A2 in HeLa cells resulted in localization both throughout the cell and in puncta that did not colocalize with LAMP1 (**Figure 3.9**). Preliminary results suggest that the diffuse staining results from accumulation of the Y268A variant at the plasma membrane with the puncta corresponding to cell surface projections or early endocytic vesicles; however, further experiments are necessary to determine whether this variant also localizes to other non-pigmented intracellular compartments.

Expression of the Y268A variant in melan-uw1 melanocytes partially restored pigmentation to these cells. When expressed transiently, 46 ± 4.5% of the melanocytes showed some degree of pigmentation 48 h post-transfection with that number increasing to 59 ± 8.5% after 72 h (**Figure 3.1D-E**). This surprisingly high degree of pigmentation is most likely a consequence of overexpression since melan-uw1 cells stably expressing the Y268A variant produce approximately half the melanin of melan-uw1 cells stably expressing wild-type HA-SLC45A2 (**Figure 3.2**; note that stable cell lines generated using the retroviral pBMN vector typically have much lower levels of protein expression compared to cells transiently transfected with multiple copies of pCI-based plasmids).

Figure 3.8

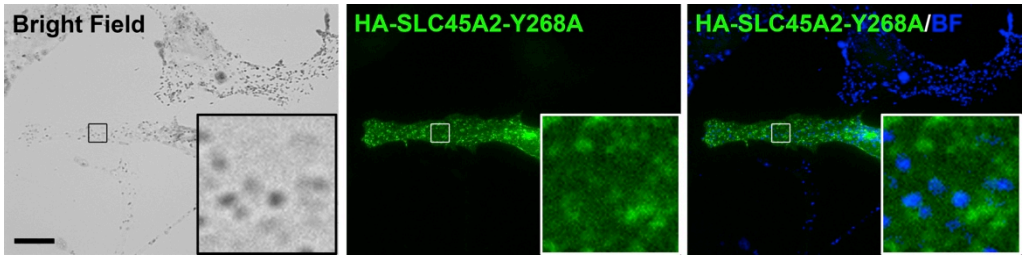

The conserved tyrosine within a putative Yxxϕ sorting signal is required for SLC45A2 localization to melanosomes. Wild-type melanocytes transiently expressing the Y268A variant of human HA-SLC45A2 were fixed 2 d after transfection, labeled with an antibody to the HA tag, and analyzed by A. Lefkovith using bright field and deconvolution immunoflourescence microscopy. Shown are representative bright field and deconvolution immunoflourescence images separately and merged together with pigment granules pseudocolored blue in the merged image. Insets show 8.25x magnifications of the boxed regions. Scale bar represents 10 μm.

Figure 3.9

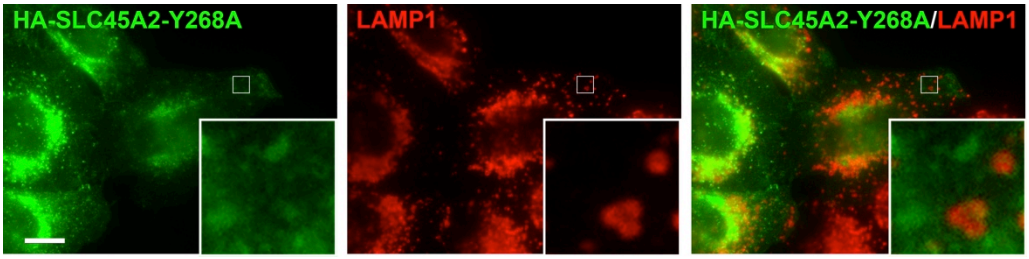

The conserved tyrosine within a putative Yxxϕ sorting signal is required for SLC45A2 localization to late endosomes and lysosomes in non-pigment HeLa cells. HeLa cells transiently expressing the Y268A variant of HA-SLC45A2 were fixed 2 d after transfection, labeled with antibodies to the HA tag (green) and LAMP1 (H4A3, red), and analyzed by T. Ho using deconvolution immunoflourescence microscopy. Shown are representative images of each label separately and merged together with insets showing 8x magnifications of the boxed regions. Scale bar represents 10 μm.

DISCUSSION

With the discovery and characterization of each gene associated with OCA, we gain new insights into the molecular mechanisms of melanosome biogenesis and grow one step closer to potentially developing treatments for OCA patients. OCA4 is caused by mutations in the proton-dependent sucrose symporter SLC45A2. In this chapter, we show that a HA-tagged version of human SLC45A2 localizes to and functions at melanosomes.

HA-SLC45A2 clusters in punctate structures on or near the melanosome limiting membrane in wild-type melanocytes and melan-uw1 melanocytes. The protein also clusters in puncta on or near the lysosomal limiting membrane in HeLa cells. Preliminary data suggest that these puncta do not co-localize with RAB38-GFP or syntaxin13-GFP (**Figure A1**). Syntaxin13 is a SNARE protein present on early endosomes (164), and RAB38 is a small G protein that localizes both to tubular domains of early endosomes and to stage III and IV melanosomes (94). Together with the observation that ectopically expressed HA-SLC45A2 in non-pigment HeLa cells localizes on/near lysosomes, these data suggest that the punctate clusters of HA-SLC45A2 most likely reflect an association with melanosomes and lysosomes – or a subdomain of melanosomes and lysosomes – and not melanocyte-specific transport intermediates.

The localization of HA-tagged SLC45A2 to melanosomes or lysosomes requires an intact tyrosine-based signaling motif between the 6^{th} and 7^{th} transmembrane domains of the protein. Mutagenesis of the critical tyrosine residue within this motif results in mislocalization of HA-SLC45A2 to the plasma membrane and a decrease in melanin synthesis suggesting that human SLC45A2 must traffic to melanosomes to efficiently

produce pigment. The decrease in melanin could also reflect decreased expression of the Y268A variant in the melan-uw1 stable cell lines in comparison to wild-type HA-SLC45A2 (**Figure A2**). However, given that overexpression of the Y268A variant by transient transfection also impairs pigmentation, we favor the more likely interpretation that melanosomal localization is required for optimal SLC45A2 function.

What is the function of human SLC45A2 under normal physiological conditions? Since many more "stalled" stage III melanosomes were observed in a preliminary electron microscopy experiment comparing melan-uw1 melanocytes with wild-type melanocytes (**Figure A3**), we hypothesize that SLC45A2 is needed for the maturation of stage III melanosomes to stage IV melanosomes. Since knockdown of OCA2 has been shown to increase the number of stage I and stage II melanosomes without significantly affecting the number of stage III melanosomes (165), we speculate that OCA2 may initiate the process of neutralizing melanosomal pH in early stage melanosomes while SLC45A2 maintains it in stage III and stage IV melanosomes. Consistent with this idea, OCA2 appears to localizes predominantly to internal structures within melanosomes and overlaps to only a minor degree with proteins on the limiting membrane of mature melanosomes such as TYRP1 (14,166), suggesting that OCA2 might be cleared from the limiting membrane of stage III melanosomes by invagination onto intraluminal membranes (88,167,168). The presence of hypopigmented late-stage melanosomes in melan-uw1 cells is also supported by preliminary immunofluorescence and bright field microscopy experiments showing co-localization of TYR and TYRP1 – but not PMEL, a marker of early stage I and stage II melanosomes – with lightly pigmented structures (**Figure A4**). The notion that both OCA2 and SLC45A2 increase the pH of melanosomes

to provide an optimal environment for tyrosinase activity is further supported by another preliminary experiment in which, surprisingly, transient overexpression of OCA2-HA in SLC45A2-deficient melan-uw1 mouse melanocytes resulted in complete restoration of pigment by bright field microscopy (**Figure A5**).

Together, these experiments suggest that OCA4 is caused by stage III melanosomes that are too acidic for optimal TYR activity. It remains to be tested whether melan-uw1 mouse melanocytes "rescued" with OCA2-HA are equivalent to those rescued using HA-SLC45A2 and whether overexpression of SLC45A2 can restore pigmentation in OCA2-deficient melan-p1 mouse melanocytes. Why or how HA-SLC45A2 clusters in discrete puncta on or near the limiting membrane of melanosomes is also unclear and may hinder attempts to record current flow using patch-clamp techniques. However, we plan to examine melan-uw1 mouse melanocytes stably expressing HA-SLC45A2 by immunoelectron microscopy and hope that this experiment will provide the resolution necessary to determine whether the punctate structures we observe by light microscopy correspond to regions near or within the melanosomal membrane.

CHAPTER 4

Discussion

Testing the toxicity of a functional amyloid protein

While pathogenic amyloid proteins have been studied for decades, functional amyloid proteins are still a relatively recent discovery. In chapter 2, we proposed one mechanism of regulation for the functional amyloid protein PMEL in which the oligomeric state of PMEL regulates its propensity for amyloid formation. Our model suggests that disulfide-bonded PMEL dimers prevent premature fibril formation in early secretory compartments but must be resolved prior to functional amyloid assembly in early endosomes/stage I melanosomes. This process provides an additional layer of regulation to ensure that PMEL forms amyloid at exactly the right place and time. We speculate that other functional and pathogenic amyloid proteins might share a similar mechanism of regulation and that breakdown of this mechanism – at least for PMEL – could lead to inappropriate and potentially toxic amyloid formation earlier in the secretory pathway.

But would it? Identification of the toxic amyloid species remains a huge area of controversy within the field of amyloid biology, and the number of questions only multiplied with the discovery of functional amyloid proteins. Study of these proteins demonstrated that the final product of amyloid formation was not necessarily toxic. However, it remains unknown what separates functional amyloid proteins from pathogenic amyloid proteins. It might simply be a matter of context. For example, accumulation of the (normally extracellular) bacterial amyloid protein curli inside cells lacking the chaperone protein CsgC has been shown to increase cell death (46). Would other functional amyloid proteins also exhibit toxicity if expressed in different tissues and/or without robust regulation? Would PMEL?

Two naturally occurring dominant variants of PMEL suggest that the manner in which PMEL fibril formation occurs is not inconsequential. The *Dominant white* (*DW*) and *Silver* (*HoSi*) PMEL alleles form aberrant, tightly packed PMEL fibrils that impair pigmentation when expressed in melanocytes. Surprisingly, however, the mutations responsible for the loss of pigment in *Dominant white* chickens and *Silver* horses are not located in amyloid-forming regions of the protein but near the transmembrane domain. The *DW* allele involves the insertion of 3 additional amino acids in the PMEL transmembrane domain (TM^{insWAP}), while the *Silver* allele is defined by a single amino acid mutation in an arginine residue adjacent to the PMEL transmembrane domain (TM^{R625C}). How exactly these changes affect PMEL fibril formation is not known; however, their distance from the NTR and PKD domains (which most likely constitute the core of PMEL amyloid fibrils (86)) suggest that they influence the manner by which PMEL subunits assemble to form amyloid and/or the structure of the final product. Moreover, their dramatic effect on chicken plumage and horse hair suggest that changes in the regulation of PMEL amyloid assembly can radically alter PMEL function.

The C301S PMEL mutant is not a naturally occurring PMEL allele, and therefore, how the protein affects pigmentation *in vivo* is not known. However, it would be interesting to test whether C301S PMEL is toxic given that the non-covalent dimers formed by this mutant are likely to be less stable than disulfide-bonded p250 dimers. Transient overexpression of the C301S mutant in non-pigment HeLa cells showed no noticeable increase in toxicity when compared to the wild-type protein, and there was no obvious accumulation of C301S amyloid fibrils elsewhere in cells examined by electron microscopy. However, the *DW* variant of PMEL also formed normal-appearing amyloid

fibrils when overexpressed in HeLa cells; closely packed fibrils that inhibit melaninization were only observed upon expression in mouse melanocytes (147). Thus, it would be interesting to perform additional studies on the C301S mutant using high-pressure freezing to see if fibril formation occurs earlier in the secretory pathway or if fibril morphology is affected when the mutant protein is expressed at endogenous levels in mouse melanocytes.

If reduced cell viability and/or premature fibril formation were to be observed *in vitro*, we would then express the C301S mutant *in vivo*, a process we have already begun for *DW* PMEL. Because we only achieve low levels of protein expression using stable transfectants and because long-term effects on cell survival are difficult to assess using transient expression systems, we are generating transgenic mice that conditionally express PMEL under the control of the CAG promoter. The targeting construct was produced by insertion of wild-type PMEL or *DW* PMEL into the CAG-STOP-eGFP-ROSA Targeting Vector (**Figure A6**) and has been electroporated into C57BL/6 embryonic stem (ES) cells. These ES cells have been screened by the Gene Targeting Core at the University of Pennsylvania using Southern hybridization and by myself using PCR. These cells currently await injection into mouse blastocysts. One preliminary experiment suggests that these animals will be worth the wait. When co-transfected with Cre recombinase and a plasmid containing a puromycin selection cassette by T. Raabe of the Gene Targeting Core, ES cells expressing *DW* PMEL have decreased viability in comparison to control cells transfected with only the puromycin plasmid. In contrast, no difference in survival was observed for ES cells expressing wild-type PMEL. These data suggest that the formation of *DW* amyloid is toxic to ES cells, whereas that of wild-type

PMEL is not. It will be interesting to see whether this result holds true in primary melanocytes derived from newborn transgenic mice and treated with Cre recombinase *in vitro*, and it will be even more exciting to test whether mice expressing wild-type or *DW* PMEL in dopaminergic neurons of the substantia nigra show signs of neurodegeneration.

If this same experiment were to be performed using C301S PMEL, we would predict that mice carrying the C301S PMEL mutant would exhibit signs of neurodegeneration earlier than mice expressing wild-type PMEL in their dopaminergic neurons. The phenotype may also be more severe due to increased neuronal loss caused by amyloid fibrils that have formed in a different manner, in an earlier location, at the incorrect time, and/or with different structural properties. However, dopaminergic neurons of C301S mice may be less damaged than those of mice expressing *DW* PMEL as the ability to form noncovalent C301S dimers will likely enable the majority of the protein to undergo normal, nontoxic amyloid assembly.

The function of the PMEL KLD

PMEL amyloid, like all amyloid, is comprised of fibrils in which the β strands are organized perpendicular to the long axis of the fibril. Once formed, this hydrogen-bonded cross-β sheet structure is incredibly stable and highly insoluble, not to mention potentially toxic. Therefore, the conversion of PMEL from a non-amyloid protein to an amyloid one is likely to be highly regulated to ensure that the conformational change occurs quickly and efficiently in early stage melanosomes but not elsewhere in the cell.

While the function of the PMEL KLD is unknown, an intact KLD is clearly necessary for efficient fibril formation. Very little of the amyloidogenic Mα fragment is observed free in solution within MNT-1 cells and virtually none is observed in HeLa cells transiently expressing wild-type PMEL suggesting that (1) free Mα is rapidly processed into amyloid fibrils and (2) association with the KLD in p250, p160, and Mα+Mβ' species may antagonize adoption of the amyloid fold. Our results additionally indicate that the KLD forms a disulfide bond with PMEL C301 and therefore must be located near the PKD and the RPT domains in the three-dimensional structure of p250 and p160. In this position, the KLD could easily influence the structure of fibril-forming fragments by tethering the region in such a way as to be incompatible with the cross-β sheet amyloid fold. The idea that a disulfide bond can tether a protein in an amyloid-resistant conformation is not new and was previously reported for the pathologic amyloid protein tau (150).

Alternatively, the KLD could function to promote an association between the RPT domain and the fibril-forming NTR and PKD domains. Despite reports to the contrary (92,93), the RPT is unlikely to be a core component of amyloid fibrils since PMEL fibrils form much more rapidly *in vivo* than reported for the recombinant RPT domain *in vitro* (91), PMEL fibrils *in vivo* are stable within melanosomes at neutral pH whereas those produced from the RPT domain are stable only under acidic conditions, and the RPT domain is heavily O-glycosylated *in vivo*. However, the RPT domain may stabilize fully formed fibrils and/or facilitate the assembly of amyloid fibrils that have a particular structure. Indeed, a PMEL variant lacking the RPT domain forms much more closely packed fibrils (141) that could be harder to distinguish from unstructured aggregates by electron microscopy.

As previously discussed, the KLD could also catalyze a disulfide bond rearrangement that converts PMEL from an amyloid-resistant to an amyloid-prone conformation. While catalytic activity has never been reported for a KLD, the sensitivity of C301-KLD disulfide bonds to reduction during cell lysis if not adequately protected by NEM suggests that (1) the C301-KLD disulfide bond is solvent exposed and not buried deep within the globular core of the protein and (2) the catalytic cysteine that facilitates the reduction of this disulfide bond is either part of an abundant protein disulfide isomerase present nearby or located within PMEL itself. Since the only known protein disulfide isomerase of the endocytic pathway – GILT – is not expressed in melanocytes unless treated with γ-interferon ((145,146) and M. Marks, unpublished data), this would require the recruitment of an unknown protein disulfide isomerase. Thus, until additional protein disulfide isomerases are identified within secretory and/or endocytic compartments, we favor the interpretation that cysteine residues of the KLD can initiate disulfide bond rearrangements within PMEL in an autocatalytic manner. Note, however, that we have no structural information to suggest that one disulfide bond arrangement is more conducive to amyloid formation than another and that the proposed catalytic activity of the KLD in no way precludes it from also tethering or recruiting other PMEL domains.

Following up on p250

Functional amyloid proteins that are non-toxic in multiple cellular systems suggest the presence of regulatory mechanisms that are (1) intrinsic to the proteins themselves and/or (2) common to all cell types. We have proposed the formation of stable, non-toxic p250

dimers as one intrinsic mechanism of regulation preventing premature PMEL fibril formation early in the secretory pathway since p250 accumulation correlates with impaired fibril formation in the C566S variant of PMEL. To more rigorously test our model, however, we could tag PMEL with an FKBP domain, chemically induce dimerization with the dimerizing agent FK1012 (169), and examine the effect this has on PMEL fibril formation.

By chemically inducing dimerization, we might accumulate p250 PMEL dimers without introducing mutations into the KLD domain of the protein. If, as we speculate, the cysteine residues within the KLD can catalyze the resolution of p250, the inducible dimerization domain should preserve the p250 dimer even after disulfide rearrangement enabling us to determine whether dimerization alone is sufficient to inhibit PMEL amyloid formation or whether the decrease in fibril formation observed in the C566S PMEL variant results from a defective KLD. Alternatively or in conjunction with this experiment, the F36M variant of FKBP could be used to make ligand-reversible PMEL dimers. The advantage of this system is that the accumulated homodimers can be completely dissociated within minutes by the addition of synthetic ligands (170). Therefore, with this mutant we could test not only the effect of p250 accumulation on amyloid fibril formation but also observe how the p250 dimers are processed once released into the cell as monomeric protein. We could examine whether p250 dimers are on-pathway intermediates of PMEL amyloid formation by monitoring p160, free Mα, and Mα' fragment formation. We could even analyze these cells by immunofluorescence microscopy at various time points after the addition of FKBP ligand to see whether the

released monomeric protein is targeted to melanosomes for incorporation into growing amyloid fibrils or trafficked to lysosomes for degradation.

Subtleties of the C566S mutant

If our model was the only mechanism governing PMEL fibril formation, then all of PMEL should be packaged into disulfide-bonded p250 dimers concomitant with ER exit. These dimers would absolutely prevent unwanted fibril formation early in the secretory pathway, and any disruption in dimer resolution would bring fibril assembly to a standstill. In our experiments, however, fibril formation is not completely ablated in the C566S variant of PMEL, suggesting that either not all PMEL exits the ER as p250 dimers or that the dimers can be incorporated into fibrillar structures, albeit with decreased efficiency. Since very little free P2 or free Mα is observed in HeLa cells expressing the C566S mutant, it is unlikely that a significant portion of PMEL is exported from the ER in a monomeric form. Therefore, we speculate that the single cysteine point mutation C566S does not completely destroy the function of the KLD and that the C566S dimers are converted to p160 at a reduced rate. Alternatively, the dimers themselves may inefficiently polymerize into amyloid fibrils that resemble those formed by wild-type PMEL, at least by thin section electron microscopy. To test for a p160 "leak," cells expressing the C566S variant of p250 could be treated with a BACE2 inhibitor to prevent minute amounts of p160 from being rapidly assembled into amyloid fibrils. A metabolic pulse-chase experiment would also be useful to determine whether the C566S mutant is more slowly incorporated into detergent-insoluble fractions.

Help from chaperone proteins

Many chaperone proteins were detected in our mass spectrometry analysis of affinity-purified PMEL including PDI family members, UGGT1, ERp44, and BiP. Given that PMEL takes a long time to fold and exit the ER, it was not surprising to find that PMEL associated with many components of the glycoprotein quality control system. We considered the possibility that some of these chaperones continue to associate with PMEL past ER exit and even investigated ERp57 (a PDI family member also known as PDIA3) as a potential PMEL binding partner. The results showed that ERp57 associates with immature PMEL isoforms but not mature Golgi-modified PMEL species, suggesting that most of the chaperones we identified by mass spectrometry interact only with immature forms of PMEL in the ER.

However, chaperones are important components of other functional amyloid systems (46), and ER chaperones have been shown to traffic with aggregation-prone proteins (171). Thus, it seems not improbable that a chaperone might traffic with mature PMEL to ensure proper folding and prevent premature amyloid formation in secretory and endocytic compartments. In our previous attempts to identify covalent binding partners of PMEL by mass spectrometry, we used beads covalently conjugated to the αPMEL-C antibody for affinity purification. Because this antibody does not distinguish between mature and immature PMEL isoforms and because chaperones interacting with immature ER folding intermediates likely outnumber those interacting with mature forms of PMEL, it is hardly surprising that most of the peptides recovered in these experiments were derived from chaperones that function exclusively within the ER. To enrich for

noncovalent interactions involving mature PMEL isoforms, however, lysates could be pre-cleared using beads covalently conjugated to αPMEL-I prior to affinity chromatography using αPMEL-C. By pre-clearing the lysate over beads specific to ER forms of PMEL, proteins that interact with immature PMEL can not only be removed from the final sample but also serve as a useful point of comparison if eluted and analyzed separately by mass spectrometry. Note that HMB45, the antibody specific for mature forms of PMEL, is not suitable for immunoprecipitation or affinity purification.

Two regulators of PMEL fibril formation that should be enriched by the proposed experiment are CD63 and apolipoprotein E (ApoE). Neither protein was detected in our previous experiment, but both are involved in sorting mature PMEL to the ILVs of early endosomes/stage I melanosomes and have been shown to co-immunoprecipate with PMEL (78,79). The absence of these two proteins from our previous affinity chromatography/mass spectrometry analysis, however, is not a flaw in that experiment since we were specifically searching for covalent binding partners of PMEL and did not analyze many regions of the gel outside p250 and p160.

A protein chaperone that might interact with both mature and immature forms of PMEL is the 78 kDa glucose-regulated protein (GRP78, or BiP). BiP is an Hsp70 family member that typically resides within the ER but has been observed outside the ER during times of stress, especially on the cell surface of cancer cells (172). In addition, enormous quantities of BiP were detected in a separate Coomassie-stained band in our affinity chromatography/mass spectrometry experiment (data not shown) such that any mechanism masking the ER retention motif of BiP would likely result in its co-secretion.

PMEL *in vitro*

Some of the most tantalizing experiments await the purification of properly folded PMEL isoforms. Thus far, this has been a huge challenge for the field as Mα isolated from *E. coli* inclusion bodies retains very few (if any) of the regulatory mechanisms that govern PMEL amyloid formation *in vivo*. At the same time, extraction of pre-amyloid PMEL isoforms from mammalian tissue is not a viable strategy since (1) melanocytes comprise only a minor fraction of skin cells and (2) melanosome biogenesis within the RPE occurs primarily during prenatal development. Therefore, the best option currently available is to purify the secreted form of PMEL (sPMEL) from the culture medium of MNT-1 human melanoma cells.

Unlike recombinant Mα produced in bacteria, however, sPMEL is surprisingly resistant to aggregation. Even after exposure to low pH, the reducing agent DTT, or the denaturant urea, the vast majority of the protein remained in the soluble fraction following ultracentrifugation at 100,000g (D. Harper, unpublished results). This suggests that regulatory mechanisms governing the conversion of Mα from a non-amyloid to an amyloid form are intact in sPMEL but that an additional factor might be necessary to reconstitute fibril formation *in vitro*. Since fibril assembly typically occurs on ILVs, we hypothesize that the missing component is a protein or lipid associated with ILVs. Until that component can be identified, though, it may be useful to supply the reaction with purified exosomes (which are, essentially, secreted ILVs).

If/when an *in vitro* system using correctly folded and processed PMEL is operational, we will finally be able to perform kinetic and structural studies directly comparing PMEL

amyloid with other pathologic amyloid proteins. At a minimum, the kinetics of wild-type PMEL amyloid formation will be compared with that of Aβ and the C301S variant and the final products examined by CD, FTIR, and X-ray fiber diffraction. But we could also examine what types of stable oligomers and protofibrils are produced by the different PMEL mutants, use synthetic protein modifications to monitor the conformational change that occurs as PMEL converts from p250 to p160 to an amyloid form, or test the effect of PMEL pre-formed fibrils (PFFs) on melanocytes versus neurons in culture to try and gain additional insight into the question of whether PMEL amyloid is intrinsically less toxic than that of pathological amyloid proteins – or whether differences in toxicity are entirely a matter of context/regulation.

PMEL *in vivo*

While plenty of data support the amyloid structure of PMEL fibrils generated *in vitro* using recombinant Mα produced in bacteria, the only evidence that PMEL forms amyloid *in vivo* is that (1) melanosomes purified from bovine retinal pigment epithelia stain with amyloid dyes and (2) detergent-insoluble clusters extracted from bovine melanosomes stain with both Thioflavin S and PMEL. To perform additional structural studies, however, we either need to purify μg-mg quantities of PMEL amyloid from bovine retina or develop a way to generate sufficient material in cell culture. To start, melanosomes might be isolated from wild-type or TYR-deficient melanocytes, and membrane depleted using 1% Lubrol PX as was previously done for peptide hormones in pituitary secretory granules (59). Even if the quantity of fibrils obtained is insufficient for structural studies,

the material could be used to seed the formation of sPMEL fibrils that could then be analyzed by CD, FTIR, and X-ray diffraction.

Concluding remarks

To date, mammalian functional amyloid proteins have been identified in the pituitary (173), in the innate immune system (17), and in melanosomes (174). Of these, the structure and function of PMEL in the melanosome is by far the best studied, yet very little is known about how the protein converts from a non-amyloid to an amyloid form. Here we described the formation of p250 PMEL dimers and proposed that resolution of this species by the KLD contributes one layer of regulation to the timing of PMEL amyloid formation. Future studies on the toxicity of wild-type PMEL and associated variants, the biophysical characteristics of properly folded and processed PMEL fragments, and the contribution of protein chaperones will continue to shed light on the physiology and pathophysiology of amyloid in health and disease.

APPENDIX A

Supplementary Figures

Figure A1

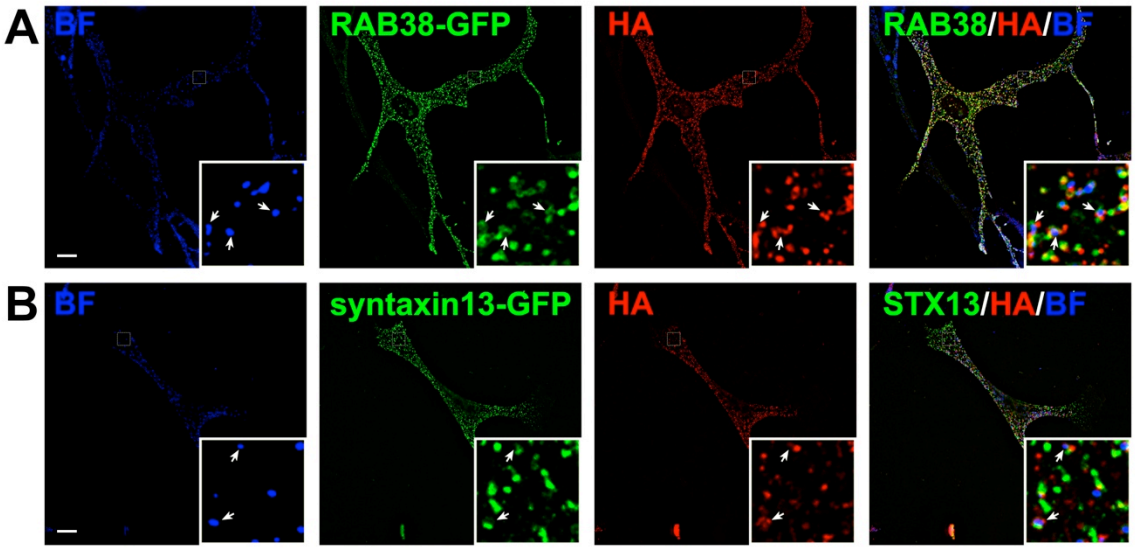

Punctate HA-SLC45A2 structures do not co-localize with RAB38 or syntaxin-13. Immortalized melan-uw1 melanocytes stably rescued with HA-SLC45A2 and transiently transfected with RAB38-GFP (A) or syntaxin-13-GFP (B) were fixed, labeled with an antibody against the HA tag and AF594-conjugated secondary antibody, and analyzed by bright field (pseudocolored blue) and deconvolution immunofluorescence microscopy. Shown are representative images of each channel separately and merged together. Insets show 8.4x magnifications of the boxed regions. Scale bars represent 10 μm.

Figure A2

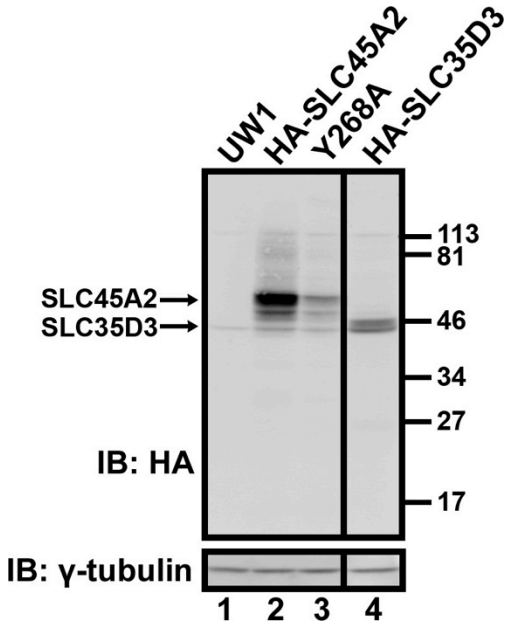

Expression of HA-SLC45A2, HA-SLC45A2 Y268A, or HA-SLC35D3 protein in melan-uw1 stable cell lines. Immortalized melan-uw1 melanocytes stably expressing HA-SLC45A2 (lane 2), the Y268A variant of HA-SLC45A2 (lane 3), HA-SLC35D3 (lane 4), or the uninfected parental cell line (lane 1) were lysed in buffer containing 1% Triton X-100. The detergent-soluble material was fractionated by SDS-PAGE, transferred to a membrane, and immunoblotted with an antibody to the HA tag followed by an antibody to γ-tubulin as a loading control. The migration of molecular weight standards is indicated to the right. Arrows highlight bands corresponding to SLC45A2 and SLC35D3. Lane numbers are indicated across the bottom.

Figure A3

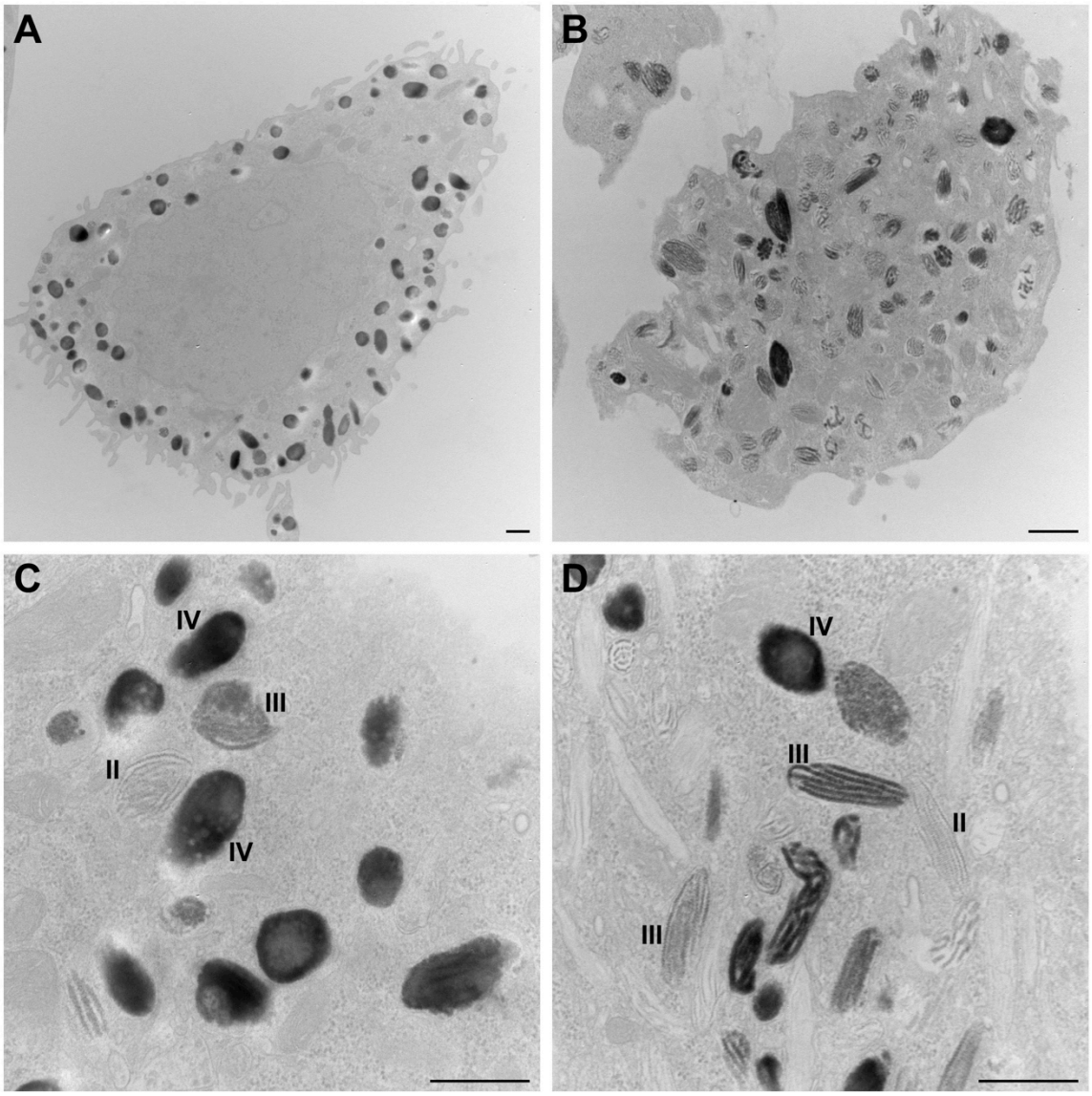

Immortalized melan-uw1 mouse melanocytes have more stage III and fewer stage IV melanosomes. Electron micrographs of melan-ink (A, C) and melan-uw1 (B, D) mouse melanocytes at low (A, B) and high magnifications (C, D). Scale bars represent 500 nm.

Figure A4

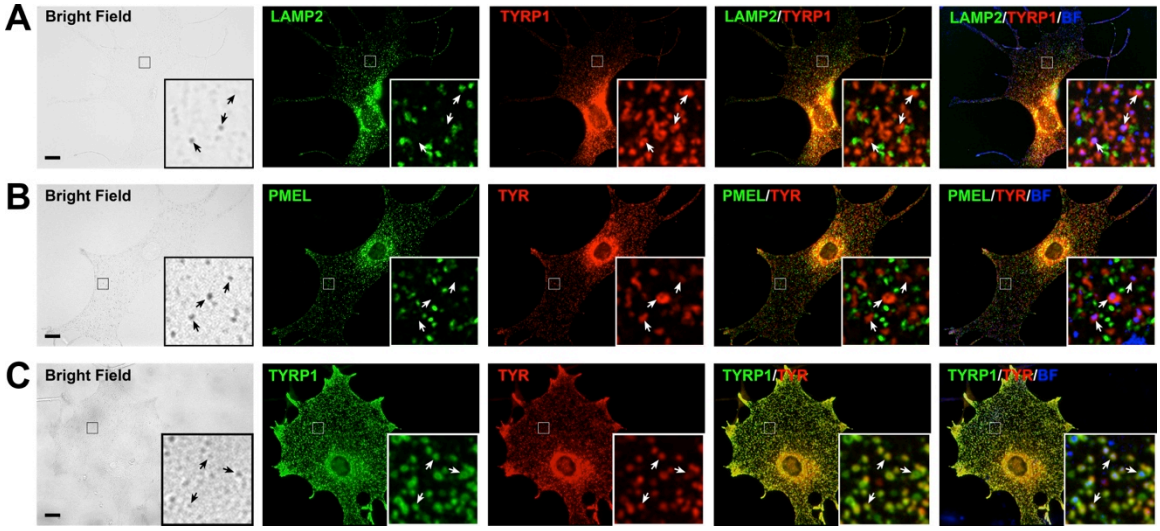

TYR and TYRP1 co-localize with faint pigment granules in melan-uw1 mouse melanocytes. Immortalized melan-uw1 mouse melanocytes were fixed, labeled with antibodies to TYR (PEP7), TYRP1 (TA99), PMEL (HMB45), and/or LAMP2 (GL2A7), and analyzed by bright field and deconvolution immunofluorescence microscopy. Shown are representative images of each channel separately and merged together. Insets show 8.25x magnifications of the boxed regions. Scale bars represent 10 μm.

Figure A5

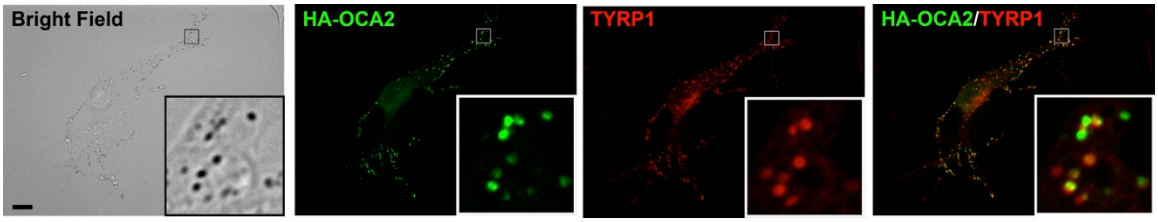

SLC45A2-deficient melan-uw1 melanocytes expressing OCA2 are highly pigmented. Immortalized melan-uw1 mouse melanocytes transiently expressing OCA2-HA were fixed, labeled with antibodies to TYRP1 (TA99) and the HA tag, and analyzed by bright field and deconvolution immunofluorescence microscopy. Shown are representative images of each channel separately and merged together. Insets show 8.25x magnifications of the boxed regions. Scale bar represents 10 μm.

Figure A6

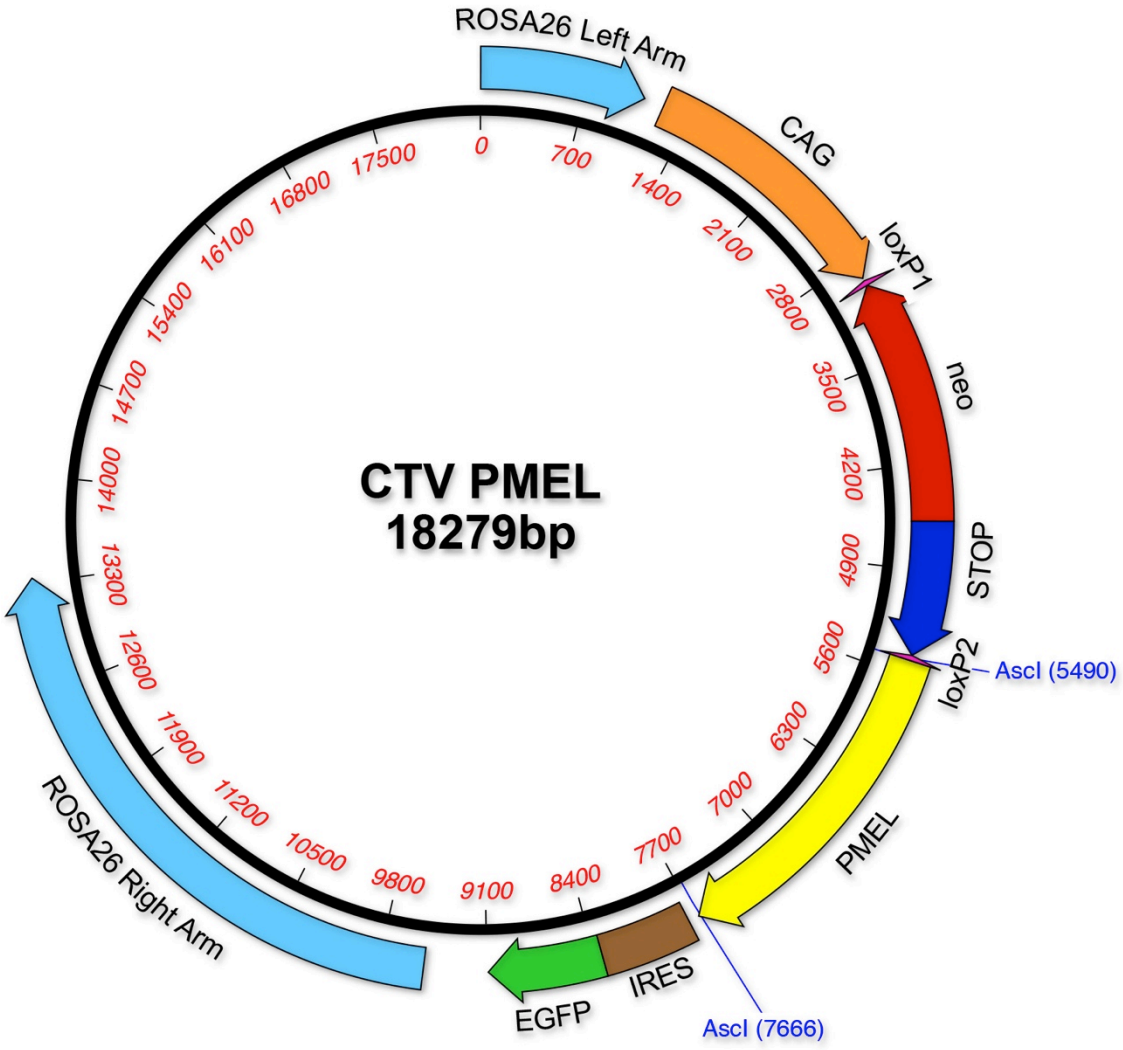

Targeting vector used to generate conditional knock-in mice expressing wild-type or TM^{insWAP} (*DW*) PMEL. Map of plasmid with left and right arms of homology for insertion into the ROSA26 locus, the strong CAG promoter (CAG), a neomycin resistance gene (neo) and a synthetic polyA transcriptional terminator (STOP) surrounded

by loxP sites, the location of the wild-type or *DW* PMEL cDNA (PMEL), and an IRES-GFP cassette.

APPENDIX B

Materials and Methods

Antibodies and reagents

Unless otherwise specified, chemicals were obtained from Sigma-Aldrich (St. Louis, MO) and tissue culture reagents from Life Technologies (Carlsbad, CA). Protease inhibitors were purchased from Roche Diagnostics (Indianapolis, IN), gene amplification primers from Integrated DNA Technologies (Coralville, IA), GoTaq DNA polymerase from Promega Corp. (Madison, WI), and restriction enzymes and T4 DNA ligase from New England Biolabs (Ipswich, MA). HMB45, a mouse monoclonal antibody to PMEL, was purchased from Enzo Life Sciences (Catalog # ENZ-C34930; Farmingdale, NY). Rabbit polyclonal antibodies PMEL-I, PMEL-N, PMEL-C, and PEP7 were affinity purified as previously described (64,72,133,175). The mouse monoclonal antibody NKI-beteb was obtained from Lab Vision (Freemont, CA), and the anti-HA antibodies used were 3F10 from Roche Diagnostics (Indianapolis, IN) and 16B12 from Covance (Princeton, NJ). The antibody TA99 to TYRP1 was obtained from ATCC (Rockville, MD), ab18528 to LAMP2A from abcam (Cambridge, MA), and GL2A7 to LAMP2 and H4A3 to LAMP1 both from the Developmental Studies Hybridoma Bank (University of Iowa, Iowa City, IA). Secondary antibodies conjugated to Alexa Fluor 488 or Alexa Fluor 594 for immunofluorescence microscopy or to alkaline phosphatase for immunoblotting were obtained from Jackson ImmunoResearch Laboratories (West Grove, PA). Secondary antibodies conjugated to IRDye 800CW or IRDye 680LT for immunoblotting were obtained from LI-COR Biotechnology (Lincoln, NE).

Cell culture and transfection conditions

The highly pigmented MNT-1 human melanoma cell line was cultured as previously described (129). The immortalized melanocyte cell lines melan-Ink4a and melan-uw1 were cultured in RPMI 1640 supplemented with 10% FBS (Atlanta Biologicals, Atlanta, GA) and 200 nM 12-tetradecanoylphorbol 13-acetate (TPA) in 10% CO_2 at 37˚C. The culture medium of melan-uw1 melanocytes and derived stable transfectants was also supplemented with 200 pM cholera toxin. Immortalized melanocyte cell lines were transfected using Lipofectamine 2000 (Thermo Fisher Scientific, Waltham, MA). HeLa cells were cultured in DMEM supplemented with 10% FBS in 5% CO_2 at 37°C and transfected with FuGENE 6 (Roche), FuGENE HD (Promega), GeneJuice (EMD Millipore, Billerica, MA), jetPRIME (Polyplus-transfection SA, Illkirch, France), or Xfect (Clontech Laboratories, Mountain View, CA) transfection reagents.

DNA constructs and cloning

The pCDM8.1 HA-SLC35D3 plasmid has been previously described (176). Wild-type hPMEL (long form) and the cleavage site mutant ΔCS in the pCI vector (Promega) have also been previously described (64,82) with cysteine mutants generated by site-directed mutagenesis using two-step gene amplification (177). The human SLC45A2 cDNA in the pCDNA4/TO-GFP vector was a gift from Dr. Elena Oancea (Brown University, Providence, RI). This insert was PCR amplified with an N-terminal HA tag and inserted into the pCI vector (Promega Corp., Madison, WI) to create HA-SLC45A2. The Y268A variant of HA-SLC45A2 was generated by A. Lefkovith via site-directed mutagenesis using two-step amplification (177). All inserts were verified by DNA sequencing.

Sequences of primers used for gene amplification and for the production of all mutants are available upon request.

Immunoblotting

Cells were harvested by centrifugation following release from plates with PBS, 5 mM EDTA, then treated with PBS, 50 mM *N*-ethylmaleimide (NEM), and then lysed (~10^7 cells per mL) in lysis buffer [1% (w/v) Triton X-100, 150 mM sodium chloride, 0.02% (w/v) sodium azide, 10 mM HEPES pH 7.4 supplemented with protease inhibitors and 50 mM NEM]. After centrifugation at 19,000g for 20 min, 1 volume of 6x SDS sample buffer [0.4 M Tris pH 6.8, 12% (w/v) SDS, 34% glycerol, 0.02% (w/v) bromophenol blue] with or without 11% β-mercaptoethanol was added to 5 volumes of detergent-soluble lysate. Samples were then heated at 60°C for 20 min, fractionated by SDS-PAGE on Tris-glycine gels containing 7%, 10%, or 12% acrylamide, and electrophoretically transferred to PVDF membranes. Membranes were blocked using blocking buffer [TBS pH 7.4, 0.2% Tween-20, 5% (w/v) nonfat dry milk] or Odyssey Blocking Buffer (LI-COR Biotechnology), incubated with primary antibodies diluted in blocking buffer, and washed with TBST [TBS pH 7.4, 0.2% Tween-20]. In some experiments, membranes were subsequently incubated with secondary antibodies conjugated to alkaline phosphatase diluted in blocking buffer, washed with TBST, detected using enhanced chemifluorescence (GE Healthcare Life Sciences, Piscataway, NJ), and analyzed using a Molecular Dynamics Storm 860 Molecular Imager Phosphorimager (GE Healthcare Life Sciences). In others, membranes were probed using secondary antibodies conjugated to

IRDye-800CW or IRDye-680LT diluted in blocking buffer, washed with TBST, and analyzed using an Odyssey Infrared Imaging System (LI-COR Biotechnology). Quantification of bands was performed using the ImageJ Gel Analyzer tool (http://fiji.sc/Fiji; National Institutes of Health) or Image Studio Lite (LI-COR).

Sucrose gradient sedimentation

Cells treated with PBS, 50 mM NEM were lysed in fractionation buffer [150 mM sodium chloride, 0.02% (w/v) sodium azide, 100 mM Tris pH 7.4 supplemented with protease inhibitor tablets, 50 mM NEM, and 20 mM iodoacetamide] containing 250 mM *n*-octylglucoside. The lysate was clarified by centrifugation at 19,000g for 15 min, layered on top of 5-20% sucrose gradients in 150 mM sodium chloride, 0.02% (w/v) sodium azide, 25 mM *n*-octylglucoside, 100 mM Tris pH 8, and fractionated by sedimentation velocity as described (178). Briefly, gradients were subjected to ultracentrifugation in a Beckman L8-70M Ultracentrifuge (Beckman Coulter Inc., Brea, CA) for 38 h at 30,000 rpm in an SW-41 rotor. Fractions were collected from bottom to top using a peristaltic pump, and aliquots of each fraction analyzed by non-reducing SDS-PAGE and immunoblotting. Standard proteins (ovalbumin, rabbit IgG, bovine liver catalase, and/or bovine thyroid thyroglobulin) were fractionated on parallel gradients; these fractions were analyzed by reducing SDS-PAGE followed by staining with Coomassie Brilliant Blue R-250.

Size exclusion chromatography

Cells were lysed in fractionation buffer containing either 250 mM *n*-octylglucoside, 40 mM dodecyl-β-D-maltoside, or 4% (w/v) Triton X-100. After clarification at 19,000g for 15 min, detergent-soluble lysates were analyzed by size exclusion chromatography on an ÄKTAFPLC system (GE Healthcare Life Sciences) using a Superose 6 10/300 GL column (GE Healthcare Life Sciences) in running buffer [150 mM sodium chloride, 0.02% (w/v) sodium azide, 10 mM HEPES pH 7.4] containing a lower concentration of the same detergent used for lysis – either 25 mM *n*-octylglucoside, 1 mM dodecyl-β-D-maltoside, or 0.1% (w/v) Triton X-100. The column was eluted at a flow rate of 0.4 – 0.45 mL/min with a fraction volume of 300 or 600 µL. Aliquots of each fraction were analyzed by non-reducing SDS-PAGE and immunoblotting. The elution volumes of thyroglobulin (669 kDa), α_2-macroglobulin (720 kDa), rabbit IgG (150 kDa), ovalbumin (45 kDa), and/or cytochrome C (12 kDa) were also evaluated in separate runs with fractions analyzed by SDS-PAGE followed by staining with Coomassie Brilliant Blue R-250.

Metabolic labeling and immunoprecipitation

Metabolic labeling with ^{35}S-methionine/cysteine and immunoprecipitation analyses were conducted essentially as described (64). Briefly, cells were harvested by centrifugation following digestion with trypsin-EDTA, washed, and cultured in suspension for 30 min in methionine/cysteine-free DMEM containing 5% dialyzed FBS. Cells were then pelleted and metabolically labeled in suspension in the same medium containing ^{35}S-Met/Cys Express Mix (PerkinElmer, Waltham, MA) for 10-15 min (pulse/chase analyses) or 2 h

(steady-state labeling for 2D-PAGE). For pulse/chase analyses, cells were pelleted again and chased for the indicated periods of time in standard growth medium containing excess methionine/cysteine as described (64). Cells were then lysed in lysis buffer and clarified by centrifugation at 19,000g for 20 min. After first pre-clearing the lysates over unconjugated protein A beads (Life Technologies) and then over protein A beads conjugated to normal rabbit serum, normal mouse serum, or a mouse isotype control antibody, the samples were subjected to immunoprecipitation using the antibodies specified. The immunoprecipitated material was fractionated by SDS-PAGE, and the resulting gels were dried and analyzed on a Phosphorimager as described above.

2-dimensional non-reducing/reducing SDS-PAGE

Triton X-100 lysates from cells metabolically labeled for 2 h were subject to immunoprecipitation using the PMEL antibodies αPMEL-N, NKI-beteb, or αPMEL-C after pre-clearing first with unconjugated protein A beads and then with protein A beads conjugated to either normal rabbit serum or normal mouse serum as described above. The immunoprecipitated material was then fractionated by SDS-PAGE in a 7% polyacrylamide tube gel under non-reducing conditions. The tube gel was reduced by incubation in 0.5% (w/v) DTT, 0.5% (w/v) SDS, 125 mM Tris pH 6.8 for 2 hours at room temperature and then mounted and sealed (with 1% agarose) on top of a standard SDS polyacrylamide gel. After fractionation by SDS-PAGE, the gels were dried and analyzed on a Phosphorimager as detailed above.

Immunoprecipitation/immunoblotting

HeLa cells expressing wild-type hPMEL or the C301S variant were released from plates using PBS, 5 mM EDTA and harvested by centrifugation. The cells were treated with PBS, 50 mM NEM on ice, pelleted, frozen, and subsequently lysed (~3 x 10^6 cells per mL) in lysis buffer. Following clarification at 19,000g, lysates were pre-cleared over unconjugated protein A beads prior to immunoprecipitation using NKI-beteb, αPMEL-C, normal rabbit serum, or a mouse isotype control antibody pre-bound to protein A beads. The beads were washed four times with wash buffer [0.1% (w/v) Triton X-100, 150 mM sodium chloride, 0.02% (w/v) sodium azide, 10 mM HEPES pH 7.4] followed by one wash with PBS. The immunoprecipitated material was then eluted by adding 2x SDS sample buffer containing 3.6% β-mercaptoethanol and heating the samples for 20 min at 60°C. After fractionation by SDS-PAGE and transfer to PVDF membranes, immunoblots were probed with αPMEL-C or HMB45 and analyzed using the Odyssey Imaging System detailed above.

Proteomic analysis of p250 and p160

Affinity purification. Pellets of 2.6 – 7.8 x 10^8 NEM-treated MNT-1 cells were either homogenized with a Dounce homogenizer and enriched for the total membrane fraction as previously described (82) or lysed directly in lysis buffer and clarified by centrifugation at 19,000g for 15 min. The detergent-soluble fraction was then loaded onto 3 columns in tandem containing Sepharose 4B (Sigma), rabbit IgG-conjugated agarose (Sigma), and αPMEL-C-conjugated Sepharose (generated by combining 3 mL of 1

mg/mL αPMEL-C with 3 mL of packed CNBr-activated Sepharose 4B from GE Healthcare Life Sciences according to manufacturer's instructions). The αPMEL-C column was subsequently washed with 600 mL wash buffer and eluted using 0.63 μg/mL PMEL-C peptide (CPIGENSPLLSGQQV, Peptide 2.0 Inc., Chantilly, VA). Eluate was collected in 0.5 – 1 mL fractions and aliquots analyzed by immunoblotting for PMEL content. Peak fractions were precipitated using a 5-fold volume of either methanol or acetone at -20°C. The concentrated eluate was then fractionated on a 3-8% Tris-Acetate protein gel (Life Technologies) and stained with Coomassie Brilliant Blue G-250.

In-gel digestion. Each sample was excised from the gel and cut into 1 mm cubes, destained in a solution containing 50% methanol, 1.25% acetic acid, reduced with 5 mM DTT (Thermo Fisher Scientific, Waltham, MA), and alkylated with 20 mM iodoacetamide (Sigma). Gel pieces were then washed with 20 mM ammonium bicarbonate (Sigma) and dehydrated with acetonitrile (Thermo Fisher Scientific). Trypsin (Promega; 5 ng/mL in 20 mM ammonium bicarbonate) was added to the gel pieces, and proteolysis was allowed to proceed overnight at 37ºC. Peptides were extracted with 0.3% triflouroacetic acid (J.T.Baker of Avantor Performance Materials, Center Valley, PA), followed by 50% acetonitrile. Extracts were combined and the volume was reduced by vacuum centrifugation.

Mass spectrometry analysis. Tryptic digests were analyzed by LC-MS/MS on a hybrid LTQ Orbitrap Elite mass spectrometer (Thermo Fisher Scientific) coupled with a nanoLC Ultra (Eksigent Technologies Inc., Dublin, CA). Peptides were separated by reverse phase (RP)-HPLC on a nanocapillary column, 75 μm x 15 cm Reprosil-pur 3 μm, 120 Å

(Dr. Maisch, Ammerbuch, Germany) in a Nanoflex chip system (Eksigent). Mobile phase A consisted of 1% methanol (Thermo Fisher Scientific), 0.1% formic acid (Thermo Fisher Scientific) and mobile phase B of 1% methanol, 0.1% formic acid, 80% acetonitrile. Peptides were eluted into the mass spectrometer at 300 nL/min with each RP-LC run comprising a 90 min gradient from 10 to 25% B in 65 min, 25 to 40% B in 25 min. The mass spectrometer was set to repetitively scan m/z from 300 to 1800 (R = 240,000 for LTQ-Orbitrap Elite) followed by data-dependent MS/MS scans on the twenty most abundant ions with a minimum signal of 1500, dynamic exclusion with a repeat count of 1, repeat duration of 30 s, exclusion size of 500 and duration of 60 s, isolation width of 2.0, normalized collision energy of 33, and waveform injection and dynamic exclusion enabled. Fourier transform mass spectroscopy full scan automatic gain control target value was 1E6, while MSn automatic gain control was 1E4. Fourier transform mass spectroscopy full scan maximum fill time was 500 ms, while ion trap MSn fill time was 50 ms; microscans were set at one. FT preview mode, charge state screening, and monoisotopic precursor selection were all enabled with rejection of unassigned and 1+ charge states.

Protein Identification. MaxQuant/Andromeda version 1.5.2.8 was used to identify proteins by searching against a human complete proteome sequence database downloaded from Uniprot.org on 20140714. MaxQuant search parameters are detailed in the parameters and summary tabs (see supplementary Microsoft Excel file), and the identified protein groups and their estimated MS1 summed spectral intensities for each gel slice are listed in the proteinGroups tab.

Immunofluorescence microscopy

Cells grown on uncoated or Matrigel-coated coverslips were fixed with 2% formaldehyde in PBS or HBSS, permeabilized and labeled with primary antibodies and fluorochrome-conjugated secondary antibodies in PBS, 0.2% (w/v) saponin, 0.1% (w/v) BSA as described previously (179), and analyzed on either a DM IRBE microscope (Leica Microsystems, Wetzlar, Germany) equipped with a 63x or 100x Plan Apochromat objective lens (1.4 NA; Leica), a Retiga Exi Fast 1394 digital camera (QImaging, Surrey, Canada), and OpenLab software (Improvision, Lexington, MA) or a DMI 6000B microscope (Leica Microsystems) equipped with the same objectives, an Orca Flash 4.0 V2 camera (Hamamatsu, Bridgewater, NJ), and Leica Application Suite X software (Leica Microsystems). Images captured in sequential z-planes separated by 0.2 μm were deconvolved and manipulated using the Volume Deconvolution module in OpenLab or Gold's 3D deconvolution algorithm with 3-4 iterations in the Leica Application Suite. Insets were magnified and further adjustments in brightness and contrast were performed using Adobe Photoshop (Adobe Systems, Mountain View, CA).

Electron microscopy

For electron microscopy, melan-ink4a and melan-uw1 mouse melanocytes were grown in 10-cm dishes and fixed *in situ*, while HeLa cells transfected with pCI-PMEL wild-type, C301S, or C566S with or without pEGFP-C1 (Clontech Laboratories) in a 9:1 ratio were either fixed *in situ*, high-pressure frozen, or sorted for GFP expression prior to fixation in

suspension. For fixation *in situ*, cells were incubated in Karnovsky's Fixative [4% paraformaldehyde, 4 mM calcium chloride, 72 mM sodium cacodylate pH 7.4] containing 0.5% glutaraldehyde for 1-2 h. This solution was then removed and replaced with Karnovsky's Fixative containing 2% glutaraldehyde and the cells fixed overnight at room temperature. After the cells were scraped using a rubber policeman, the overnight fixative was replaced with Karnovsky's Fixative containing 0.5% glutaraldehyde and the cells stored at 4°C. For high-pressure freezing, cells were released from plates using PBS, 5 mM EDTA, pelleted by centrifugation, and high-pressure frozen using an HPM 010 (ABRA Fluid, Widnow, Switzerland) by the Electron Microscopy Resource Laboratory at the University of Pennsylvania. Sample dehydration by freeze substitution was performed in a Leica AFSII (Leica Microsystems) over 72 h at -90°C in glass-distilled acetone supplemented with 0.1% uranyl acetate and 2% OsO_4. Cells were then embedded in EPON resin at room temperature followed by polymerization for 48 h at 60°C. HeLa cells sorted prior to fixation were co-transfected with pEGFP, released from plates using PBS, 5 mM EDTA, and sorted for GFP expression on a Moflo Astrios EQ (Beckman Coulter Inc.) by the CHOP Flow Cytometry Core. Similar to the cells sorted *in situ*, these sorted cells were fixed for 1-2 hours in Karnovsky's Fixative containing 0.5% glutaraldehyde, overnight in Karnovsky's Fixative containing 2% glutaraldehyde, and stored in Karnovsky's Fixative with 0.5% glutaraldehyde at 4°C. Both cells fixed *in situ* and cells sorted prior to fixation were subsequently dehydrated and embedded in EMbed-812 (Electron Microscopy Sciences, Fort Washington, PA) at the Electron Microscopy Resource Laboratory. Ultrathin sections were cut on either a Reichert-Jung Ultracut E or a Reichert Ultracut S microtome (now Leica Microsystems), placed on either uncoated

copper mesh grids or Formvar-coated copper slot grids, and stained with 50% ethanol, 1% uranyl acetate, 1% lead citrate as previously described (180). The specimens were then examined with a JEOL 1010 electron microscope fitted with a Hamamatsu C4742-95 digital camera (Hamamatsu, Bridgewater, NJ) and AMT Advantage image capture software (Advanced Microscopy Techniques, Woburn, MA). For quantification of fibril-containing organelles, a combined total of at least 30 cells from the three independent experiments were analyzed for each transfected cell type. The number of multivesicular bodies that lacked fibrils and the number of multivesicular bodies that contained fibrils (or fibrillar compartments lacking other internal structure) were quantified, and the percentage of fibril-containing multivesicular bodies calculated for each cell. These data were analyzed and plotted using Prism 6 (GraphPad Prism 6, La Jolla, CA), and statistical analyses were performed using a two-tailed unpaired t-test.

Melanin quantification

Melanin from melan-uw1 stable cell lines was quantified by K. Haltaufderhyde as previously described (181). Briefly, mouse melanocytes 50-90% confluent were lysed in Triton X-100 and centrifuged at 14,000g for 30 min to obtain detergent-soluble and detergent-insoluble fractions. The total protein present in the detergent-soluble fraction was determined using a Bradford assay (Bio-Rad Laboratories, Hercules, CA). The insoluble fraction was solubilized in 1 N NaOH, and total melanin content quantified by comparing the optical density of each sample at 405 nm with that of synthetic melanin

standards (Sigma). Average cellular melanin was then calculated as the ratio of total melanin to total protein for each sample.

REFERENCES

1. Hubbard, J. K., Uy, J. A., Hauber, M. E., Hoekstra, H. E., and Safran, R. J. (2010) Vertebrate pigmentation: from underlying genes to adaptive function. *Trends Genet.* **26**, 231-239
2. Ito, S., and Wakamatsu, K. (2008) Chemistry of mixed melanogenesis--pivotal roles of dopaquinone. *Photochem. Photobiol.* **84**, 582-592
3. Marks, M. S., Heijnen, H. F., and Raposo, G. (2013) Lysosome-related organelles: unusual compartments become mainstream. *Curr. Opin. Cell Biol.* **25**, 495-505
4. Sitaram, A., and Marks, M. S. (2012) Mechanisms of protein delivery to melanosomes in pigment cells. *Physiology* **27**, 85-99
5. Seiji, M., Shimao, K., Birbeck, M. S., and Fitzpatrick, T. B. (1963) Subcellular localization of melanin biosynthesis. *Ann. N. Y. Acad. Sci.* **100**, 497-533
6. Watt, B., van Niel, G., Raposo, G., and Marks, M. S. (2013) PMEL: a pigment cell-specific model for functional amyloid formation. *Pigment cell & melanoma research* **26**, 300-315
7. Ancans, J., Tobin, D. J., Hoogduijn, M. J., Smit, N. P., Wakamatsu, K., and Thody, A. J. (2001) Melanosomal pH controls rate of melanogenesis, eumelanin/phaeomelanin ratio and melanosome maturation in melanocytes and melanoma cells. *Exp. Cell Res.* **268**, 26-35
8. Berson, J. F., Harper, D. C., Tenza, D., Raposo, G., and Marks, M. S. (2001) Pmel17 initiates premelanosome morphogenesis within multivesicular bodies. *Mol. Biol. Cell* **12**, 3451-3464
9. Raposo, G., Tenza, D., Murphy, D. M., Berson, J. F., and Marks, M. S. (2001) Distinct protein sorting and localization to premelanosomes, melanosomes, and lysosomes in pigmented melanocytic cells. *J. Cell Biol.* **152**, 809-824
10. Setty, S. R., Tenza, D., Sviderskaya, E. V., Bennett, D. C., Raposo, G., and Marks, M. S. (2008) Cell-specific ATP7A transport sustains copper-dependent tyrosinase activity in melanosomes. *Nature* **454**, 1142-1146
11. Wei, A. H., Zang, D. J., Zhang, Z., Liu, X. Z., He, X., Yang, L., Wang, Y., Zhou, Z. Y., Zhang, M. R., Dai, L. L., Yang, X. M., and Li, W. (2013) Exome sequencing identifies SLC24A5 as a candidate gene for nonsyndromic oculocutaneous albinism. *J. Invest. Dermatol.* **133**, 1834-1840
12. Lamason, R. L., Mohideen, M. A., Mest, J. R., Wong, A. C., Norton, H. L., Aros, M. C., Jurynec, M. J., Mao, X., Humphreville, V. R., Humbert, J. E., Sinha, S., Moore, J. L., Jagadeeswaran, P., Zhao, W., Ning, G., Makalowska, I., McKeigue, P. M., O'Donnell, D., Kittles, R., Parra, E. J., Mangini, N. J., Grunwald, D. J., Shriver, M. D., Canfield, V. A., and Cheng, K. C. (2005) SLC24A5, a putative cation exchanger, affects pigmentation in zebrafish and humans. *Science* **310**, 1782-1786
13. Bellono, N. W., Escobar, I. E., Lefkovith, A. J., Marks, M. S., and Oancea, E. (2014) An intracellular anion channel critical for pigmentation. *Elife* **3**, e04543
14. Sitaram, A., Piccirillo, R., Palmisano, I., Harper, D. C., Dell'Angelica, E. C., Schiaffino, M. V., and Marks, M. S. (2009) Localization to mature melanosomes

by virtue of cytoplasmic dileucine motifs is required for human OCA2 function. *Mol. Biol. Cell* **20**, 1464-1477
15. Newton, J. M., Cohen-Barak, O., Hagiwara, N., Gardner, J. M., Davisson, M. T., King, R. A., and Brilliant, M. H. (2001) Mutations in the human orthologue of the mouse underwhite gene (uw) underlie a new form of oculocutaneous albinism, OCA4. *Am. J. Hum. Genet.* **69**, 981-988
16. Chapman, M. R., Robinson, L. S., Pinkner, J. S., Roth, R., Heuser, J., Hammar, M., Normark, S., and Hultgren, S. J. (2002) Role of Escherichia coli curli operons in directing amyloid fiber formation. *Science* **295**, 851-855
17. Li, J., McQuade, T., Siemer, A. B., Napetschnig, J., Moriwaki, K., Hsiao, Y. S., Damko, E., Moquin, D., Walz, T., McDermott, A., Chan, F. K., and Wu, H. (2012) The RIP1/RIP3 necrosome forms a functional amyloid signaling complex required for programmed necrosis. *Cell* **150**, 339-350
18. Fowler, D. M., Koulov, A. V., Alory-Jost, C., Marks, M. S., Balch, W. E., and Kelly, J. W. (2006) Functional amyloid formation within mammalian tissue. *PLoS Biol.* **4**, e6
19. Chiti, F., and Dobson, C. M. (2006) Protein misfolding, functional amyloid, and human disease. *Annu. Rev. Biochem.* **75**, 333-366
20. Eichner, T., and Radford, S. E. (2011) A diversity of assembly mechanisms of a generic amyloid fold. *Mol. Cell* **43**, 8-18
21. Fandrich, M. (2012) Oligomeric intermediates in amyloid formation: structure determination and mechanisms of toxicity. *J. Mol. Biol.* **421**, 427-440
22. Chartier-Harlin, M. C., Crawford, F., Houlden, H., Warren, A., Hughes, D., Fidani, L., Goate, A., Rossor, M., Roques, P., Hardy, J., and et al. (1991) Early-onset Alzheimer's disease caused by mutations at codon 717 of the beta-amyloid precursor protein gene. *Nature* **353**, 844-846
23. Roher, A. E., Lowenson, J. D., Clarke, S., Woods, A. S., Cotter, R. J., Gowing, E., and Ball, M. J. (1993) beta-Amyloid-(1-42) is a major component of cerebrovascular amyloid deposits: implications for the pathology of Alzheimer disease. *Proc. Natl. Acad. Sci. U. S. A.* **90**, 10836-10840
24. Iwatsubo, T., Saido, T. C., Mann, D. M., Lee, V. M., and Trojanowski, J. Q. (1996) Full-length amyloid-beta (1-42(43)) and amino-terminally modified and truncated amyloid-beta 42(43) deposit in diffuse plaques. *Am. J. Pathol.* **149**, 1823-1830
25. Jarrett, J. T., Berger, E. P., and Lansbury, P. T., Jr. (1993) The carboxy terminus of the beta amyloid protein is critical for the seeding of amyloid formation: implications for the pathogenesis of Alzheimer's disease. *Biochemistry* **32**, 4693-4697
26. Burdick, D., Soreghan, B., Kwon, M., Kosmoski, J., Knauer, M., Henschen, A., Yates, J., Cotman, C., and Glabe, C. (1992) Assembly and aggregation properties of synthetic Alzheimer's A4/beta amyloid peptide analogs. *J. Biol. Chem.* **267**, 546-554
27. Borchelt, D. R., Thinakaran, G., Eckman, C. B., Lee, M. K., Davenport, F., Ratovitsky, T., Prada, C. M., Kim, G., Seekins, S., Yager, D., Slunt, H. H., Wang, R., Seeger, M., Levey, A. I., Gandy, S. E., Copeland, N. G., Jenkins, N. A., Price,

D. L., Younkin, S. G., and Sisodia, S. S. (1996) Familial Alzheimer's disease-linked presenilin 1 variants elevate Abeta1-42/1-40 ratio in vitro and in vivo. *Neuron* **17**, 1005-1013

28. McLean, C. A., Cherny, R. A., Fraser, F. W., Fuller, S. J., Smith, M. J., Beyreuther, K., Bush, A. I., and Masters, C. L. (1999) Soluble pool of Abeta amyloid as a determinant of severity of neurodegeneration in Alzheimer's disease. *Ann. Neurol.* **46**, 860-866
29. Mc Donald, J. M., Savva, G. M., Brayne, C., Welzel, A. T., Forster, G., Shankar, G. M., Selkoe, D. J., Ince, P. G., Walsh, D. M., Medical Research Council Cognitive, F., and Ageing, S. (2010) The presence of sodium dodecyl sulphate-stable Abeta dimers is strongly associated with Alzheimer-type dementia. *Brain* **133**, 1328-1341
30. Shankar, G. M., Li, S., Mehta, T. H., Garcia-Munoz, A., Shepardson, N. E., Smith, I., Brett, F. M., Farrell, M. A., Rowan, M. J., Lemere, C. A., Regan, C. M., Walsh, D. M., Sabatini, B. L., and Selkoe, D. J. (2008) Amyloid-beta protein dimers isolated directly from Alzheimer's brains impair synaptic plasticity and memory. *Nat. Med.* **14**, 837-842
31. Polymeropoulos, M. H., Lavedan, C., Leroy, E., Ide, S. E., Dehejia, A., Dutra, A., Pike, B., Root, H., Rubenstein, J., Boyer, R., Stenroos, E. S., Chandrasekharappa, S., Athanassiadou, A., Papapetropoulos, T., Johnson, W. G., Lazzarini, A. M., Duvoisin, R. C., Di Iorio, G., Golbe, L. I., and Nussbaum, R. L. (1997) Mutation in the alpha-synuclein gene identified in families with Parkinson's disease. *Science* **276**, 2045-2047
32. Spillantini, M. G., Schmidt, M. L., Lee, V. M., Trojanowski, J. Q., Jakes, R., and Goedert, M. (1997) Alpha-synuclein in Lewy bodies. *Nature* **388**, 839-840
33. Saito, Y., Ruberu, N. N., Sawabe, M., Arai, T., Kazama, H., Hosoi, T., Yamanouchi, H., and Murayama, S. (2004) Lewy body-related alpha-synucleinopathy in aging. *J. Neuropathol. Exp. Neurol.* **63**, 742-749
34. Kalia, L. V., Kalia, S. K., McLean, P. J., Lozano, A. M., and Lang, A. E. (2013) alpha-Synuclein oligomers and clinical implications for Parkinson disease. *Ann. Neurol.* **73**, 155-169
35. Winner, B., Jappelli, R., Maji, S. K., Desplats, P. A., Boyer, L., Aigner, S., Hetzer, C., Loher, T., Vilar, M., Campioni, S., Tzitzilonis, C., Soragni, A., Jessberger, S., Mira, H., Consiglio, A., Pham, E., Masliah, E., Gage, F. H., and Riek, R. (2011) In vivo demonstration that alpha-synuclein oligomers are toxic. *Proc. Natl. Acad. Sci. U. S. A.* **108**, 4194-4199
36. Bartels, T., Choi, J. G., and Selkoe, D. J. (2011) alpha-Synuclein occurs physiologically as a helically folded tetramer that resists aggregation. *Nature* **477**, 107-110
37. Wang, W., Perovic, I., Chittuluru, J., Kaganovich, A., Nguyen, L. T., Liao, J., Auclair, J. R., Johnson, D., Landeru, A., Simorellis, A. K., Ju, S., Cookson, M. R., Asturias, F. J., Agar, J. N., Webb, B. N., Kang, C., Ringe, D., Petsko, G. A., Pochapsky, T. C., and Hoang, Q. Q. (2011) A soluble alpha-synuclein construct forms a dynamic tetramer. *Proc. Natl. Acad. Sci. U. S. A.* **108**, 17797-17802

38. Weinreb, P. H., Zhen, W., Poon, A. W., Conway, K. A., and Lansbury, P. T., Jr. (1996) NACP, a protein implicated in Alzheimer's disease and learning, is natively unfolded. *Biochemistry* **35**, 13709-13715
39. Trexler, A. J., and Rhoades, E. (2012) N-Terminal acetylation is critical for forming alpha-helical oligomer of alpha-synuclein. *Protein Sci.* **21**, 601-605
40. Bartels, T., Kim, N. C., Luth, E. S., and Selkoe, D. J. (2014) N-alpha-acetylation of alpha-synuclein increases its helical folding propensity, GM1 binding specificity and resistance to aggregation. *PLoS One* **9**, e103727
41. Fowler, D. M., Koulov, A. V., Balch, W. E., and Kelly, J. W. (2007) Functional amyloid--from bacteria to humans. *Trends Biochem. Sci.* **32**, 217-224
42. Majumdar, A., Cesario, W. C., White-Grindley, E., Jiang, H., Ren, F., Khan, M. R., Li, L., Choi, E. M., Kannan, K., Guo, F., Unruh, J., Slaughter, B., and Si, K. (2012) Critical role of amyloid-like oligomers of Drosophila Orb2 in the persistence of memory. *Cell* **148**, 515-529
43. Wang, X., Smith, D. R., Jones, J. W., and Chapman, M. R. (2007) In vitro polymerization of a functional Escherichia coli amyloid protein. *J. Biol. Chem.* **282**, 3713-3719
44. Hammer, N. D., Schmidt, J. C., and Chapman, M. R. (2007) The curli nucleator protein, CsgB, contains an amyloidogenic domain that directs CsgA polymerization. *Proc. Natl. Acad. Sci. U. S. A.* **104**, 12494-12499
45. Nenninger, A. A., Robinson, L. S., and Hultgren, S. J. (2009) Localized and efficient curli nucleation requires the chaperone-like amyloid assembly protein CsgF. *Proc. Natl. Acad. Sci. U. S. A.* **106**, 900-905
46. Evans, M. L., Chorell, E., Taylor, J. D., Aden, J., Gotheson, A., Li, F., Koch, M., Sefer, L., Matthews, S. J., Wittung-Stafshede, P., Almqvist, F., and Chapman, M. R. (2015) The bacterial curli system possesses a potent and selective inhibitor of amyloid formation. *Mol. Cell* **57**, 445-455
47. Hammar, M., Arnqvist, A., Bian, Z., Olsen, A., and Normark, S. (1995) Expression of two csg operons is required for production of fibronectin- and congo red-binding curli polymers in Escherichia coli K-12. *Mol. Microbiol.* **18**, 661-670
48. Robinson, L. S., Ashman, E. M., Hultgren, S. J., and Chapman, M. R. (2006) Secretion of curli fibre subunits is mediated by the outer membrane-localized CsgG protein. *Mol. Microbiol.* **59**, 870-881
49. Goyal, P., Krasteva, P. V., Van Gerven, N., Gubellini, F., Van den Broeck, I., Troupiotis-Tsailaki, A., Jonckheere, W., Pehau-Arnaudet, G., Pinkner, J. S., Chapman, M. R., Hultgren, S. J., Howorka, S., Fronzes, R., and Remaut, H. (2014) Structural and mechanistic insights into the bacterial amyloid secretion channel CsgG. *Nature* **516**, 250-253
50. Knowles, T. P., and Buehler, M. J. (2011) Nanomechanics of functional and pathological amyloid materials. *Nature nanotechnology* **6**, 469-479
51. Baxa, U., Cheng, N., Winkler, D. C., Chiu, T. K., Davies, D. R., Sharma, D., Inouye, H., Kirschner, D. A., Wickner, R. B., and Steven, A. C. (2005) Filaments of the Ure2p prion protein have a cross-beta core structure. *J. Struct. Biol.* **150**, 170-179

52. Blinder, D., Coschigano, P. W., and Magasanik, B. (1996) Interaction of the GATA factor Gln3p with the nitrogen regulator Ure2p in Saccharomyces cerevisiae. *J. Bacteriol.* **178**, 4734-4736
53. King, C. Y., Tittmann, P., Gross, H., Gebert, R., Aebi, M., and Wuthrich, K. (1997) Prion-inducing domain 2-114 of yeast Sup35 protein transforms in vitro into amyloid-like filaments. *Proc. Natl. Acad. Sci. U. S. A.* **94**, 6618-6622
54. Stansfield, I., Jones, K. M., Kushnirov, V. V., Dagkesamanskaya, A. R., Poznyakovski, A. I., Paushkin, S. V., Nierras, C. R., Cox, B. S., Ter-Avanesyan, M. D., and Tuite, M. F. (1995) The products of the SUP45 (eRF1) and SUP35 genes interact to mediate translation termination in Saccharomyces cerevisiae. *EMBO J.* **14**, 4365-4373
55. Osherovich, L. Z., and Weissman, J. S. (2001) Multiple Gln/Asn-rich prion domains confer susceptibility to induction of the yeast [PSI(+)] prion. *Cell* **106**, 183-194
56. Shorter, J. (2008) Hsp104: a weapon to combat diverse neurodegenerative disorders. *Neurosignals* **16**, 63-74
57. Si, K., Choi, Y. B., White-Grindley, E., Majumdar, A., and Kandel, E. R. (2010) Aplysia CPEB can form prion-like multimers in sensory neurons that contribute to long-term facilitation. *Cell* **140**, 421-435
58. Raveendra, B. L., Siemer, A. B., Puthanveettil, S. V., Hendrickson, W. A., Kandel, E. R., and McDermott, A. E. (2013) Characterization of prion-like conformational changes of the neuronal isoform of Aplysia CPEB. *Nat. Struct. Mol. Biol.* **20**, 495-501
59. Maji, S. K., Perrin, M. H., Sawaya, M. R., Jessberger, S., Vadodaria, K., Rissman, R. A., Singru, P. S., Nilsson, K. P., Simon, R., Schubert, D., Eisenberg, D., Rivier, J., Sawchenko, P., Vale, W., and Riek, R. (2009) Functional amyloids as natural storage of peptide hormones in pituitary secretory granules. *Science* **325**, 328-332
60. Hurbain, I., Geerts, W. J., Boudier, T., Marco, S., Verkleij, A. J., Marks, M. S., and Raposo, G. (2008) Electron tomography of early melanosomes: implications for melanogenesis and the generation of fibrillar amyloid sheets. *Proc. Natl. Acad. Sci. U. S. A.* **105**, 19726-19731
61. Orlow, S. J., Zhou, B. K., Boissy, R. E., and Pifko-Hirst, S. (1993) Identification of a mammalian melanosomal matrix glycoprotein. *J. Invest. Dermatol.* **101**, 141-144
62. Donatien, P. D., and Orlow, S. J. (1995) Interaction of melanosomal proteins with melanin. *Eur. J. Biochem.* **232**, 159-164
63. Hellstrom, A. R., Watt, B., Fard, S. S., Tenza, D., Mannstrom, P., Narfstrom, K., Ekesten, B., Ito, S., Wakamatsu, K., Larsson, J., Ulfendahl, M., Kullander, K., Raposo, G., Kerje, S., Hallbook, F., Marks, M. S., and Andersson, L. (2011) Inactivation of Pmel alters melanosome shape but has only a subtle effect on visible pigmentation. *PLoS Genet* **7**, e1002285
64. Berson, J. F., Harper, D., Tenza, D., Raposo, G., and Marks, M. S. (2001) Pmel17 initiates premelanosome morphogenesis within multivesicular bodies. *Mol. Biol. Cell* **12**, 3451-3464

65. Du, J., Miller, A. J., Widlund, H. R., Horstmann, M. A., Ramaswamy, S., and Fisher, D. E. (2003) MLANA/MART1 and SILV/PMEL17/GP100 are transcriptionally regulated by MITF in melanocytes and melanoma. *Am. J. Pathol.* **163**, 333-343
66. Kobayashi, T., Vieira, W. D., Potterf, B., Sakai, C., Imokawa, G., and Hearing, V. J. (1995) Modulation of melanogenic protein expression during the switch from eu- to pheomelanogenesis. *J. Cell Sci.* **108 (Pt 6)**, 2301-2309
67. Nasti, T. H., and Timares, L. (2015) MC1R, eumelanin and pheomelanin: their role in determining the susceptibility to skin cancer. *Photochem. Photobiol.* **91**, 188-200
68. Kwon, B. S., Halaban, R., Kim, G. S., Usack, L., Pomerantz, S., and Haq, A. K. (1987) A melanocyte-specific complementary DNA clone whose expression is inducible by melanotropin and isobutylmethyl xanthine. *Mol. Biol. Med.* **4**, 339-355
69. Maresh, G. A., Marken, J. S., Neubauer, M., Aruffo, A., Hellström, I., Hellström, K. E., and Marquardt, H. (1994) Cloning and expression of the gene for the melanoma-associated ME20 antigen. *DNA Cell Biol.* **13**, 87-95
70. Adema, G. J., de Boer, A. J., Vogel, A. M., Loenen, W. A., and Figdor, C. G. (1994) Molecular characterization of the melanocyte lineage-specific antigen gp100. *J. Biol. Chem.* **269**, 20126-20133
71. Valencia, J. C., Rouzaud, F., Julien, S., Chen, K. G., Passeron, T., Yamaguchi, Y., Abu-Asab, M., Tsokos, M., Costin, G. E., Yamaguchi, H., Jenkins, L. M., Nagashima, K., Appella, E., and Hearing, V. J. (2007) Sialylated core 1 O-glycans influence the sorting of Pmel17/gp100 and determine its capacity to form fibrils. *J. Biol. Chem.* **282**, 11266-11280
72. Harper, D. C., Theos, A. C., Herman, K. E., Tenza, D., Raposo, G., and Marks, M. S. (2008) Premelanosome amyloid-like fibrils are composed of only golgi-processed forms of Pmel17 that have been proteolytically processed in endosomes. *J. Biol. Chem.* **283**, 2307-2322
73. Leonhardt, R. M., Vigneron, N., Rahner, C., and Cresswell, P. (2011) Proprotein convertases process Pmel17 during secretion. *J. Biol. Chem.* **286**, 9321-9337
74. Theos, A. C., Truschel, S. T., Tenza, D., Hurbain, I., Harper, D. C., Berson, J. F., Thomas, P. C., Raposo, G., and Marks, M. S. (2006) A lumenal domain-dependent pathway for sorting to intralumenal vesicles of multivesicular endosomes involved in organelle morphogenesis. *Dev. Cell* **10**, 343-354
75. Theos, A. C., Berson, J. F., Theos, S. C., Herman, K. E., Harper, D. C., Tenza, D., Sviderskaya, E. V., Lamoreux, M. L., Bennett, D. C., Raposo, G., and Marks, M. S. (2006) Dual loss of ER export and endocytic signals with altered melanosome morphology in the silver mutation of Pmel17. *Mol. Biol. Cell* **17**, 3598-3612
76. Kummer, M. P., Maruyama, H., Huelsmann, C., Baches, S., Weggen, S., and Koo, E. H. (2009) Formation of Pmel17 amyloid is regulated by juxtamembrane metalloproteinase cleavage, and the resulting C-terminal fragment is a substrate for gamma-secretase. *J. Biol. Chem.* **284**, 2296-2306
77. Theos, A. C., Berson, J. F., Theos, S. C., Herman, K. E., Harper, D. C., Tenza, D., Sviderskaya, E. V., Lamoreux, M. L., Bennett, D. C., Raposo, G., and Marks, M.

S. (2006) Dual loss of ER export and endocytic signals with altered melanosome morphology in the *silver* mutation of Pmel17. *Mol. Biol. Cell* **17**, 3598-3612

78. van Niel, G., Charrin, S., Simoes, S., Romao, M., Rochin, L., Saftig, P., Marks, M. S., Rubinstein, E., and Raposo, G. (2011) The tetraspanin CD63 regulates ESCRT-independent and -dependent endosomal sorting during melanogenesis. *Dev. Cell* **21**, 708-721
79. van Niel, G., Bergam, P., Di Cicco, A., Hurbain, I., Lo Cicero, A., Dingli, F., Palmulli, R., Fort, C., Potier, M. C., Schurgers, L. J., Loew, D., Levy, D., and Raposo, G. (2015) Apolipoprotein E Regulates Amyloid Formation within Endosomes of Pigment Cells. *Cell Rep*
80. Rochin, L., Hurbain, I., Serneels, L., Fort, C., Watt, B., Leblanc, P., Marks, M. S., De Strooper, B., Raposo, G., and van Niel, G. (2013) BACE2 processes PMEL to form the melanosome amyloid matrix in pigment cells. *Proc. Natl. Acad. Sci. U. S. A.* **110**, 10658-10663
81. Corder, E. H., Saunders, A. M., Strittmatter, W. J., Schmechel, D. E., Gaskell, P. C., Small, G. W., Roses, A. D., Haines, J. L., and Pericak-Vance, M. A. (1993) Gene dose of apolipoprotein E type 4 allele and the risk of Alzheimer's disease in late onset families. *Science* **261**, 921-923
82. Berson, J. F., Theos, A. C., Harper, D. C., Tenza, D., Raposo, G., and Marks, M. S. (2003) Proprotein convertase cleavage liberates a fibrillogenic fragment of a resident glycoprotein to initiate melanosome biogenesis. *J. Cell Biol.* **161**, 521-533
83. Kawaguchi, M., Hozumi, Y., and Suzuki, T. (2015) ADAM protease inhibitors reduce melanogenesis by regulating PMEL17 processing in human melanocytes. *J. Dermatol. Sci.* **78**, 133-142
84. Hoashi, T., Tamaki, K., and Hearing, V. J. (2010) The secreted form of a melanocyte membrane-bound glycoprotein (Pmel17/gp100) is released by ectodomain shedding. *FASEB J.* **24**, 916-930
85. Maresh, G. A., Wang, W.-C., Beam, K. S., Malacko, A. R., Hellström, I., Hellström, K. E., and Marquardt, H. (1994) Differential processing and secretion of the melanoma-associated ME20 antigen. *Arch. Biochem. Biophys.* **311**, 95-102
86. Watt, B., van Niel, G., Fowler, D. M., Hurbain, I., Luk, K. C., Stayrook, S. E., Lemmon, M. A., Raposo, G., Shorter, J., Kelly, J. W., and Marks, M. S. (2009) N-terminal domains elicit formation of functional Pmel17 amyloid fibrils. *J. Biol. Chem.* **284**, 35543-35555
87. Kwon, B. S., Chintamaneni, C., Kozak, C. A., Copeland, N. G., Gilbert, D. J., Jenkins, N., Barton, D., Francke, U., Kobayashi, Y., and Kim, K. K. (1991) A melanocyte-specific gene, Pmel 17, maps near the silver coat color locus on mouse chromosome 10 and is in a syntenic region on human chromosome 12. *Proc. Natl. Acad. Sci. U. S. A.* **88**, 9228-9232
88. Theos, A. C., Truschel, S. T., Raposo, G., and Marks, M. S. (2005) The Silver locus product Pmel17/gp100/Silv/ME20: controversial in name and in function. *Pigment Cell Res.* **18**, 322-336
89. Hoashi, T., Muller, J., Vieira, W. D., Rouzaud, F., Kikuchi, K., Tamaki, K., and Hearing, V. J. (2006) The repeat domain of the melanosomal matrix protein

PMEL17/GP100 is required for the formation of organellar fibers. *J. Biol. Chem.* **281**, 21198-21208
90. McGlinchey, R. P., Jiang, Z., and Lee, J. C. (2014) Molecular origin of pH-dependent fibril formation of a functional amyloid. *Chembiochem* **15**, 1569-1572
91. Pfefferkorn, C. M., McGlinchey, R. P., and Lee, J. C. (2010) Effects of pH on aggregation kinetics of the repeat domain of a functional amyloid, Pmel17. *Proc. Natl. Acad. Sci. U. S. A.* **107**, 21447-21452
92. McGlinchey, R. P., Shewmaker, F., McPhie, P., Monterroso, B., Thurber, K., and Wickner, R. B. (2009) The repeat domain of the melanosome fibril protein Pmel17 forms the amyloid core promoting melanin synthesis. *Proc. Natl. Acad. Sci. U. S. A.* **106**, 13731-13736
93. McGlinchey, R. P., Shewmaker, F., Hu, K. N., McPhie, P., Tycko, R., and Wickner, R. B. (2011) Repeat domains of melanosome matrix protein Pmel17 orthologs form amyloid fibrils at the acidic melanosomal pH. *J. Biol. Chem.* **286**, 8385-8393
94. Gronskov, K., Ek, J., and Brondum-Nielsen, K. (2007) Oculocutaneous albinism. *Orphanet J. Rare Dis.* **2**, 43
95. Lerner, A. B., Fitzpatrick, T. B., and et al. (1949) Mammalian tyrosinase; preparation and properties. *J. Biol. Chem.* **178**, 185-195
96. Kwon, B. S., Haq, A. K., Pomerantz, S. H., and Halaban, R. (1987) Isolation and sequence of a cDNA clone for human tyrosinase that maps at the mouse c-albino locus. *Proc. Natl. Acad. Sci. U. S. A.* **84**, 7473-7477
97. Spritz, R. A., Ho, L., Furumura, M., and Hearing, V. J., Jr. (1997) Mutational analysis of copper binding by human tyrosinase. *J. Invest. Dermatol.* **109**, 207-212
98. Yamaguchi, Y., Heiny, M. E., Suzuki, M., and Gitlin, J. D. (1996) Biochemical characterization and intracellular localization of the Menkes disease protein. *Proc. Natl. Acad. Sci. U. S. A.* **93**, 14030-14035
99. Mellman, I., Fuchs, R., and Helenius, A. (1986) Acidification of the endocytic and exocytic pathways. *Annu. Rev. Biochem.* **55**, 663-700
100. Saeki, H., and Oikawa, A. (1978) Effects of pH and type of sugar in the medium on tyrosinase activity in cultured melanoma cells. *J. Cell. Physiol.* **94**, 139-145
101. Manga, P., and Orlow, S. J. (2001) Inverse correlation between pink-eyed dilution protein expression and induction of melanogenesis by bafilomycin A1. *Pigment Cell Res.* **14**, 362-367
102. Simon, J. D., Peles, D., Wakamatsu, K., and Ito, S. (2009) Current challenges in understanding melanogenesis: bridging chemistry, biological control, morphology, and function. *Pigment cell & melanoma research* **22**, 563-579
103. Bartolke, R., Heinisch, J. J., Wieczorek, H., and Vitavska, O. (2014) Proton-associated sucrose transport of mammalian solute carrier family 45: an analysis in Saccharomyces cerevisiae. *Biochem. J.* **464**, 193-201
104. Kausar, T., Bhatti, M. A., Ali, M., Shaikh, R. S., and Ahmed, Z. M. (2013) OCA5, a novel locus for non-syndromic oculocutaneous albinism, maps to chromosome 4q24. *Clin. Genet.* **84**, 91-93

105. Gronskov, K., Dooley, C. M., Ostergaard, E., Kelsh, R. N., Hansen, L., Levesque, M. P., Vilhelmsen, K., Mollgard, K., Stemple, D. L., and Rosenberg, T. (2013) Mutations in c10orf11, a melanocyte-differentiation gene, cause autosomal-recessive albinism. *Am. J. Hum. Genet.* **92**, 415-421
106. Beermann, F., Orlow, S. J., Boissy, R. E., Schmidt, A., Boissy, Y. L., and Lamoreux, M. L. (1995) Misrouting of tyrosinase with a truncated cytoplasmic tail as a result of the murine platinum (cp) mutation. *Exp. Eye Res.* **61**, 599-607
107. Vijayasaradhi, S., Xu, Y., Bouchard, B., and Houghton, A. N. (1995) Intracellular sorting and targeting of melanosomal membrane proteins: identification of signals for sorting of the human brown locus protein, gp75. *J. Cell Biol.* **130**, 807-820
108. Honing, S., Sandoval, I. V., and von Figura, K. (1998) A di-leucine-based motif in the cytoplasmic tail of LIMP-II and tyrosinase mediates selective binding of AP-3. *EMBO J.* **17**, 1304-1314
109. Theos, A. C., Tenza, D., Martina, J. A., Hurbain, I., Peden, A. A., Sviderskaya, E. V., Stewart, A., Robinson, M. S., Bennett, D. C., Cutler, D. F., Bonifacino, J. S., Marks, M. S., and Raposo, G. (2005) Functions of adaptor protein (AP)-3 and AP-1 in tyrosinase sorting from endosomes to melanosomes. *Mol. Biol. Cell* **16**, 5356-5372
110. Delevoye, C., Hurbain, I., Tenza, D., Sibarita, J. B., Uzan-Gafsou, S., Ohno, H., Geerts, W. J., Verkleij, A. J., Salamero, J., Marks, M. S., and Raposo, G. (2009) AP-1 and KIF13A coordinate endosomal sorting and positioning during melanosome biogenesis. *J. Cell Biol.* **187**, 247-264
111. Setty, S. R., Tenza, D., Truschel, S. T., Chou, E., Sviderskaya, E. V., Theos, A. C., Lamoreux, M. L., Di Pietro, S. M., Starcevic, M., Bennett, D. C., Dell'Angelica, E. C., Raposo, G., and Marks, M. S. (2007) BLOC-1 is required for cargo-specific sorting from vacuolar early endosomes toward lysosome-related organelles. *Mol. Biol. Cell* **18**, 768-780
112. Di Pietro, S. M., Falcon-Perez, J. M., Tenza, D., Setty, S. R., Marks, M. S., Raposo, G., and Dell'Angelica, E. C. (2006) BLOC-1 interacts with BLOC-2 and the AP-3 complex to facilitate protein trafficking on endosomes. *Mol. Biol. Cell* **17**, 4027-4038
113. Dennis, M. K., Mantegazza, A. R., Snir, O. L., Tenza, D., Acosta-Ruiz, A., Delevoye, C., Zorger, R., Sitaram, A., de Jesus-Rojas, W., Ravichandran, K., Rux, J., Sviderskaya, E. V., Bennett, D. C., Raposo, G., Marks, M. S., and Setty, S. R. (2015) BLOC-2 targets recycling endosomal tubules to melanosomes for cargo delivery. *J. Cell Biol.* **209**, 563-577
114. Bonifacino, J. S., and Traub, L. M. (2003) Signals for sorting of transmembrane proteins to endosomes and lysosomes. *Annu. Rev. Biochem.* **72**, 395-447
115. Kondo, T., Namiki, T., Coelho, S. G., Valencia, J. C., and Hearing, V. J. (2015) Oculocutaneous albinism: developing novel antibodies targeting the proteins associated with OCA2 and OCA4. *J. Dermatol. Sci.* **77**, 21-27
116. Cullinane, A. R., Vilboux, T., O'Brien, K., Curry, J. A., Maynard, D. M., Carlson-Donohoe, H., Ciccone, C., Program, N. C. S., Markello, T. C., Gunay-Aygun, M., Huizing, M., and Gahl, W. A. (2011) Homozygosity mapping and whole-exome

sequencing to detect SLC45A2 and G6PC3 mutations in a single patient with oculocutaneous albinism and neutropenia. *J. Invest. Dermatol.* **131**, 2017-2025
117. Bin, B. H., Bhin, J., Yang, S. H., Shin, M., Nam, Y. J., Choi, D. H., Shin, D. W., Lee, A. Y., Hwang, D., Cho, E. G., and Lee, T. R. (2015) Membrane-Associated Transporter Protein (MATP) Regulates Melanosomal pH and Influences Tyrosinase Activity. *PLoS One* **10**, e0129273
118. Costin, G. E., Valencia, J. C., Vieira, W. D., Lamoreux, M. L., and Hearing, V. J. (2003) Tyrosinase processing and intracellular trafficking is disrupted in mouse primary melanocytes carrying the underwhite (uw) mutation. A model for oculocutaneous albinism (OCA) type 4. *J. Cell Sci.* **116**, 3203-3212
119. Dooley, C. M., Schwarz, H., Mueller, K. P., Mongera, A., Konantz, M., Neuhauss, S. C., Nusslein-Volhard, C., and Geisler, R. (2013) Slc45a2 and V-ATPase are regulators of melanosomal pH homeostasis in zebrafish, providing a mechanism for human pigment evolution and disease. *Pigment cell & melanoma research* **26**, 205-217
120. Skovronsky, D. M., Lee, V. M., and Trojanowski, J. Q. (2006) Neurodegenerative diseases: new concepts of pathogenesis and their therapeutic implications. *Annu. Rev. Pathol.* **1**, 151-170
121. Burgoyne, T., O'Connor, M. N., Seabra, M. C., Cutler, D. F., and Futter, C. E. (2015) Regulation of melanosome number, shape and movement in the zebrafish retinal pigment epithelium by OA1 and PMEL. *J. Cell Sci.* **128**, 1400-1407
122. Chakraborty, A. K., Platt, J. T., Kim, K. K., Kwon, B. S., Bennett, D. C., and Pawelek, J. M. (1996) Polymerization of 5,6-dihydroxyindole-2-carboxylic acid to melanin by the pmel 17/silver locus protein. *Eur. J. Biochem.* **236**, 180-188
123. Lee, Z. H., Hou, L., Moellmann, G., Kuklinska, E., Antol, K., Fraser, M., Halaban, R., and Kwon, B. S. (1996) Characterization and subcellular localization of human Pmel 17/silver, a 110-kDa (pre)melanosomal membrane protein associated with 5,6,-dihydroxyindole-2-carboxylic acid (DHICA) converting activity. *J. Invest. Dermatol.* **106**, 605-610
124. Kerje, S., Sharma, P., Gunnarsson, U., Kim, H., Bagchi, S., Fredriksson, R., Schutz, K., Jensen, P., von Heijne, G., Okimoto, R., and Andersson, L. (2004) The Dominant white, Dun and Smoky color variants in chicken are associated with insertion/deletion polymorphisms in the PMEL17 gene. *Genetics* **168**, 1507-1518
125. Schonthaler, H. B., Lampert, J. M., von Lintig, J., Schwarz, H., Geisler, R., and Neuhauss, S. C. (2005) A mutation in the silver gene leads to defects in melanosome biogenesis and alterations in the visual system in the zebrafish mutant fading vision. *Dev. Biol.* **284**, 421-436
126. Brunberg, E., Andersson, L., Cothran, G., Sandberg, K., Mikko, S., and Lindgren, G. (2006) A missense mutation in PMEL17 is associated with the Silver coat color in the horse. *BMC Genet.* **7**, 46
127. Clark, L. A., Wahl, J. M., Rees, C. A., and Murphy, K. E. (2006) Retrotransposon insertion in SILV is responsible for merle patterning of the domestic dog. *Proc. Natl. Acad. Sci. U. S. A.* **103**, 1376-1381

128. Dunn, L. C., and Thigpen, L. W. (1930) The silver mouse: a recessive color variation. *J. Hered.* **21**, 495-498
129. Raposo, G., Tenza, D., Murphy, D. M., Berson, J. F., and Marks, M. S. (2001) Distinct protein sorting and localization to premelanosomes, melanosomes, and lysosomes in pigmented melanocytic cells. *J. Cell Biol.* **152**, 809-823
130. Kushimoto, T., Basrur, V., Valencia, J., Matsunaga, J., Vieira, W. D., Ferrans, V. J., Muller, J., Appella, E., and Hearing, V. J. (2001) A model for melanosome biogenesis based on the purification and analysis of early melanosomes. *Proc. Natl. Acad. Sci. U.S.A.* **98**, 10698-10703
131. Chng, S. S., Xue, M., Garner, R. A., Kadokura, H., Boyd, D., Beckwith, J., and Kahne, D. (2012) Disulfide rearrangement triggered by translocon assembly controls lipopolysaccharide export. *Science* **337**, 1665-1668
132. Chiamenti, A. M., Vella, F., Bonetti, F., Pea, M., Ferrari, S., Martignoni, G., Benedetti, A., and Suzuki, H. (1996) Anti-melanoma monoclonal antibody HMB-45 on enhanced chemiluminescence-western blotting recognizes a 30-35 kDa melanosome-associated sialated glycoprotein. *Melanoma Res.* **6**, 291-298
133. Nichols, S. E., Harper, D. C., Berson, J. F., and Marks, M. S. (2003) A novel splice variant of Pmel17 expressed by human melanocytes and melanoma cells lacking some of the internal repeats. *J. Invest. Dermatol.* **121**, 821-830
134. Lorber, B., Bishop, J. B., and DeLucas, L. J. (1990) Purification of octyl beta-D-glucopyranoside and re-estimation of its micellar size. *Biochim. Biophys. Acta* **1023**, 254-265
135. Nishigai, M., Osada, T., and Ikai, A. (1985) Structural changes in alpha-2- and ovomacroglobulins studied by gel chromatography and electron microscopy. *Biochim. Biophys. Acta* **831**, 236-241
136. VanAken, T., Foxall-VanAken, S., Castleman, S., and Ferguson-Miller, S. (1986) Alkyl glycoside detergents: synthesis and applications to the study of membrane proteins. *Methods Enzymol.* **125**, 27-35
137. Biaselle, C. J., and Millar, D. B. (1975) Studies on Triton X-100 detergent micelles. *Biophys. Chem.* **3**, 355-361
138. Vennegoor, C., Hageman, P., Van Nouhuijs, H., Ruiter, D. J., Calafat, J., Ringens, P. J., and Rumke, P. (1988) A monoclonal antibody specific for cells of the melanocyte lineage. *Am. J. Pathol.* **130**, 179-192
139. Tartakoff, A. M. (1983) Perturbation of vesicular traffic with the carboxylic ionophore monensin. *Cell* **32**, 1026-1028
140. Stachel, S. J., Coburn, C. A., Steele, T. G., Jones, K. G., Loutzenhiser, E. F., Gregro, A. R., Rajapakse, H. A., Lai, M. T., Crouthamel, M. C., Xu, M., Tugusheva, K., Lineberger, J. E., Pietrak, B. L., Espeseth, A. S., Shi, X. P., Chen-Dodson, E., Holloway, M. K., Munshi, S., Simon, A. J., Kuo, L., and Vacca, J. P. (2004) Structure-based design of potent and selective cell-permeable inhibitors of human beta-secretase (BACE-1). *J. Med. Chem.* **47**, 6447-6450
141. Leonhardt, R. M., Vigneron, N., Hee, J. S., Graham, M., and Cresswell, P. (2013) Critical residues in the PMEL/Pmel17 N-terminus direct the hierarchical assembly of melanosomal fibrils. *Mol. Biol. Cell* **24**, 964-981

142. Leonhardt, R. M., Vigneron, N., Rahner, C., Van den Eynde, B. J., and Cresswell, P. (2010) Endoplasmic reticulum export, subcellular distribution, and fibril formation by Pmel17 require an intact N-terminal domain junction. *J. Biol. Chem.* **285**, 16166-16183
143. Oka, O. B., and Bulleid, N. J. (2013) Forming disulfides in the endoplasmic reticulum. *Biochim. Biophys. Acta* **1833**, 2425-2429
144. Liu, Y. D., Chen, X., Enk, J. Z., Plant, M., Dillon, T. M., and Flynn, G. C. (2008) Human IgG2 antibody disulfide rearrangement in vivo. *J. Biol. Chem.* **283**, 29266-29272
145. West, L. C., and Cresswell, P. (2013) Expanding roles for GILT in immunity. *Curr. Opin. Immunol.* **25**, 103-108
146. O'Donnell, P. W., Haque, A., Klemsz, M. J., Kaplan, M. H., and Blum, J. S. (2004) Cutting edge: induction of the antigen-processing enzyme IFN-gamma-inducible lysosomal thiol reductase in melanoma cells Is STAT1-dependent but CIITA-independent. *J. Immunol.* **173**, 731-735
147. Watt, B., Tenza, D., Lemmon, M. A., Kerje, S., Raposo, G., Andersson, L., and Marks, M. S. (2011) Mutations in or near the transmembrane domain alter PMEL amyloid formation from functional to pathogenic. *PLoS Genet* **7**, e1002286
148. Anoop, A., Ranganathan, S., Das Dhaked, B., Jha, N. N., Pratihar, S., Ghosh, S., Sahay, S., Kumar, S., Das, S., Kombrabail, M., Agarwal, K., Jacob, R. S., Singru, P., Bhaumik, P., Padinhateeri, R., Kumar, A., and Maji, S. K. (2014) Elucidating the role of disulfide bond on amyloid formation and fibril reversibility of somatostatin-14: relevance to its storage and secretion. *J. Biol. Chem.* **289**, 16884-16903
149. Li, Y., Gong, H., Sun, Y., Yan, J., Cheng, B., Zhang, X., Huang, J., Yu, M., Guo, Y., Zheng, L., and Huang, K. (2012) Dissecting the role of disulfide bonds on the amyloid formation of insulin. *Biochem. Biophys. Res. Commun.* **423**, 373-378
150. Walker, S., Ullman, O., and Stultz, C. M. (2012) Using intramolecular disulfide bonds in tau protein to deduce structural features of aggregation-resistant conformations. *J. Biol. Chem.* **287**, 9591-9600
151. Stefani, M., and Dobson, C. M. (2003) Protein aggregation and aggregate toxicity: new insights into protein folding, misfolding diseases and biological evolution. *J. Mol. Med. (Berl.)* **81**, 678-699
152. Spritz, R. A., Strunk, K. M., Giebel, L. B., and King, R. A. (1990) Detection of mutations in the tyrosinase gene in a patient with type IA oculocutaneous albinism. *N. Engl. J. Med.* **322**, 1724-1728
153. Rinchik, E. M., Bultman, S. J., Horsthemke, B., Lee, S. T., Strunk, K. M., Spritz, R. A., Avidano, K. M., Jong, M. T., and Nicholls, R. D. (1993) A gene for the mouse pink-eyed dilution locus and for human type II oculocutaneous albinism. *Nature* **361**, 72-76
154. Bellono, N. W., and Oancea, E. V. (2014) Ion transport in pigmentation. *Arch. Biochem. Biophys.* **563**, 35-41
155. Boissy, R. E., Zhao, H., Oetting, W. S., Austin, L. M., Wildenberg, S. C., Boissy, Y. L., Zhao, Y., Sturm, R. A., Hearing, V. J., King, R. A., and Nordlund, J. J. (1996) Mutation in and lack of expression of tyrosinase-related protein-1 (TRP-1)

in melanocytes from an individual with brown oculocutaneous albinism: a new subtype of albinism classified as "OCA3". *Am. J. Hum. Genet.* **58**, 1145-1156
156. Montoliu, L., Gronskov, K., Wei, A. H., Martinez-Garcia, M., Fernandez, A., Arveiler, B., Morice-Picard, F., Riazuddin, S., Suzuki, T., Ahmed, Z. M., Rosenberg, T., and Li, W. (2014) Increasing the complexity: new genes and new types of albinism. *Pigment cell & melanoma research* **27**, 11-18
157. Lehman, A. L., Silvers, W. K., Puri, N., Wakamatsu, K., Ito, S., and Brilliant, M. H. (2000) The underwhite (uw) locus acts autonomously and reduces the production of melanin. *J. Invest. Dermatol.* **115**, 601-606
158. Lamoreux, M. L., Wakamatsu, K., and Ito, S. (2001) Interaction of major coat color gene functions in mice as studied by chemical analysis of eumelanin and pheomelanin. *Pigment Cell Res.* **14**, 23-31
159. Ozeki, H., Ito, S., Wakamatsu, K., and Thody, A. J. (1996) Spectrophotometric characterization of eumelanin and pheomelanin in hair. *Pigment Cell Res.* **9**, 265-270
160. Ito, S., and Wakamatsu, K. (2003) Quantitative analysis of eumelanin and pheomelanin in humans, mice, and other animals: a comparative review. *Pigment Cell Res.* **16**, 523-531
161. Potterf, S. B., Furumura, M., Sviderskaya, E. V., Santis, C., Bennett, D. C., and Hearing, V. J. (1998) Normal tyrosine transport and abnormal tyrosinase routing in pink-eyed dilution melanocytes. *Exp. Cell Res.* **244**, 319-326
162. Simmen, T., Schmidt, A., Hunziker, W., and Beermann, F. (1999) The tyrosinase tail mediates sorting to the lysosomal compartment in MDCK cells via a di-leucine and a tyrosine-based signal. *J. Cell Sci.* **112 (Pt 1)**, 45-53
163. Papadopoulos, J. S., and Agarwala, R. (2007) COBALT: constraint-based alignment tool for multiple protein sequences. *Bioinformatics* **23**, 1073-1079
164. Prekeris, R., Klumperman, J., Chen, Y. A., and Scheller, R. H. (1998) Syntaxin 13 mediates cycling of plasma membrane proteins via tubulovesicular recycling endosomes. *J. Cell Biol.* **143**, 957-971
165. Park, S., Morya, V. K., Nguyen, D. H., Singh, B. K., Lee, H. B., and Kim, E. K. (2015) Unrevealing the role of P-protein on melanosome biology and structure, using siRNA-mediated down regulation of OCA2. *Mol. Cell. Biochem.* **403**, 61-71
166. Sitaram, A., Dennis, M. K., Chaudhuri, R., De Jesus-Rojas, W., Tenza, D., Setty, S. R., Wood, C. S., Sviderskaya, E. V., Bennett, D. C., Raposo, G., Bonifacino, J. S., and Marks, M. S. (2012) Differential recognition of a dileucine-based sorting signal by AP-1 and AP-3 reveals a requirement for both BLOC-1 and AP-3 in delivery of OCA2 to melanosomes. *Mol. Biol. Cell* **23**, 3178-3192
167. Turner, W. A., Taylor, J. D., and Tchen, T. T. (1975) Melanosome formation in the goldfish: the role of multivesicular bodies. *J. Ultrastruct. Res.* **51**, 16-31
168. Jimbow, K., Oikawa, O., Sugiyama, S., and Takeuchi, T. (1979) Comparison of eumelanogenesis and pheomelanogenesis in retinal and follicular melanocytes; role of vesiculo-globular bodies in melanosome differentiation. *J. Invest. Dermatol.* **73**, 278-284

169. Spencer, D. M., Wandless, T. J., Schreiber, S. L., and Crabtree, G. R. (1993) Controlling signal transduction with synthetic ligands. *Science* **262**, 1019-1024
170. Rollins, C. T., Rivera, V. M., Woolfson, D. N., Keenan, T., Hatada, M., Adams, S. E., Andrade, L. J., Yaeger, D., van Schravendijk, M. R., Holt, D. A., Gilman, M., and Clackson, T. (2000) A ligand-reversible dimerization system for controlling protein-protein interactions. *Proc. Natl. Acad. Sci. U. S. A.* **97**, 7096-7101
171. Genereux, J. C., Qu, S., Zhou, M., Ryno, L. M., Wang, S., Shoulders, M. D., Kaufman, R. J., Lasmezas, C. I., Kelly, J. W., and Wiseman, R. L. (2015) Unfolded protein response-induced ERdj3 secretion links ER stress to extracellular proteostasis. *EMBO J.* **34**, 4-19
172. Ni, M., Zhang, Y., and Lee, A. S. (2011) Beyond the endoplasmic reticulum: atypical GRP78 in cell viability, signalling and therapeutic targeting. *Biochem. J.* **434**, 181-188
173. Maji, S. K., Perrin, M. H., Sawaya, M. R., Jessberger, S., Vadodaria, K., Rissman, R. A., Singru, P. S., Nilsson, K. P., Simon, R., Schubert, D., Eisenberg, D., Rivier, J., Sawchenko, P., Vale, W., and Riek, R. (2009) Functional amyloids as natural storage of peptide hormones in pituitary secretory granules. *Science* **325**, 328-332
174. Fowler, D. M., Koulov, A. V., Alory-Jost, C., Marks, M. S., Balch, W. E., and Kelly, J. W. (2006) Functional amyloid formation within mammalian tissue. *PLoS biology* **4**, e6
175. Jimenez, M., Tsukamoto, K., and Hearing, V. J. (1991) Tyrosinases from two different loci are expressed by normal and by transformed melanocytes. *J. Biol. Chem.* **266**, 1147-1156
176. Meng, R., Wang, Y., Yao, Y., Zhang, Z., Harper, D. C., Heijnen, H. F., Sitaram, A., Li, W., Raposo, G., Weiss, M. J., Poncz, M., and Marks, M. S. (2012) SLC35D3 delivery from megakaryocyte early endosomes is required for platelet dense granule biogenesis and is differentially defective in Hermansky-Pudlak syndrome models. *Blood* **120**, 404-414
177. Higuchi, R., Krummel, B., and Saiki, R. K. (1988) A general method of in vitro preparation and specific mutagenesis of DNA fragments: study of protein and DNA interactions. *Nucleic Acids Res.* **16**, 7351-7367
178. Marks, M. S. (2001) Determination of molecular size by zonal sedimentation analysis on sucrose density gradients. *Curr. Protoc. Cell Biol.* **Chapter 5**, Unit 5 3
179. Humphrey, J. S., Peters, P. J., Yuan, L. C., and Bonifacino, J. S. (1993) Localization of TGN38 to the trans-Golgi network: involvement of a cytoplasmic tyrosine-containing sequence. *J. Cell Biol.* **120**, 1123-1135
180. Reynolds, E. S. (1963) The use of lead citrate at high pH as an electron-opaque stain in electron microscopy. *J. Cell Biol.* **17**, 208-212
181. Oancea, E., Vriens, J., Brauchi, S., Jun, J., Splawski, I., and Clapham, D. E. (2009) TRPM1 forms ion channels associated with melanin content in melanocytes. *Sci Signal* **2**, ra21